Medizinische Klinik I
Director: Prof. Dr. Jens Marquardt

UNIVERSITÄT ZU LÜBECK

"Nesfatin-1's effects on energy homeostasis: dissecting the role of PVN and NTS neurons"

Dissertation
for Fulfillment of
Requirements
for the Doctoral Degree
of the University of Lübeck

from the Department of Natural Sciences

Submitted by

Sandro Catzeddu
from Oristano, Italy
Lübeck, 2021

First referee: .....

Second referee: .....

Date of oral examination: .....

Approved for printing. Lübeck, ...

Abstract

Nesfatin-1 (NUCB2/nesfatin-1), the N-terminal fragment of NEFA/nucleobindin2, is a potent anorexigenic peptide, and promoter of energy expenditure, expressed in the periphery and the brain in organs and areas related to the regulation of energy homeostasis. To date, a dedicated receptor has not been discovered, limiting our knowledge on the central mechanisms of action of NUCB2/nesfatin-1. In this work, we focused on the effects of exogenous nesfatin-1 on feeding and energy expenditure. First, we compared the effects of intracerebroventricular injections of NUCB2/nesfatin-1 in food-deprived vs. *ad libitum* fed animals; in this latter group, NUCB2/nesfatin-1 is seen to promote energy expenditure quicker than in the food-deprived group. Second, we focused specifically on the paraventricular hypothalamus (PVN). Here, NUCB2/nesfatin-1 reduces food intake, and increases energy expenditure by recruiting the interscapular brown adipose tissue (iBAT); these effects are abolished by blockade of the MAPK/ERK system. Furthermore, knockdown of the expression of the melanocortin type-4-receptors in the brainstem abolished the intra-PVN NUCB2/nesfatin-1-mediated increase in energy expenditure. Third, we investigated the role of endogenous nesfatin-1 in the brainstem (using nesfatin-1-directed antibodies) and its interaction with the GLP-1 system in the context of homeostatic and hedonic food behavior. Blockade of endogenous nesfatin-1 does not affect hedonic behavior, nor affected the anti-hedonic properties of GLP-1, as measured with a progressive ratio paradigm. However, it completely blocks the anorexigenic effect GLP-1, in male but not female animals. In summary, we underline the PVN and brainstem as crucial areas for the NUCB2/nesfatin-1 regulation of food intake and energy expenditure. We propose that nesfatinergic signals from the PVN are relayed to the brainstem and from here to the periphery, acting through the ERK1/2 and melanocortin system respectively to modulate food intake and energy expenditure.

Abstrakt

Nesfatin-1 (NUCB2/Nesfatin-1), das N-terminale Fragment von NEFA/Nucleobindin2, ist ein potentes anorexigenes Peptid und Promotor des Energieverbrauchs, das in der Peripherie und im Gehirn in Organen und Bereichen exprimiert wird, die mit der Regulation der Energiehomöostase in Verbindung stehen. Bis heute wurde kein eigener Rezeptor entdeckt, was unser Wissen über die zentralen Wirkmechanismen von NUCB2/Nesfatin-1 einschränkt. In dieser Arbeit haben wir uns auf die Auswirkungen von exogenem Nesfatin-1 auf die Nahrungsaufnahme und den Energieverbrauch konzentriert. Erstens verglichen wir die Auswirkungen von intrazerebroventrikulären Injektionen von NUCB2/Nesfatin-1 bei Tieren mit Nahrungsentzug im Vergleich zu Tieren, die *ad libitum* gefüttert wurden; in der letztgenannten Gruppe wurde festgestellt, dass NUCB2/Nesfatin-1 den Energieverbrauch schneller fördert als in der Gruppe mit Nahrungsentzug. Zweitens haben wir uns speziell auf den paraventrikulären Hypothalamus (PVN) fokussiert. Hier reduziert NUCB2/Nesfatin-1 die Nahrungsaufnahme und erhöht den Energieverbrauch durch Rekrutierung des interskapulären braunen Fettgewebes (iBAT); diese Effekte werden durch Blockade des MAPK/ERK-Systems aufgehoben. Darüber hinaus hob der Knockdown der Expression der Melanocortin-Typ-4-Rezeptoren im Hirnstamm die durch Gabe von NUCB2/Nesfatin-1 in den PVN vermittelte Steigerung des Energieverbrauchs auf. Drittens untersuchten wir die Rolle von endogenem Nesfatin-1 im Hirnstamm (unter Verwendung von gegen Nesfatin-1-gerichteten Antikörpern) und seine Interaktion mit dem GLP-1-System im Zusammenhang mit homöostatischem und hedonischem Essverhalten. Die Blockade von endogenem Nesfatin-1 beeinflusst weder das hedonische Verhalten noch die anti-hedonischen Eigenschaften von GLP-1, wie wir mit Hilfe eines progressive ratio Paradigmas zeigen konnten. Allerdings blockiert es vollständig die anorexigene Wirkung von GLP-1 bei männlichen, jedoch nicht bei weiblichen Tieren. Zusammenfassend belegen wir die entscheidende Rolle von PVN und Hirnstamm für die NUCB2/Nesfatin-1-vermittelte Regulation der Nahrungsaufnahme und des

Energieverbrauchs. Hierbei könnten nesfatinerge Signale aus dem PVN an den Hirnstamm und von dort an die Peripherie weitergeleitet werden und über das ERK1/2- bzw. Melanocortin-System wirken, um Nahrungsaufnahme und Energieverbrauch zu modulieren.

Table of contents

Introduction

Energy homeostasis

The term "homeostasis" indicates the propensity to maintain a stable state, be it either at a cellular or at a whole-organism level. Food supplies the body with the nutrients and energy that are essential for the normal continuation of its function. In return, the body employs several processes aimed at maintaining an equilibrium between energy intake via food intake and energy expenditure, an equilibrium also defined as "energy homeostasis", to maintain and defend a stable body weight.

The central nervous system (CNS) is the cornerstone of energy homeostasis regulation. First and foremost, the brain possesses so-called "glucose-sensing" neurons, whose electrical activity can be modulated by glucose levels and enact appropriate responses aimed at controlling, for example, food intake. Glucose-sensing neurons are located mainly in the hypothalamus, and especially in the arcuate (Arc) and ventromedial nuclei, but their presence has been noted also in other areas that span from the brainstem to the cortex, hippocampus, amygdala, and more (Fioramonti et al., 2017).

Second, the brain can receive, interpret, and respond to a vast range of signals that convey the body's energy status of both sensory (e.g. mechanoreceptors in the gut) and humoral (e.g. fat and glucose levels, but also meal-related peptides) nature conveyed via vagal afferent fibers predominantly to the nucleus of the solitary tract (NTS) and dorsal motor nucleus of the vagus nerve (DMNV). The brain can then integrate these signals and relay them to other appropriate food-related brain areas such as the hypothalamus and dorsal striatum to make appropriate adjustments in both food intake and energy expenditure (Figure. I.1). Adiposity signals represent the main source of energy-related information that the body – and especially the brain – employ to constantly be informed about energetic reserves. Following a model called "adiposity negative-feedback" (Kennedy, 1953), adiposity signals must first circulate on levels dependent on the body's fat mass and be able to enter the CNS where their receptors can be found. And second, these receptors should be expressed in energy homeostasis-relevant areas within the CNS, and their manipulation promotes

alteration in food intake and/or energy expenditure. Leptin and insulin fully meet all these criteria, but many other signals both anorexigenic (glucagon-like peptide 1 (GLP-1), cholecystokinin (CCK), nesfatin-1) and orexigenic (ghrelin) that convey important afferent information to the brain have been identified (G. Morton & Schwartz, 2006).

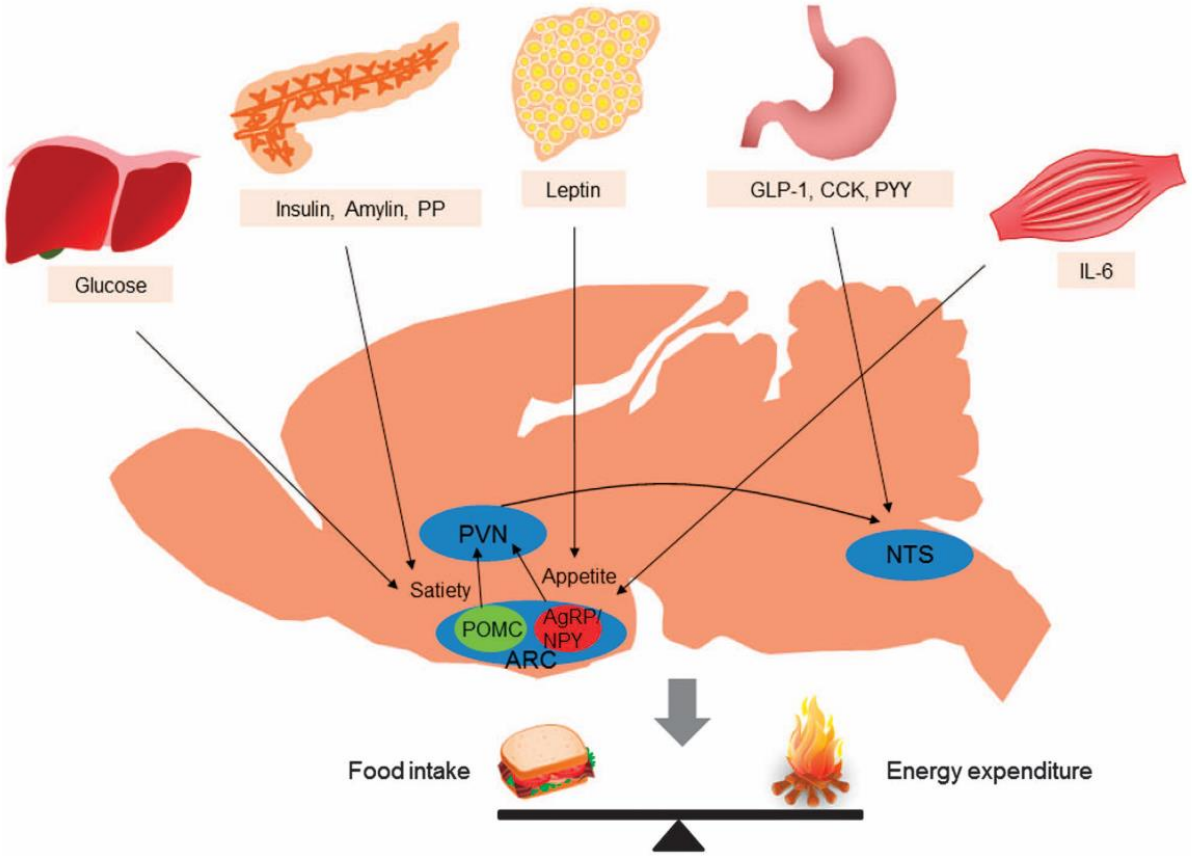

Figure I.1.: Representation of peripheral organs and brain areas involved in the homeostatic regulation of energy homeostasis.

Cues related to the nutritional state of the body reach the brain from the periphery and act mainly in the hypohtamalus and brainstem to balance energy intake and energy expenditure, modulating energy homeostasis. PP = Pancreatic polypeptide, GLP-1 = Glucagon-like peptide 1, CCK = cholecystokinin, PYY = peptide YY, IL-6 = Interleukin-6, PVN = Paraventricular nucleus, NTS Nucleus of the Solitary Tract=,

POMC = Proopiomelanocortin, AgRP = Agouti-related peptide, NPY = Neuropeptide Y, ARC = Arcuate nucleus. From (Roh et al., 2016).

Hedonic control of food intake. While the homeostatic mechanisms aim to maintain an equilibrium between energy intake and energy expenditure, they are supported by an additional system that drives food consumption: the hedonic system. Hedonic regulation of food intake can promote the consumption of

highly palatable, caloric, rewarding food even during periods of energy abundance and satiated states. Food is now considered as a reward rather than a means of survival, opening to overconsumption, weight gain, and obesity.

Two major aspects of food as a reward are here to be considered: "liking" and "wanting". Liking refers to how much palatable rewarding food is while wanting is generally associated with the motivation to obtain it (Berridge, 1996). Appropriately, the regulation of hedonic feed behaviors falls upon the dopaminergic mesolimbic system, a term that encompasses circuits within the limbic system that regulate motivated behaviors (Nestler, 2005).

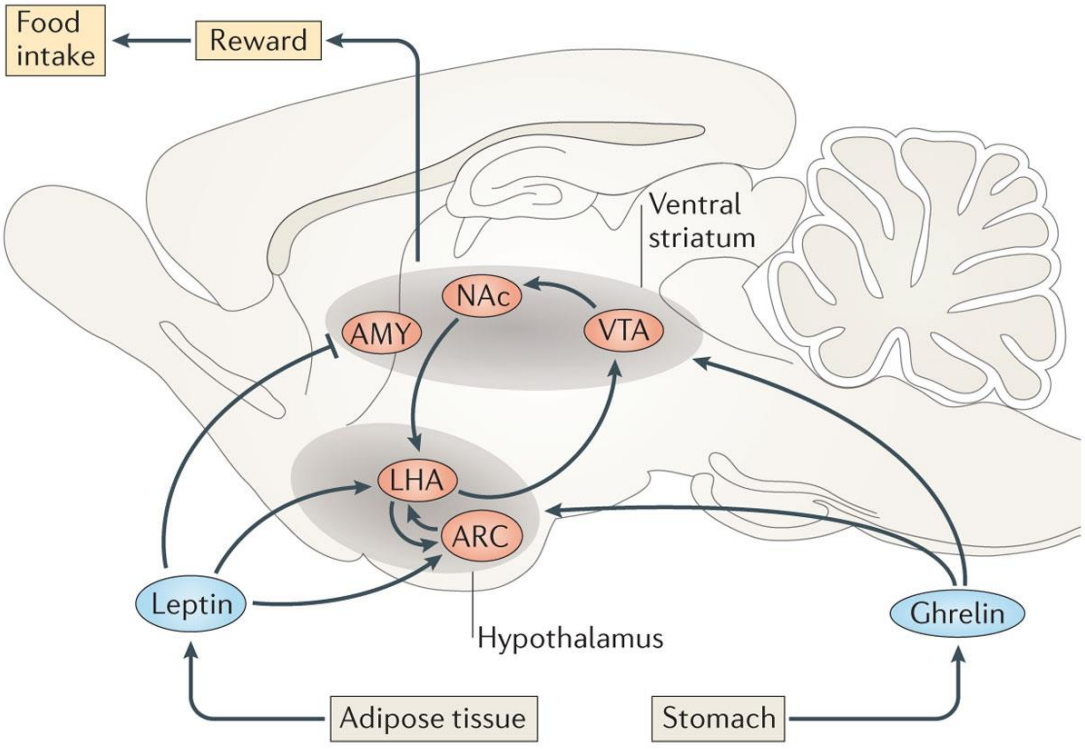

Figure I.2.: Representation of brain circuitry involved in the hedonic regulation of energy homeostasis. Homeostatic signals from the periphery such as leptin, ghrelin, GLP-1, CKK, etc., act in the brain to modulate the hedonic value of food. Here, dopaminergic neurons located in the VTA are known to project mainly to the NAc codifying the rewarding value of palatable food. Projections to and from other areas such as the hypothalamus and hindbrain (not shown) integrate homeostatic cues.
VTA = Ventral Tegmental Area, NAc = Nucleus Accumbes, AMY = Amygdala, LHA = Lateral Hypothamalic Area, ARC = Arcuate nucleus. From (G. J. Morton et al., 2014).

This system originates in the ventral tegmental area (VTA) and includes the dopaminergic projections that from here reach several regions such as the amygdala, hippocampus, prefrontal cortex, brainstem, and nucleus accumbens (NAc) (Lutter & Nestler, 2009). The connection between VTA and NAc is of particular interest, as dopamine release in this latter area are the fundaments of how our brain encodes rewarding and pleasurable stimuli, regardless of their nature (for a review on reward, addiction in the dopaminergic mesolimbic system see Nestler, 2001; Clifford B. Saper et al., 2002).

Hypothalamic and brainstem nuclei, and their role in energy homeostasis

Responsibility for the control of energy homeostasis is shared among several brain regions, with the hypothalamus and the brainstem representing perhaps the most important regions involved.

The hypothalamus is among the first and perhaps most studied areas when it comes to feeding. Already in the 1940s, surgical and chemical lesions of this area would lead to alteration of feeding behavior, from hyperphagia and obesity to complete cessation of feeding depending on which area was damaged in the process (Dietrich & Horvath, 2009). In fact, the hypothalamus is an area composed of various intercommunicating nuclei that often control and influence feeding behavior: located at the base of the third ventricle, above the median eminence where the blood-brain barrier (BBB) becomes more permeable, the arcuate nucleus is in the perfect position to come in contact with circulating peptides and hormones, detect changes in their levels, and regulate the body metabolism accordingly. This area possesses neuronal populations that express both neuropeptide Y/agouti-related peptide (neuropeptide Y (NPY)/AgRP), whose activation promotes feeding and decreases energy expenditure, and proopiomelanocortin/cocaine and amphetamine-regulated transcript (POMC/CART), whose activation decreases feeding and promotes energy expenditure, mainly via activation of the central melanocortin system (Cone, 2005). These neuronal populations make extensive connections with other hypothalamic nuclei, for example, the dorsomedial nucleus of the hypothalamus (DMH), that combines homeostatic signals coming from the arcuate with

circadian and body temperature inputs from other hypothalamic nuclei, and enacts appropriate autonomic responses to modulate thermogenesis, heart rate, blood pressure and more (Myers et al., 2016).

Both the arcuate nucleus and the DMH send projections also to the paraventricular nucleus of the hypothalamus (PVN) a nucleus in charge of feeding and autonomic functions regulation. The PVN consists of two major cell types, described as parvo (small) or magno (large) –cellular, based on the cell size. Magnocellular neurons express oxytocin and vasopressin, and through their axons reach down to the neurohypophysis to release these hormones in the bloodstream, regulating mainly fluid balance and reproductive functions. Parvocellular neurons and are important endocrine regulators, acting on the activity of the HPA axis (by secreting corticotropin-release hormone (CRH)), thyroid axis (thyrotropin-releasing hormone (TRH)), regulating body growth (somatostatin), and reproductive functions (e.g. dopamine). These peptides are released in the medial eminence and reach the adenohypophysis through the portal system, thus gaining access to the peripheral circulation (Myers et al., 2016).

The PVN has a special role in the hypothalamus. It functions as a converging site for energy-related signals from other brain regions, integrating them to generate an appropriate response mainly involving the activation of the autonomic nervous system with the ultimate goal of maintaining energy balance. Accordingly, this area shows extensive connections within the hypothalamus itself (e.g. arcuate and the DMH as described above) but also with the lateral hypothalamic area and VTA, where it participates mostly in reward and wanting.

Connections with the suprachiasmatic nucleus give the PVN access to circadian inputs, while connections to other extra-hypothalamic feeding areas and sympathetic premotor regions in the brainstem give a more thorough control of feeding and sympathetic nervous system activity. These areas include, but are not limited to, the dorsal vagal complex (that encompasses the dorsal motor nucleus of the vagus (DMX), NTS and area postrema (AP)), lateral parabrachial nucleus, and Edinger-Westphal nucleus (Geerling et al., 2010; C.B. Saper et al., 1976; Swanson, 1977; Swanson et al., 1980).

Fittingly, lesions of the PVN or disruption of its connections lead to sustained overeating and consequently obesity (Leibowitz et al., 1981; Sims & Lorden, 1986). Finally, the PVN communicates extensively also with the periphery, contacting peripheral organs and tissues involved in energy regulation such as WAT, pancreas, liver, and iBAT (Hill, 2012).

As mentioned before, the brain relies heavily on peripheral signals conveying information on the body's energy state. The brainstem and the NTS specifically is a fundamental component for the processing of such signals receiving information both from the arcuate nucleus and the PVN (Blevins & Baskin, 2010) but as well from the periphery. The NTS is reached by projections coming directly from the gustatory receptors (Bradley & Grabauskas, 1998) at its rostral level, from here relayed to the forebrain for taste recognition, while its caudal level is reached prominently by vagal nerve afferents that carry information related to food intake coming from the gastrointestinal tract (e.g. gastric distension). Neurons in the NTS are also exposed to circulating endocrine signals (e.g. leptin, insulin) and nutrients (e.g. glucose, lipids) as the BBB is more permeable at the level of the AP, thus allowing the NTS to be constantly informed about the nutritional status of the body and modulate food intake accordingly (G. Morton & Schwartz, 2006). The NTS contains a diverse variety of neuronal population involved in energy homeostasis, namely POMC, GLP-1, and catecholaminergic neurons (Rui, 2013) all of which are activated by vagal afferent glutamatergic inputs in response to food intake (Appleyard et al., 2005, 2007; Hisadome et al., 2011). In addition to its role in the regulation of homeostatic food intake, GLP-1 neurons in the NTS send direct projections to both the VTA and the NAc suggesting that the NTS might participate also in the regulation of hedonic food intake. Accordingly, agonism of the GLP-1 receptors in these areas VTA or NAc decreases food intake, body weight, and the rewarding value of food (Alhadeff et al., 2012; Dickson et al., 2012).

Nesfatin-1

Expression, release, and mechanisms of action

Nesfatin-1 is the N-terminal fragment of NEFA/nucleobindin2 (*Nucb2*), a peroxisome proliferator γ receptor (PPARG)-activated gene whose product, NUCB2, was first described as a protein of unknown function (Miura et al., 1992). Rediscovered in 2006 as a potent anorexigenic peptide involved in homeostatic feeding (Oh-I et al., 2006), NUCB2/nesfatin-1 (as common antibodies used for research are generally unable to distinguish between NUCB2 and the derivative fragment nesfatin-1) has been since described to regulate a variety of physiological functions that span from the regulation of energy homeostasis as a whole to cardiovascular and reproductive functions, to stress, and more (see Dore, Levata, Lehnert, et al., 2017 for an extensive review).

NUCB2 is a 396 amino acids long peptide (the original product from the *Nucb2* gene consist of NUCB2 and a 24 amino acids long signal peptide, for a total of 420 amino acids) presenting cleaving sites for the enzyme protein convertases 1/3 and protein convertase 2. The presence of these sites suggests further processing in three sub-fragments, called nesfatin-1 (amino acids 1 to 82), nesfatin-2 (amino acids 85 to 163), and nesfatin-3 (amino acids 166 to 396). Notably, only nesfatin-1 is anorexigenic, and the function of nesfatin-2/3 is still unclear to date (Oh-I et al., 2006). It should however be noted that while the presence of nesfatin-1 has been detected in rat cerebrospinal fluid (Oh-I et al., 2006) and thus proved *in vivo*, the cleaving from its parent peptide NUCB2 has yet to be shown *in vitro* or *in vivo*. Chinese hamster ovary (CHO) cells overexpressing Nucb2 and protein convertase 1/3 and 2 failed to produce the various NUCB2 fragments (Oh-I S, 2013), suggesting that NUBC2 processing might happen under enzymes that cleave similar sequences like the cell surface membrane-bound protein furin (Seidah & Prat, 2002).

The *Nucb2* mRNA expression in the brain is prominent in areas that participate in feeding, especially in the hypothalamus (and here in the paraventricular, arcuate, and supraoptic nucleus) and in the brainstem (notably in the medio-caudal NTS); *Nucb2* mRNA expression is also found in reward-related brain regions

like the ventral and dorsal striatum, lateral hypothalamus, dorsal and dorsolateral tegmental nucleus (Brailoiu et al., 2007; Goebel-Stengel et al., 2011).

In the brain (at least in the PVN) nesfatin-1 is thought to be released in an autocrine or paracrine fashion since on a cellular level it appears to be stored mainly in vesicles surrounding the Golgi apparatus while being absent from axon terminals (Maejima et al., 2009). Once out of the cell, nesfatin-1 general mechanism of action is to alter calcium (Ca^{2+}) influx of the target cell, either via L- (Brailoiu et al., 2007; Ishida et al., 2012; Nakata et al., 2011) P/Q (Brailoiu et al., 2007, 2013) or N- (Iwasaki et al., 2009) Ca^{2+} channels, causing either hyperpolarization or depolarization (Brailoiu et al., 2007, 2013; Ozcan et al., 2016) depending on the area considered.

But considerably less is known about *how* nesfatin-1 can exert its effects: a dedicated receptor has not been discovered yet, and while nesfatin-1 has been proposed – but not proven – very early after its rediscovery to interact in the brain with G-protein coupled receptors (Brailoiu et al., 2007) little to no progress on that front has been made since: nesfatin-1 remains an orphan neuropeptide.

But despite being rediscovered and characterized as anorexigenic peptide acting in the brain, NUCB2/nesfatin-1 is mainly produced in the periphery: its major source is, in fact, the gastric mucosa, expressing roughly 10-times the levels of NUCB2/nesfatin-1 that are found in the hypothalamus (Stengel, Goebel, Yakubov, Wang, Witcher, Coskun, Taché, et al., 2009). Other peripheral sites for NUCB2/nesfatin-1 production are white adipose tissue, (WAT) pancreatic beta cells, and, to a lesser extent, testes (Kylie S. Foo et al., 2010; Gonzalez et al., 2009; Ramanjaneya et al., 2010). Finally, peripheral nesfatin-1 can cross the BBB in both directions by non-saturable transmembrane diffusion, opening to the possibility that nesfatin-1 might access the CNS from the periphery to exert its functions (Pan et al., 2007; T. O. Price et al., 2007).

Effects on feeding and thermogenesis

Homeostatic feeding. NUCB2/nesfatin-1 is a potent anorexigenic peptide, and it has been shown to reduce food intake and body weight during the dark phase as well as the light phase, and after both central

and peripheral administration (K. Könczöl et al., 2012; Maejima et al., 2009; Oh-I et al., 2006; Shimizu et al., 2009; Wernecke et al., 2014; Gina L C Yosten & Samson, 2010). The connection/interaction between NUCB2/nesfatin-1 and energy metabolism is reciprocal: both *Nucb2* mRNA expression and NUCB2/nesfatin-1 protein level are reduced by fasting or states of negative energy balance and raised following a meal on in states of positive energy balance, in CNS (García-Galiano et al., 2010; Kohno et al., 2008; Oh-I et al., 2006), plasma (Stengel et al., 2009), and adipose tissue alike (Ramanjaneya et al., 2010). The mechanisms by which nesfatin-1 regulates food intake are not clear to date, but the melanocortin and the oxytocinergic system are the most studied and proposed mediators for its effects. The melanocortin system is perhaps the most relevant partner system, as blockade of the central melanocortin receptors 3/4 has been shown to reduce or abolish multiple nesfatin-1 effects, from feeding (Oh-I et al., 2006), to anxiety and stress response as well as cardiovascular effects (G. L. C. Yosten & Samson, 2009) and iBAT thermogenesis (Dore, Levata, Gachkar, et al., 2017).

Oxytocin and nesfatin-1 co-localize in both the PVN and the SON, and nesfatin-1 seem to alter the excitability of oxytocinergic neurons in the PVN (C. J. Price et al., 2008). Similarly to what was described for the melanocortin receptors, also blockade of the central oxytocinergic receptors reduces the anorexigenic and hypertensive effects of nesfatin-1 (Maejima et al., 2009; Gina L C Yosten & Samson, 2010).

Notably, nesfatin-1 is capable of causing anorexia even in Zucker rats (Oh-I et al., 2006) and animals that have developed obesity after being fed a high-fat diet (Prinz et al., 2015; Shimizu et al., 2009), settings where the leptin-mediated regulation of food intake fails to work. Rather, leptin itself might depend on nesfatin-1 to reduce food intake: leptin administration increases *Nucb2* mRNA expression in the PVN, and NUCB2-knockdown in this very area abolishes the anorexigenic effect of leptin (Shimizu et al., 2009).

Hedonic feeding. Nesfatin-1 is involved also in the regulation of the hedonic aspect of feeding, albeit its role here is far less characterized. NUCB2/nesfatin-1 is expressed in various reward-related areas such as the VTA, NAc, lateral hypothalamus, and tegmental nuclei (Goebel-Stengel et al., 2011), and has been reported to alter the excitability of neurons in the VTA and *substantia nigra* (Dore et al., 2020; Ilango et

al., 2014; C. Li et al., 2014), the latter also involved in reward-related behaviors. Direct injections of nesfatin-1 in the VTA are anorexigenic (X. Chen et al., 2015), and i.c.v. administration of nesfatin-1 has recently been shown to reach the VTA hyperpolarizing its dopaminergic neurons via outward potassium current and causing a reduction in the rewarding value of sucrose (Dore et al., 2020).

Thermogenesis. Besides being an anorexigenic peptide, nesfatin-1 is a promoter of energy expenditure as well. Central nesfatin-1 increases energy expenditure by increasing core body temperature and thermogenesis (K. Könczöl et al., 2012; Wernecke et al., 2014). This increase has been shown to depend on an increased sympathetic nervous system (Levata et al., 2019) and consequently iBAT activation (Dore et al., 2017). It is abolished by blockade of the central melanocortin system (Dore et al., 2017).

Research aims

Overall, nesfatin-1 is a promising target for the development of treatments against obesity and related pathologies. Obesity has more than tripled in the last decades and it is steadily increasing to date, making it one of the most significant and urgent world problems from both a health and economic standpoint. The discovery of leptin and its potent anorexigenic effect generated much enthusiasm for the development of therapeutic agents to counteract obesity. Alas, such enthusiasm rapidly collapsed with the discovery of leptin resistance in obese individuals (Friedman, 2004), leaving a void to be filled with more effective treatments.

Like leptin, nesfatin-1 is emerging as an important modulator of energy homeostasis, with a potent anorexigenic and thermogenic effect. Unlike leptin, however, no phenomena of resistance have been described to date for nesfatin-1 thus making it a very promising therapeutic target even in settings where leptin fails to be effective. The biggest obstacle behind the employment of nesfatin-1 as a therapeutic agent lays in its receptor, which eludes researchers to date hampering the development of synthetic receptor agonists, as well as a yet incomplete understanding of the mechanisms of action of nesfatin-1 and the areas involved.

Overall, this study aimed at investigating the physiological effects of nesfatin-1 on both energy intake and energy expenditure. Special attention was given to the PVN and NTS as we hypothesized a pivotal role for both areas in mediating the anorexigenic and energy expenditure effects of nesfatin-1.

In brief, we first characterized the effects of exogenous nesfatin-1 after i.c.v. or intra-PVN administration. Animals fed *ad libitum* or food-deprived for 24 hours were compared after i.c.v. administration of nesfatin-1 to investigate if feeding state would affect response to nesfatin-1. Intra-PVN nesfatin-1 injections were then employed to determine the effects of nesfatin-1 on food intake, energy expenditure, and iBAT thermogenesis.

Subsequently, we shifted towards investigating putative downstream effectors for nesfatin-1, by focusing on the pharmacological manipulation of the ERK1/2 system first, and on the knockdown of the melanocortin receptor 4 (MCR4) in the NTS second in two separate experiments. Both systems are established players in the regulation of energy homeostasis, and their interaction with nesfatin-1 has been hinted at by various studies. We hypothesized that nesfatin-1 would recruit the ERK1/2 system in the PVN to acutely reduce food intake and promote energy expenditure. We also hypothesized that the neurons in the PVN would communicate with MCR4-expressing neurons in the NTS when stimulated with nesfatin-1. Knockdown of said receptors would then weaken the effects of intra-PVN nesfatin-1.

Lastly, we hypothesized that nesfatin-1 would regulate hedonic and homeostatic food behavior in the NTS by interacting with the GLP-1-ergic system. The NTS is an established regulator of homeostatic food intake and has rapidly gained importance also as a hedonic regulator thanks to the effects of GLP-1 agonists in this area (Karolina P. Skibicka, 2013). Nesfatin-1 is also an important regulator of hedonic behavior (Dore et al., 2020) and its interaction with GLP-1 in the regulation of homeostatic food intake has been suggested previously (Saito et al., 2016).

Materials and Methods

General methods: Animals

For *in vivo* studies conducted in Germany, male Wistar (Charles River Laboratories, Sulzfeld, Germany) weighing 225-275g at arrival were group-housed in individually ventilated cages (Double-decker, Tecniplast, Varese, Italy) in a 12-h/12-h light/dark cycle (lights on at 5:00 h) temperature-controlled (21˚C) vivarium at the CBBM (Center of Brain, Behavior, and Metabolism, Lübeck, Germany). Animals had *ad libitum* access to regular chow (Altromin 1324, Altromin, Lage, Germany) and water unless otherwise reported. Animals were single-housed in individually ventilated cages after surgery. All animal experiments and their care were performed in accordance with the German law and approved by the committee on animal care of Schleswig-Holstein, Germany (licenses 4(77-6/17), 4(27-4/18), 4(46-4/19)).

For *in vivo* studies conducted in Sweden, male and female Sprague Dawley rats (180-300g at surgery, Charles River Laboratories, Sulzfeld, Germany) were single-housed in individual wire-topped cages in a 12-hour light/dark cycle (lights on at 7:00 h) temperature-controlled (21 ˚C) vivarium at the EBM (Laboratory for Experimental Biomedicine, Gothenburg, Sweden) with *ad libitum* access to regular chow rodent (Envigo 2016 Teklad global, 16% protein) and water, unless otherwise reported. All studies were carried out with ethical permissions (license 137/15) from the Animal Welfare Committee of the University of Gothenburg, in accordance with the legal requirements of the European Community (Decree 86/609/EEC). All efforts were made to minimize suffering.

General methods: Stereotactic surgery

Animals were given a minimum of three days to adapt to the new housing condition before any procedure could be carried and get accustomed to light hand restraint.

To investigate the effects of treatments on the central nervous system or within a specific brain area, guide cannulas were implanted in the site of interest via stereotaxic surgery. All surgical procedures were

performed as previously described (Dore et al., 2013). Rats were anesthetized with a mix of Ketamine (80 mg/kg) and Xylazine (6 mg/kg) administered with an intraperitoneal (i.p.) injection and fixed in a stereotaxic frame (Kopf Instruments, Tujunga, US) after verifying the absence of reflexes upon pinch of the distal portion of the tail and the toes on the hind legs; the depth of anesthetized state was frequently checked through the responsiveness to the reflexes as stated above. During the whole surgical procedure, body temperature regulation was maintained by a heating pad.

Once the head was fixed in position its skin was first shaved, cut open with a scalpel, and finally kept spread via bulldog clamps to expose the skull underneath. The skull was then cleaned with a scraper to remove the periosteum and reveal the bregma.

After reaching the implantation site (using the coordinates provided in Table M.1 and before implanting the cannula, up to six holes in the skull were primed with the aid of a manual drill, and a corresponding number of jewelry screws was implanted to aid stability of the whole intracranial implant. Lastly, a hole above the area of interest was drilled with the aid of an electric drill to allow the insertion of the guide cannula. Thereafter, a 24-gauge stainless steel guide cannula (Plastics One, Roanoke, US) was implanted either unilaterally (lateral ventricle (i.c.v.), intra-PVN) or bilaterally (intra-NTS) following the coordinates obtained from Paxinos and Watson's rat brain atlas (Paxinos & Watson, 2007). For each area of interest, the coordinates are presented with respect to bregma and the incisor bar set at - 3.3 mm below the interaural line.

After cannula implantation, a solution of dental cement (Paladur®, self-curing methyl-methacrylate copolymer and liquid methyl-methacrylate with 2(2H-Benzoltriazol-2-yl)-4-methyl phenol) was applied to the skull to fully submerge both the base of the guide cannula and the jewelry screws and let it cure fully to grant stability to the implant. Finally, the guide cannula was closed with an obturator to keep it patent. Carprofen was administered twice daily for 3 days post-surgery (5 mg/kg at an application volume of 1

µL/g body weight). Animals were granted at least one week to recover from the procedure, during which health, body weight, food, and water intake were strictly monitored.

General methods: Viral Knockdown of NTS-MC4Rs

Animals were assigned to either a nucleus of the solitary tract (NTS) melanocortin receptor type 4 (MC4R) knockdown group or a control scramble group by matching body weight, food intake, fat, and lean mass pre-surgery. After reaching a bodyweight of at least 270 g, animals were anesthetized via i.p. injection, fixed to a stereotaxic frame and the skull was exposed as described above. After reaching the NTS coordinates given in Table M.1, a hole was drilled in the skull to allow the insertion of a glass capillary used to deliver the viral solution. Thereafter, 1 µL of the viral solution (an AAV carrying an shRNA sequence against the MC4R or a scramble shRNA sequence used as a control solution) was applied via a glass capillary mounted on an electrode holder within 1 minute. Subsequently, the capillary was left in place for a total of 10 minutes to allow the viral solution to diffuse and avoid backflow when removing the capillary before proceeding to the other hemisphere for a bilateral injection. The same procedure was followed for the contralateral NTS.

General methods: Microinfusion procedures

The microinjection apparatus consisted of an injector for intracranial applications (Plastics One, Roanoke, US) connected to a plastic tube. The tube was then filled with injectable water (Ampuwa®, Fresenius Kabi Deutschland GmbH, Bad Homburg vor der Höhe, Germany) to allow greater accuracy of the volume injected by avoiding air compression. The tube was then connected to a 10 or 5 µL Hamilton syringe (Hamilton Bonaduz AG, Switzerland). Finally, a 1 µL air bubble was loaded in the tube to allow separation between the injectable water and the drug solution.

For the injections, the animals were taken out of the home cage and left freely moving on the operator's lap. The obturator was then removed from the guide cannula and the injector of the appropriate protrusion was inserted into the guide cannula reaching the area of interest. Treatments were administered at a rate of

2 µL/minute after which the injector was kept in place for an additional minute to allow diffusion and prevent the backflow of the drug upon the removal of the injector.

General methods: Body composition

Body composition in fat tissue, lean mass, and free fluid was measured via nuclear magnetic resonance (Minispec LF110, Bruker Biospin GmbH, Rheinstetten, Germany). Before each measurement, the instrument was calibrated as per company instruction with a daily check sample that consisted of a glass tube containing rape seeds.

After completing the calibration, animals were weighed, inserted in a plastic restrainer, and immediately placed inside the Minispec for analysis. After ~ 2 minutes, animals were removed from the restrainer and placed back in their home cage. Results were analyzed and quantified via Measure minispec Plus NF and Opus 7.0 software, and exported into Microsoft Excel for further analysis.

General methods: Sacrifice and tissue collection

For *in vivo* studies conducted in Germany, on the day of the sacrifice, animals received a final injection before sacrifice according to the experimental protocol. Animals were then rapidly killed by decapitation and the brains quickly removed and frozen in dry ice before being stored at - 80 °C. Blood samples, inguinal white adipose tissue (iWAT), epididymal WAT (eWAT), and iBAT were collected and quickly frozen on dry ice before being stored at - 80 °C. To verify cannula placement, 1 µL of 1% bromphenol-blue was injected into the brain immediately before killing (Figure A.4).

For *in vivo* studies conducted in Sweden, on the day of the sacrifice animals received a final injection of Exenidin-4 (Ex4) or aCSF two hours before sacrifice. Animals were briefly exposed to a light (4%) isoflurane (Baxter AB, Sweden) anesthesia and rapidly killed by decapitation. The brains were quickly removed and the NTS isolated using punches. Blood samples, NTS punches and the rest of the brain were then frozen in dry ice along before being stored at - 80 °C.

General methods: NTS and hypothalamic preparations

For RNA extraction and NTS gene expression, the hindbrain was moved to a cryostat adjusted to - 16 °C and cut with a razor blade at the end of the trapezoid body and at the end of the hindbrain to provide a brain slice containing the NTS. From this slide, the NTS was then extracted by a dorsal cut in the middle of the fourth ventricle, lateral cuts before the spinal tegmental tract, and ventrally cutting off 1/3 of the leftover.

For RNA extraction and whole hypothalamic gene expression, the brain was moved to a cryostat adjusted to - 16°C, and coronal cuts were made with a razor blade at the level of the optic chiasm and just posterior of the mamillary nucleus. The hypothalamic slice was turned on its posterior surface and cut laterally directly before the amygdala and dorsally just underneath the anterior commissure.

General methods: Cryostat brain sections

Brains were cut using a cryostat (Leica CM 305, Leica Biosystems Nussloch GmbH, Nussloch, Germany). Brains were transferred from a - 80 °C freezer to a - 20 °C freezer at least 3 hours prior cutting, and then to the cryostat set at a temperature of - 20±1 °C. To allow the cutting of both the PVN and the NTS, brains were divided at the very beginning of the cerebellum with a razor blade and mounted on a tissue holder via Tissue-Tek O.C.T™ (Sakura Fintek Europe, Alphen aan den Rijn, Netherlands) with the medulla or the hypothalamus facing the operator.

For the PVN, 40 µm thick brain slices containing the whole PVN region were collected, starting approximately from - 1.80 until - 2.30 from bregma according to Paxinos and Watson's rat brain atlas (Paxinos & Watson, 2007) on Superfrost™Plus slides (Gerhard Menzel B.V. & Co. KG, Braunschweig, Germany) for verification of the cannula placement via fluorescence microscopy.

For the NTS, 40 µm thick brain slices containing the most caudal and medial NTS region were collected, starting approximately from - 13.30 until - 12.00 from bregma according to Paxinos and Watson's rat brain atlas (Paxinos & Watson, 2007). Polyethylene-naphthalate (PEN) membrane slides (MembraneSlide,

1.0 mm, Carl Zeiss Microscopy GmbH, Göttingen, Germany) were used for laser capture microdissection (LCM) and every 4th slice was collected on Superfrost™Plus slides (Gerhard Menzel B.V. & Co. KG, Braunschweig, Germany) for verification of the injection placement via fluorescence microscopy.

General methods: Laser capture microdissection (LCM)

The LCM was performed to achieve area-specific resolution for mRNA expression analysis. After identification of the PVN or the NTS via specific landmarks (hippocampus, optic chiasm, and fornix for the PVN; pyramidal tracts, olive complex, and hypoglossal nuclei for the NTS) a template was designed around the region of interest with the software Robo 4.8 Pro and used for dissection with the PALM Micro Beam. For each region, 5 slices were cut and collected with forceps, and immediately transferred to a 0.2 mL tube along with 100 µL of lysis buffer containing 0.7 % β-mercaptoethanol. The tube was then frozen at - 80 ˚C.

General methods: RNA extraction – Nano preparation

When collected at the LCM, brain tissues were processed via Absolutely RNA Nanoprep Kit (Agilent Technologies, Texas, USA) according to the manufacturer's instructions: after thawing at room temperature, lysates were mixed in with 100 µL of sulfolane and mixed for 5 seconds before being transferred to an RNA-binding nano-spin cup (samples, from here on). After being centrifuged for 60 seconds, the flow-through was discarded. In the next step, after adding 300 µL 1x of low-salt wash buffer the samples were centrifuged again for 60 seconds, the flow-through was discarded and then the samples were centrifuged for 2 more minutes. Next, the samples were incubated for 15 minutes at 37 ˚C after upon adding a Deoxyribonuclease (DNase) solution consisting of 2.5 µL DNase in 12.5 µL DNase digestion buffer; then, after adding 300 µL 1x of low-salt wash buffer the samples were centrifuged for 60 seconds and the flow-through discarded. After adding 300 µL 1x of low-salt wash buffer, centrifuging and discarding the flow-through two more times, the spin cup was centrifuged again for 3 minutes and transferred to a new 2 mL collection tube. Finally, 11 µL nuclease-free water was added onto the fiber

matrix and incubated for 2 minutes at room temperature. The spin cup was centrifuged for 5 minutes, and the filtrate was stored on ice for reverse transcription. All the centrifugation steps were performed at room temperature at 12000 × g.

General methods: RNA extraction – Mini preparation

The RNA from iBAT, eWAT, and brain areas not collected via LCM were extracted using the NucleoSpin® RNA Kit (Macherey-Nagel GmbH & Co. KG, Düren, Germany). After homogenizing the samples using a disperser, 150 µL of homogenate were added and mixed with RA1 buffer (850 µL for iBAT and i/eWAT, 500 µL for NTS). The lysates were frozen at - 20 °C overnight. After thawing, 500 µL of lysates were mixed thoroughly for 1 minute with 500 µL of chloroform, and centrifuged for 1 minute. The supernatant (350 µL for iBAT and i/eWAT, 300 µL for the NTS) was then transferred to the NucleoSpin® filter in a 2 mL collection tube, centrifuged for 1 minute and the filter discarded. Next, 350 µL 70% ethanol was then added to the filtrate, mixed and transferred to a NucleoSpin® RNA Column, and centrifuged for 30 seconds. After that, 350 µL of membrane desalting buffer was added to the column, centrifuged for 1 minute and the flow-through was discarded. A DNase reaction mixture consisting of 95 µL reaction buffer for rDNase with 10% reconstituted rDNase was directly added to the membrane and incubated for 15 minutes at room temperature. Subsequently, 200 µL of RAW2 was added to the column, centrifuged for 30 seconds and the flow-through discarded. Next, 600 µL of RAW3 was added to the column, centrifuged for 30 seconds, and the flow-through discarded. Lastly, 250 µL of RAW3 was added to the column, centrifuged for 2 minutes, and the flow-through discarded. The column was transferred to a 1.5 mL collection tube, where 50 µL of RNase-free water was added and centrifuged for 1 minute. RNA was stored at - 80 °C. All the centrifugation steps were performed at room temperature at 11000 × g.

General methods: RNA-detection with NanoDrop

RNA concentration in the samples was using a spectrophotometer (NanDrop 2000, Thermo Fisher Scientific Inc., Carlsbad, CA, USA), which reads light absorption at 260 nm, the characteristic wavelength

of maximum absorption of nucleic acids. DNA contamination could be excluded as a result of previous DNase treatment of the columns during extraction RNase free water was used as a blank control, and 1 µL RNA sample measured supported by the software NanoDrop 2000, Version 1.4.0.1 that also calculates the RNA concentration.

General methods: Reverse transcription

The extracted RNA was then transcribed to complementary DNA (cDNA) for the next steps. The Reverse Transcription System A3500 kit (Promega Corporation, Madison, WI, USA), containing the avian myeloblastosis virus (AMV) reverse transcriptase (RT), and RNA dependent DNA polymerase possessing an intrinsic RNase H activity was used. Here, 10 µL of RNA (total volume of NanoPrep samples, 0.4 µg for i/eWAT and iBAT samples) was transferred to a 0.2 mL reaction tube and heated at 70 °C in the thermocycler (Thermocycler, PCR Express Thermo Hybaid, USA) to denature the RNA and allow for the annealing of primers over the entire RNA for a complete reverse transcription. In the meantime, the master mix solution was prepared. It contained $MgCl_2$ as a cofactor for the AMV-RT, reverse transcription buffer for optimal function and stabilization, RNasin for RNase inhibition, and deoxyribonucleotide triphosphates (dNTPs) for the supply of educts. The reaction steps are shown again in Table M.5. The cDNA was stored at - 20 °C.

General methods: Quantitative real-time PCR (qRT-PCR)

Quantitative real time-PCR was used for amplification of the cDNA. Primers of 18 - 25 base pair-long oligonucleotides are used, targeting the gene segment of interest with a forward primer binding to the complementary strand, and a reverse primer binding to the leading strand. The DNA needs to be denatured at high temperatures so the primers can anneal. Subsequently, the DNA-polymerase elongates the DNA strand starting from the primers in the 3' → 5' direction by annealing complementary nucleotides to the strand. After a threefold execution of the whole cycle, the DNA segment of interest is derived for the first time.

Here, the qPCR was used for gene expression analysis. The even amplification of the PCR product in the exponential phase is quantitatively measured in proportion to a fluorescence signal. The SYBR® Green I dye intercalates in the double-stranded DNA and forms a complex capable of emitting green light at a wavelength of 521 nm. For the quantification, a standard curve yielding a known copy number of the measured gene was run with the samples. For the reaction, 1.6 µL of cDNA was used. The reaction mix is shown in Table M.3, and a list of primers can be found in Table M.8. The detection and analysis were performed using the 7000 System SDS Software (Version 1.2.3, Applied Biosystems, MA, USA). The qPCR cycles are shown in Table M.5 First, the samples were heated to 50 °C to activate the uracil-DNA-glycosylase (UDG) which removes possible contaminations of previous amplifications. The master mix contains deoxyuridine-triphosphates (dUTPs) which are built into the PCR-products. In case of contamination by previous PCR reactions, UDG recognizes dUTPs in nucleotide strands and degrades these. In the following step, the UDG is denatured at 90 °C to not degrade the newly synthesized PCR products; at the same time, this step denatures the cDNA as well, making it possible for the primers to anneal. At 60 °C, the DNA polymerase is elongating the gene of interest flanked by the primers. Afterward, a dissociation step is added yielding a dissociation curve and allowing a purity check: if the melting temperatures are identical with the known ones for the primers, no dimers or contaminations are present.

Experiment I: effect of feeding state on nesfatin-1 induced increase in energy expenditure in the light phase

Stereotactic surgery

Animals were given a minimum of 3 days to adapt to the new housing condition and get accustomed to light hand restraint before any procedure could be carried. In this experiment, a single cannula was implanted in the lateral ventricle (Table M.1) via stereotactic surgery, as described in the general methods section. After a full recovery, cannula placement was confirmed by a positive dipsogenic response to an i.c.v.

injection of angiotensin II (15 ng/5 µL; Sigma Aldrich, Saint Louis, MO, US). All the animals showed an intake of ≥ 15 ml of water within 15 minutes.

Direct calorimetry

Direct calorimetry was performed to determine dry heat loss (DHL) as a measure for thermogenesis in animals fed *ad libitum* or food-deprived for 24 hours, during the animal's light phase. Animals were assigned to the experimental groups after matching their body weight and food intake. After a brief period of habituation to the procedure room (~ 30 minutes) the animals were weighed, injected as described (see general methods: microinfusion procedures), and introduced inside the calorimetry system for 8 hours (from 09:00 to 17:00) where they were left undisturbed for the whole session. The animals were weighed again at the end of the session and returned to their home cages for a washout period of at least 5 days.

The in-house built calorimetric system device ((Wernecke et al., 2014) based on (Wesolowski et al., 1985)) consists of a modified commercial cooling-box equipped with a Peltier element that functions as a heat sensor and generates an electric voltage (via the Seebeck effect) proportional to the heat difference at its two sides. A Voltcraft 820 multimeter (Conrad Electronic SE, Hirschberg, Germany) records the voltage in 1-minute intervals from the Peltier elements and sends them to a desktop computer for recording (via software, VC820/840 Interface Program Ver.1.00) and storage. To account for the effect of different body weight between animals on energy expenditure (Kaiyala & Schwartz, 2011), DHL data were adjusted to the three-fourth power of body weight according to Kleiber's law (Kleiber, 1947). Hourly or 8 hours averages were considered in the final analysis. The inner part of the calorimeter contains an aluminum box that accommodates the rat during the experiment. To prevent heat transfer through conduction, the aluminum box is separated from the inner walls of the calorimeter via polypropylene spacers. Finally, airflow in the system is granted via a vacuum pump (Schego® Schemel & Goetz GmbH, Offenbach am Main, Germany) calibrated via a flowmeter (TSI4140 Flowmeter Driesen + Kern GmbH, Bad Bramstedt, Germany) to aspirate air at a rate of 200 mL/min. The pump is connected to the calorimeter via a polyvinyl chloride (PVC) tube that sits next to a 5 × 125 mm (height × width) slit close to the bottom of the aluminum

box that allows CO_2 rich air to be aspirated; fresh new air enters passively through several holes in the upper part of the walls and the lid of the calorimeter system.

A four-point calibration was performed before each batch of sessions for each calorimeter box using a 1.5 kΩ electric resistor and a Bio-Rad (Munich, Germany) PowerPac Basic power supply unit for calibration. Briefly, the resistor was inserted into the aluminum box and connected to the power supply unit via terminal blocks. After closing the lid of the calorimetry box, the recording software was started and a voltage (in order: 15, 30, 75, and 90 V) applied by the power supply. The corresponding voltage generated by the Peltier element was subsequently recorded every 10 minutes and recorded as a point for the calibration only if stable for at least 30 minutes, after which the next step of voltage was applied and the procedure repeated until four points were collected. All calibration and measurements were done at a constant room temperature of 22±1 °C.

Experiment II: effect of intra-PVN nesfatin-1 administration on energy homeostasis

Experiment IIa: Food intake measurements

Food intake was monitored in *ad libitum* fed animals, during their dark phase. Animals were left undisturbed in the experimental room with unlimited access to food and water. Food, but not water was removed two hours before the onset of the dark phase to avoid possible individual meals before the injection. Following a unilateral intracranial injection aimed at the PVN (see general methods: microinfusion procedures) at the onset of the dark phase, animals were moved back to their home cage and the food was returned. Food intake and body weight were then measured after 1, 3, and 6 hours post-injection. At the end of the session, the animals were left undisturbed for a washout period of at least 5 days.

Experiment IIb: Direct calorimetry

Based on the results from Experiment I, direct calorimetry was performed to determine dry heat loss (DHL) as a measure for thermogenesis as previously described only in animals fed *ad libitum*, during the animal's light phase.

Experiment IIc: Infrared thermography

As a way of measuring heat production, dissipation and a surrogate for core body temperature, thermal imaging of interscapular brown adipose tissue (iBAT), tail, and ear canal (see also: region of interest) respectively was taken using an infrared camera (FLIR® A65, FLIR® Systems, Inc., Wilsonville, OH, USA) during the animal's light phase. Starting one week before the experiment, animals were shaved every 3 days on their back to expose the skin above the iBAT and habituated daily to the experimental procedure. Briefly, animals were taken to the experimental room with unlimited access to water but not food and left undisturbed for at least 2 hours before any procedure. After the first set of measurements (i.e. three pictures of each region of interest) in which the animals were handled for iBAT, ear canal, and tail imaging, a "mock"-injection was performed as described (see general methods: microinfusion procedures) using an injector that did not protrude from the implanted cannula inside the brain parenchyma, and without substance application. Subsequently, animals were returned to their home cage and another set of handling and measurements was performed at least one hour later. Animals were handled and were imaged at least thrice before returning to the vivarium. Finally, animals were then matched per body weight, food intake, and basal iBAT temperature during the habituation training.

On the day of the experiment, after the habituation period animals were gently taken from their home cage taking great care to not startle them to avoid any stress-related thermogenesis. After quickly placing them under the camera, a set of measurements for each region of interest was taken and a unilateral intracranial injection aimed at the PVN of nesfatin-1 or PBS (as a control solution) was performed as described (see general methods: microinfusion procedures) before returning the animals to their home cage, undisturbed until the next set of measurements. Animals were imaged every 15 minutes, for 90 minutes total. At the end of the experiment, food was returned and the animals were left undisturbed for a washout period of at least 5 days. Each measurement was taken over a ~ 30 second period to minimize handling-related stress, and a set of three images per region of interest was taken each time.

Images were scored via FLIR QuickReport 1.2 software (FLIR® Systems, Inc., Wilsonville, OH, USA), and the highest average temperature value of each set of images in a given measurement was considered for each region of interest for the final analysis.

Sacrifice, tissue collections, and gene expression analysis

Animals from experiment IIa/b were sacrificed as described (see general methods: Sacrifice and tissue collection) 35 minutes after receiving a final injection of either nesfatin-1 or PBS. After the final injection, the animals were returned to their home cage with free access to water but not food. Animals from experiment IIc were sacrificed as described (see general methods: Sacrifice and tissue collection) four hours after receiving a final injection of either nesfatin-1 or PBS. After the final injections, the animals were returned to their home cage with free access to water but not food and monitored every hour via infrared thermography for iBAT activation.

Corticosterone radio immunoassay

Circulating levels of corticosterone (CTS) at 35 minutes following an intra-PVN injection of nesfatin-1 were assayed in duplicate using a commercial ^{125}I radioimmunoassay (RIA) kit for CTS (#07-120102, ImmuChem™ Double antibody, MP Biomedicals, Orangeburg, NY, USA). The assay was performed as per manufacturer instruction, with a few exceptions. First, the samples were diluted at 1:400 instead of the recommended 1:200 dilution; second, the volume of all reagents and samples was scaled down by a factor of four (e.g. if the protocol calls for the addition of 0.2 mL of reagents 0.05 mL were added instead) to reduce the total used volume and allow the entire assay to take place in standard 1.5 mL tubes, that could be accommodated in a gamma counter for the final step of the assay. Lastly, samples were centrifuged at 7500 × g instead of 1000 × g to obtain a more solid pellet for the counting. Briefly, all reagents were first allowed to reach room temperature for at least 30 minutes prior to the start of the assay. Trunk blood serum samples were thawed prior to the start of the assay, and an aliquot was diluted 1:400 with steroid diluent. A seven points calibration curve was then prepared with premade provided calibrators (0 ng/mL, 25 ng/mL,

50 ng/mL, 100 ng/mL, 250 ng/mL, 500 ng/mL, 1000 ng/mL). Corticosterone ^{125}I and anti-corticosterone were finally added to the points of the calibration curve and the samples (from now on: tubes), vortexed thoroughly, and left in incubation at room temperature for two hours. In addition, a non-specific binding tube (NSB) was prepared with steroid diluent and corticosterone ^{125}I. The NSB tube gives a measure of how the radioactivity added binds to targets other than the desired one or non-specific targets like impurities, salts, molecules of structure similar to the target molecule, etc. (Mendel & Mendel, 1985). At the end of the incubation period, a precipitant solution was added to all the tubes and the NSB tube, which were then vortexed thoroughly and centrifuged at 4 °C for 15 minutes at 7500 × g. After centrifugation, great care was employed to separate the supernatant from the precipitated pellet. All tubes containing the pellet were then counted for radioactivity in a gamma counter with a counting time of 60 seconds per tube.

Experiment III: effects of ERK1/2 system inhibition on intra-PVN nesfatin-1 induced effects on energy homeostasis

Experiment IIIa: Food intake measurements

Food intake was monitored in *ad libitum* fed animals, during their dark phase as described in experiment II. Animals received a unilateral intracranial injection aimed at the PVN (see general methods: microinfusion procedures) of either U0126 (25 ng/rat, an ERK1/2 inhibitor) dissolved in DMSO:PBS (dimethyl sulfoxide:phosphate-buffered saline, 50:50, vol%) or the respective control solution (DMSO:PBS) 30 minutes prior a unilateral intracranial injection aimed at the PVN of either nesfatin-1 or PBS as control solution at the onset of the dark phase. After the injection, animals were moved back to their home cage and the food was returned. Food intake and body weight were then measured after 1, 3, 6, and 24 h post-injection (for 24 hours results: see Figure A.3.1). At the end of the session, the animals were left undisturbed for a washout period of at least 5 days.

Experiment IIIb: Infrared thermography

Heat production, dissipation, and a surrogate for core body temperature were measured via thermal imaging of interscapular brown adipose tissue (iBAT), tail, and ear canal as described in experiment II. On the day of the experiment, after the habituation period, the first set of measurements of the iBAT, ear canal, and tail was taken and immediately followed by a unilateral intracranial injection aimed at the PVN (see general methods: microinfusion procedures) of either U0126 or DMSO:PBS (50:50, vol%) as control solution, before placing the animal back in its cage. The second set of measurements was taken 30 minutes later and immediately followed by a unilateral intracranial injection aimed at the PVN of either nesfatin-1 or PBS as a control solution before placing the animal back in its cage until the next set of measurements. After this second injection, animals were imaged every 15 minutes for 90 minutes in total.

Experiment IV: effects of viral knockdown of melanocortin type 4 receptors (MC4R) on intra-PVN nesfatin-1 induced effects on energy homeostasis.

Experiment IVa: model characterization

Animals were matched per body weight, food intake, fat and lean mass and assigned to a scramble or knockdown group as described in the general methods section. After surgery, animals were monitored for body weight development and food intake thrice per week, for a total of 6 weeks. Additionally, body composition was monitored at week 0, and week 2 to week 5. Thermography of the iBAT was performed at week 4, and direct calorimetry at week 6.

Experiment IVb: infrared thermography

Heat production, dissipation, and a surrogate for core body temperature were measured via thermal imaging of interscapular brown adipose tissue (iBAT), tail, and ear canal as described in experiment II and III. After at least one week of daily training, on the day of the experiment, the animals were taken to the experimental room and left for a habituation period of two hours. The first set of measurements of the iBAT, ear canal, and tail was then taken and immediately followed by a unilateral intracranial injection aimed at the PVN

(see general methods: microinfusion procedures) of either nesfatin-1 or PBS as control solution before placing the animal back in its cage until the next set of measurements. After this second injection, animals were imaged every 15 minutes for 90 minutes in total.

Experiment V: role of NTS endogenous nesfatin-1 on hedonic and homeostatic feeding behavior, and interactions with the NTS GLP-1 system

Experiment Va: Operant conditioning

Operant conditioning was here used to establish the association between a behavior (i.e. "pressing a lever") and a specific outcome (i.e. receiving a pellet of "rewarding food", like sucrose) in regards to food reward-related behaviors. As effort (an increasing number of lever presses to obtain each subsequent reward) was here required to obtain a reward (sucrose pellet), operant conditioning was used to investigate the "wanting" component (Berridge et al., 2009) of food reward-related behaviors, meaning the motivation to work to obtain a reward.

After recovering from the implantation of a bilateral cannula aimed at the NTS surgery (see general methods: Stereotactic surgery), animals started operant training, daily, three hours after the beginning of the light phase (lights on at 07:00). Operant training and experiment IVa took place in a rat operant box (30.5 × 24.1× 21.0 cm^2; Med-Associates, Fairfax, VT, USA) based on the "Skinner box" (Jones & Skinner, 1939) consisting of a metal grid floor, a light bulb (as the experiment is done during the animal's light phase), four infrared beam break sensors to monitor locomotion, two retractable levers (one named "inactive" and one "active" depending on if its activation is coupled with the delivery of a reward) two cue lights (one for each lever, of which the one above the active one was always on during the training and experiment) a food dispenser for the delivery of sucrose pellets (45 mg sucrose pellets, Test Diet, Glaxo-SmithKline, Brentford, London, UK) and a receptacle (with a beam break) for the collection of sucrose pellets (rewards, from here on).

The protocol used for operant training and experiments was adapted from Skibicka et al (K. P. Skibicka et al., 2011). Animals fed *ad libitum* were trained for 30 minutes on a fixed ratio (FR) schedule, in which a single press (FR1) of the active lever would elicit the delivery of a reward. A minimum of 30 responses (total rewards earned *and* consumed) was required to proceed to the next training schedule; pellets delivered but not consumed (i.e. left in the receptacle) would not be counted as an actual response. FR1 was followed by FR3 and FR5 (three and five presses required per single reward, respectively) until animals were introduced to 60 minutes lasting the progressive ratio (PR) conditioning schedule. In the PR, the effort needed for a reward would increase for each subsequent reward according to the following equation: pellets obtained ($5e^{0.2 \times \text{lever presses}} - 5$) through the following series: 1, 2, 4, 9, 12, 15, 20, 25, 32, 40, 50, 62, 77, 95, 118, 145, 178, 219, 268, 328, 402, 492, 603, 737, 901. The PR schedule was repeated daily until the animals' response was deemed stable (less than 15% variation in rewards earned over three consecutive sessions) before proceeding with pharmacological treatments the day after.

To investigate the role of NTS endogenous nesfatin-1 on hedonic feeding behavior, animals were weighed and then pretreated with bilateral injections of intra-NTS NUCB2/nesfatin-1 directed antibodies (Nes-1 Ab), or control IgGs and returned to their home cage. After 30 minutes, animals were again injected bilaterally with either Ex4 or aCSF as control solution and again returned to their home cage. After 15 minutes from this injection, animals were placed in the operant chamber for a PR schedule session.

Experiments Vb/c: Food intake measurements

In experiment IVb, food intake and body weight change were measured 24 hours after the treatment of experiment IVa. In experiment IVc, short-term dark phase food intake was measured in *ad libitum* fed rats. Animals were left undisturbed in the vivarium with unlimited access to food and water. Food but not water was removed 2 hours before the onset of the dark phase to account for possible individual meals before the injection. Thirty minutes before the onset of the dark phase, animals were weighed and injected bilaterally with intra-NTS Nes-1 Ab, or control IgGs. At the onset of the dark phase, animals received a bilateral

injection of either Ex4 or aCSF as control solution after which food (30 g) was given back to the animals and food intake measured after 1, 2, and 3 hours post-injection. Additionally, bodyweight change was also measured at 3 hours post-injection.

Statistics

For i.c.v. nesfatin-1 injections, the effect of nesfatin-1 and feeding state on dry heat loss over 8 hours was analyzed using three-way repeated-measures ANOVA with nesfatin-1 and feeding state as between-subjects factors and time as a within-subject factor. Single time-point measurements were analyzed using a two-way ANOVA with nesfatin-1 and feeding state as between-subjects factors, followed by Newman-Keuls pairwise *post hoc* comparison. Correlation between two variables was performed using Spearman´s rank correlation coefficient. The efficiency time (E_t) for each animal was generated by fitting the 8 hours direct calorimetry data points a Hill equation. Differences between two groups were analyzed with Student's *t*-test.

For single intra-PVN nesfatin-1 injections, the effects of nesfatin-1 on feeding, dry heat loss over 8 hours, and iBAT activation were analyzed using two-way repeated measure ANOVA with nesfatin-1 as a between-subjects factor and time as a within-subject factor. For intra-PVN co-injections of nesfatin-1 and U0126, the effect of nesfatin-1 and U0126 on feeding and iBAT activation was analyzed using three-way repeated-measures ANOVA with nesfatin-1 as between-subjects factor and time and U0126 as within-subject factors. Single time-point measurements were analyzed using a two-way ANOVA with nesfatin-1 and U0126 as between-subjects factors, followed by Newman-Keuls pairwise *post hoc* comparison.

For MC4R knockdown experiments, the effect of the knockdown on body weight development, food and water intake, body composition, and iBAT activation was analyzed using two-way repeated measure ANOVA with MC4Rs knockdown as a between-subjects factor and time as a within-subject factor. Single time point differences between the two groups were analyzed with Student's *t*-test.

Levels of mRNA and protein expression were also analyzed using Student's *t*-test. Corticosterone levels from the radioimmunoassay were calculated as per manufacturer instructions. The average radioactivity count of all duplicate tubes was considered, and the average NSB count was subtracted from it. These corrected values were then divided by the average count of the 0 calibrator point of the calibration curve, to obtain the percent bound. The calibration curve was obtained by plotting the percent bound of the calibrator points versus the known concentration of the calibration curve (0 - 1000 ng/mL). The unknown concentrations from the samples were subsequently generated using a one phased decay least-square fit obtained by plotting the percent bound of the unknown samples against the curve and tested for differences between the two groups using Student's *t*-test.

The significance level was set to $p < 0.05$, with * for $p < 0.05$, ** for $p < 0.01$, *** for $p < 0.001$ and # for trends with $p < 0.1$. The software packages used were Excel (Microsoft, Redmond, US), Prism 7.0 (GraphPad, La Jolla, US) and Statistica 7.0 (StatSoft, Tulsa, US).

Results

Experiment I: effect of feeding state on nesfatin-1 induced increase in energy expenditure in the light phase

Figure 1.1A displays the effect of feeding state and i.c.v. treatment with nesfatin-1 on light phase dry heat loss (as a measure of energy expenditure) measured via direct calorimetry, shown in hourly averages. Animals either fed *ad libitum* or food-deprived for 24h underwent direct calorimetry as described in the Methods section. Animals fed *ad libitum* showed a significantly increased dry heat loss compared to the 24 h food-deprived control group, as shown by the effect of the feeding state ($p=0.000550$). Analysis of the single time points showed a significantly increased dry heat loss in the *ad libitum* fed control group at hour 3 ($p=0.00481$), hour 4 ($p=0.002733$), and hour 5 ($p=0.035042$), compared to the food-deprived control group, while a trend approaching significance could be seen at hour 1 ($p=0.055814$), hour 2 ($p=0.082336$), and hour 6 ($p=0.069941$).

In addition, i.c.v. treatment with nesfatin-1 strongly increased dry heat loss compared to the control animals, as shown by the effect of nesfatin-1 ($p=0.000162$), time ($p<0.0001$), and nesfatin-1 × time ($p<0.0001$). Analysis of the single time points showed a significantly increased dry heat loss in the *ad libitum* fed nesfatin-1 treated group at hour 1 ($p=0.029853$), hour 2 ($p=0.006016$), hour 3 ($p=0.001361$), hour 4 ($p=0.002522$), hour 5 ($p=0.013673$), and hour 6 ($p=0.046268$) compared to the *ad libitum* fed control group, while a trend approaching significance could be seen at hour 7 ($p=0.080082$). In the 24 hours food-deprived animals, nesfatin-1 treatment induced a significantly increased dry heat loss at hour 3 ($p=0.000772$), hour 4 ($p=0.000499$), hour 5 ($p=0.001691$), and hour 6 ($p=0.013417$) compared to the 24 hours food-deprived control group, while a trend approaching significance could be seen at hour 2 ($p= 0.058998$), and hour 7 ($p= 0.092004$).

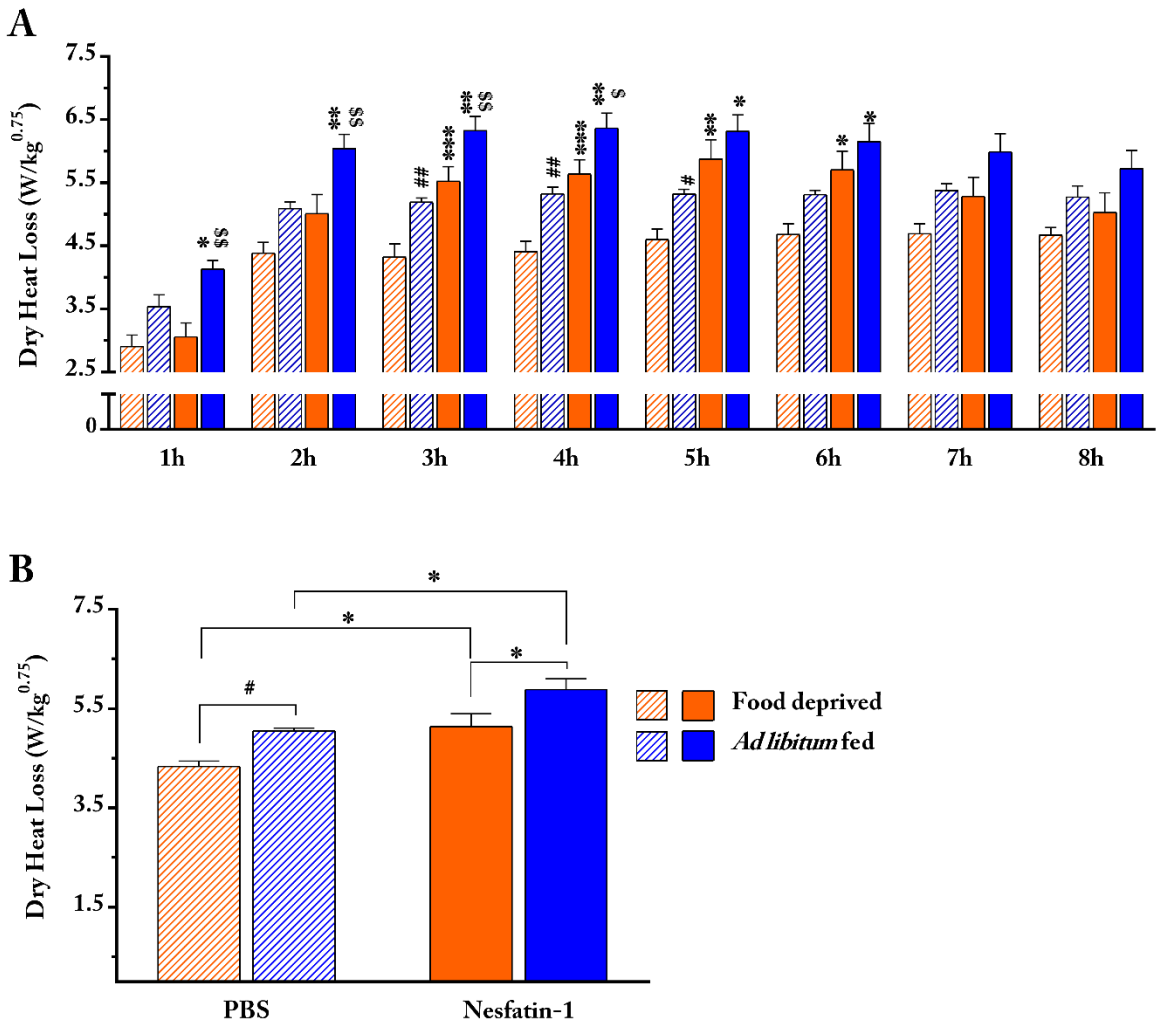

Figure 1.1.: Feeding state and i.c.v. nesfatin-1 induced light phase dry heat loss.

Effect of i.c.v. administration of nesfatin-1 (100 pmol/rat) or PBS as a control solution on dry heat loss measured through direct calorimetry. 24 hours food-deprived or *ad libitum* fed rats (7–8/group) were placed in the calorimeters immediately after drug administration and tested for 8-h during the light phase. A) 3-way ANOVA of 8 hours time course. *P < 0.05, **P < 0.01, ***P < 0.001 vs respecive food deprived group; $P < 0.05, $$P < 0.01, vs nesfatin-1 food deprived. #P < 0.05, ##P < 0.01, vs PBS food deprived (Newman–Keuls test). B) 8 hour average dry heat loss for each group. 2-way ANOVA, #P ≤ 0.1, *P < 0.05 (Student's *t*-test). All data are represented as mean ± SEM.

The feeding state *per se* did not affect the effect of nesfatin-1 on dry heat loss, as suggested by the lack of interaction between treatment and feeding state (p=0.959862). However, as shown in Figure 1.1B, analysis of the average of dry heat loss from hours 1 - 8 showed a stronger, significant effect of i.c.v. nesfatin-1 in the *ad libitum* fed group compared to the food-deprived group (p=0.0242), while only a trend is present in

the control groups (p=0.0765). Analysis of the single time points showed a significantly increased dry heat loss in the *ad libitum* fed nesfatin-1 treated group at hour 1 (p=0.001010), hour 2 (p=0.008311), hour 3 (p=0.008669), and hour 4 (p=0.014505), compared to the 24 h food-deprived nesfatin-1 treated group.

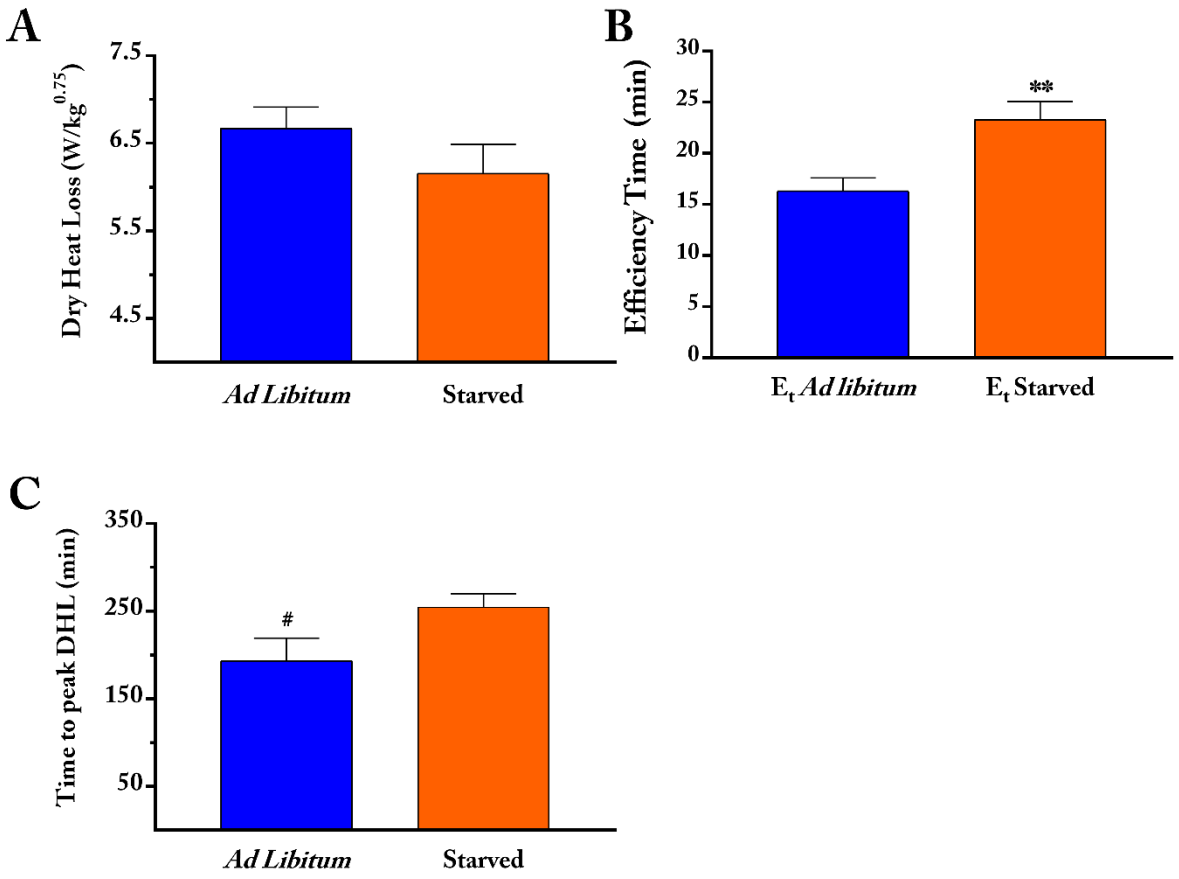

Figure 1.2.: Feeding state and i.c.v. nesfatin-1 induced energy expenditure parameters.
Effect of i.c.v. administration of nesfatin-1 (100 pmol/rat) on A) Peak dry heat loss. B) Efficiency time (or time to reach 50% of peak dry heat loss). C) Time to reach peak dry heat loss.
#P ≤ 0.1, **P < 0.01 (Student's *t*-test). All data are represented as mean ± SEM.

In the control animals, the *ad libitum* fed group significantly increased dry heat loss at hour 3 (p= 0.004881), hour 4 (p=0.002733), and hour 5 (p=0.035042) while a trend approaching significance could be seen at hour 1 (p= 0.055814), hour 2 (p=0.082336), and hour 6 (p=0.069941).

To explore the effect of feeding state on nesfatin-1's effects on dry heat loss in more detail, data were further analyzed in one-minute intervals. As shown in Figure 1.2A, animals treated i.c.v. with nesfatin-1 in both feeding conditions showed no differences in peak dry heat loss reached on any given minute during the

eight hours of the experimental session. However, animals fed *ad libitum* are more responsive to nesfatin-1's treatment as shown by the time to reach 50% of peak dry heat loss (Figure 1.2B; 16.3 vs. 23.3 minutes, p=0.007) and as shown by a trend in reaching peak dry heat loss (Figure 1.2C, p=0.0639).

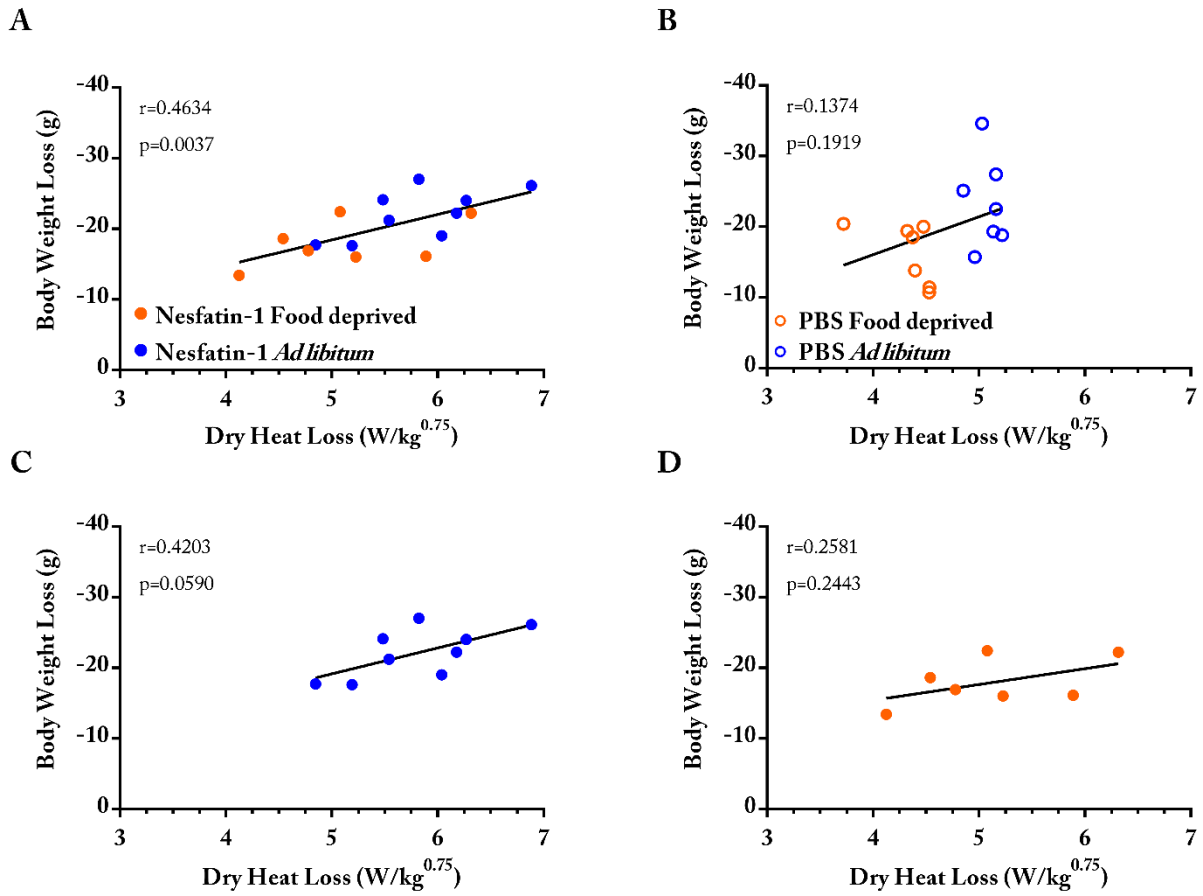

Figure 1.3.: Correlation between body weight change and dry heat loss.

Correlation analysis (Spearman´s coefficient) between body weight change and 8 hours average of dry heat loss during the direct calorimetry experiment.

A) nesfatin-1 food-deprived and nesfatin-1 fed *ad libitum*. B) PBS food-deprived and PBS fed *ad libitum*. C) nesfatin-1 *ad libitum*. D) and nesfatin-1 food-deprived alone.

Lastly, treatment with i.c.v. nesfatin-1 did not affect significantly body weight loss after eight hours of direct calorimetry (Figure A.1); nevertheless, a significant correlation between body weight loss and dry heat loss could be found in the nesfatin-1 groups when analyzed together (i.e. *ad libitum* fed and starved animals together; r=0.4634, p=0.0037) (Figure 1.3A) but not in the control groups (Figure 1.3B; r=0.1374, p=0.1919). Further analysis of the nesfatin-1 treated animals separated per feeding state, revealed an

absence of correlation in the starved group (Figure 1.3D; r=0.2581, p=0.2443) while a trend approaching significance could be seen in the *ad libitum* fed group (Figure 1.3C r=0.4203, p=0.0590).

Experiment II: effect of intra-PVN nesfatin-1 injections on energy homeostasis

Experiment IIa: effects of intra-PVN nesfatin-1 on dark phase food intake

Dark phase food intake was studied in animals fed *ad libitum*, following intra-PVN treatment with nesfatin-1 at the onset of the dark phase. Intra-PVN nesfatin-1 treatment significantly reduced cumulative food intake over 6 hours (Figure 2.1A) as indicated by the effect of nesfatin-1 ($p=0.0004$), time ($p<0.0001$), and time × nesfatin-1 ($p=0.0004$). Intra-PVN nesfatin-1 treated animals showed a significant reduction in cumulative food intake at hour 3 ($p=0.0062$) and hour 6 ($p=0.0002$) while only a trend could be seen at hour 1 ($p=0.1038$). Analysis of the incremental food intake (Figure 2.1B) revealed a significant effect of time of nesfatin-1 ($p=0.0003$), time ($p<0.0001$) but no interaction (time × nesfatin-1, $p=0.1216$). Intra-PVN nesfatin-1 treated animals showed a significant reduction in food intake at hour 3 ($p=0.0427$) and hour 6 ($p=0.0041$) while only a trend could be seen at hour one ($p=0.1038$). Lastly, intra-PVN treatment with nesfatin-1 decreased the body weight gain over six hours compared to the control group (Figure A.2; $p=0.0325$).

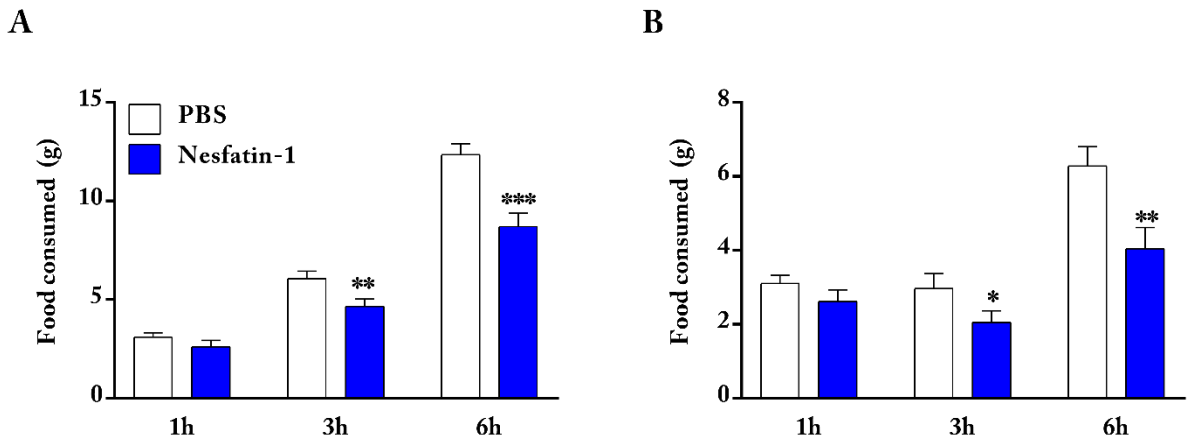

Figure 2.1.: Intra-PVN nesfatin-1 on dark phase food intake.

Effect of intra-PVN administration of nesfatin-1 (50 pmol/rat) or PBS as a control solution on dark phase food intake on *ad libitum* fed rats (12/group). A) Cumulative food intake. B) Incremental food intake. 2-way ANOVA, *P < 0.05, *P < 0.01 (Student's *t*-test). All data are represented as mean ± SEM.

Experiment IIb: effects of intra-PVN nesfatin-1 on light phase energy expenditure

Figure 2.2A shows the effect of intra-PVN treatment with nesfatin-1 on dry heat loss measured in *ad libitum* fed animals via direct calorimetry during the light phase. Animals treated with nesfatin-1 showed a significantly increased dry heat loss compared to the *ad libitum* control group, as shown by the effect of nesfatin-1 ($p=0.0134$) and time ($p<0.0001$). Analysis of the single time points showed a significantly increased nesfatin-1-induced dry heat loss at hour 2 ($p=0.027$), hour 3 ($p=0.026$), hour 4 ($p=0.029$), and hour 5 ($p=0.022$), while a trend approaching significance could be seen at hour 6 ($p=0.055$), and hour 7 ($p=0.051$), and a trend at hour 1 ($p=0.105$).

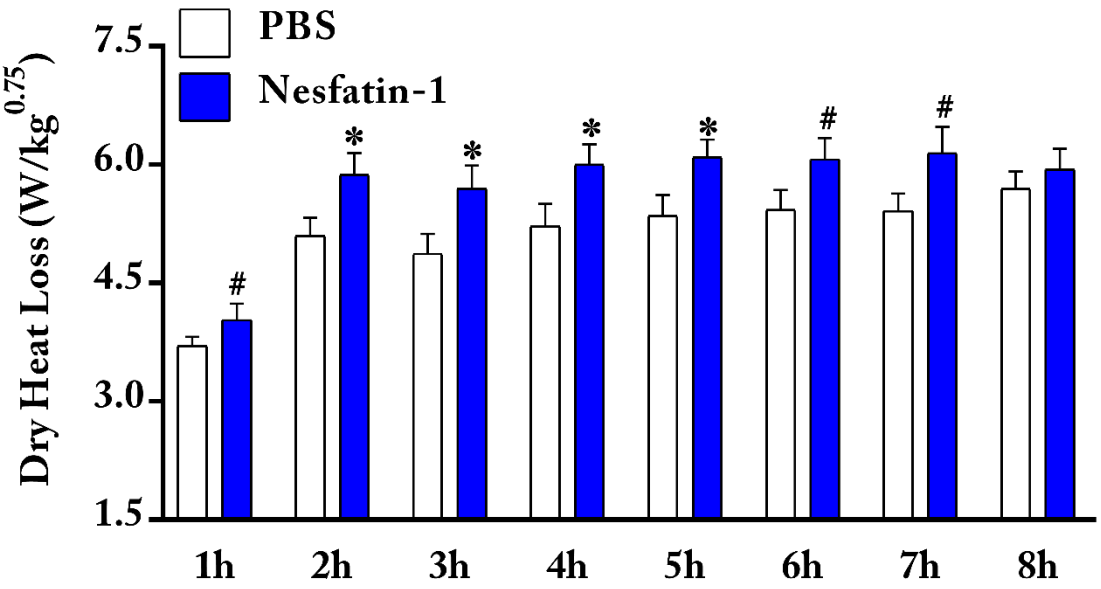

Figure 2.2.: Intra-PVN nesfatin-1 on light phase dry heat loss.
Effect of i.c.v. administration of nesfatin-1 (50 pmol/rat) or PBS as a control solution on light phase dry heat loss on *ad libitum* fed rats (8-9/group).
2-way ANOVA, #P < 0.1, *P < 0.05 (Student's *t*-test). All data are represented as mean ± SEM.

Experiment IIc: effects of intra-PVN nesfatin-1 on light phase iBAT thermogenesis

Thermal imaging of the iBAT (as a measure of iBAT thermogenesis) ear canal (as a measure of core body temperature) and tail (as a measure of heat dissipation) was assessed every 15 minutes for a total of 90 minutes, during the light phase, in animals fed *ad libitum* following intra-PVN treatment with nesfatin-1.

Treatment with nesfatin-1 elicited a strong increase in iBAT thermogenesis compared to control animals (Figure 2.3A), as indicated by the effect of nesfatin-1 ($p=0.0033$), time ($p<0.0001$), and the interaction of nesfatin-1 × time ($p=0.0082$). Analysis of the single time points showed a significantly increased iBAT thermogenesis at 15 minutes ($p=0.0131$), 30 minutes ($p=0.0012$), 45 minutes ($p=0.0013$) 60 minutes ($p=0.0176$), 75 minutes ($p=0.0361$), and 90 minutes ($p=0.0310$). Similarly, treatment with nesfatin-1 elicited a strong increase in the core body temperature compared to control animals (Figure 2.3B), as indicated by the effect of nesfatin-1 ($p=0.0030$), time ($p<0.0001$), and the interaction of nesfatin-1 × time ($p=0.0015$). Analysis of the single time points showed a significantly increased core body temperature at 15 minutes ($p=0.0438$), 30 minutes ($p=0.0013$), 45 minutes ($p=0.0215$) 60 minutes ($p=0.0030$), 75 minutes ($p=0.0141$), and 90 minutes ($p=0.0009$). Treatment with nesfatin-1 did not affect heat dissipation through the tail compared to control animals (Figure 2.3C), as indicated by a significant effect of time ($p=0.0001$) but no effect of nesfatin-1 ($p=0.7868$) and a lack of interaction of nesfatin-1 × time ($p=0.6670$). The overall impact of the treatment with nesfatin-1 on thermogenesis was also calculated as the area under the curve (AUC), taking into account the contribution of peaks that went both above and below baseline levels (net AUC). Coherently with the previous analysis, treatment with nesfatin-1 resulted in a higher net AUC compared to controls for iBAT (Figure 2.3D; $p=0.0014$) and ear (Figure 2.3E; $p=0.0020$) but not in the tail (Figure 2.3F; $p=0.39$).

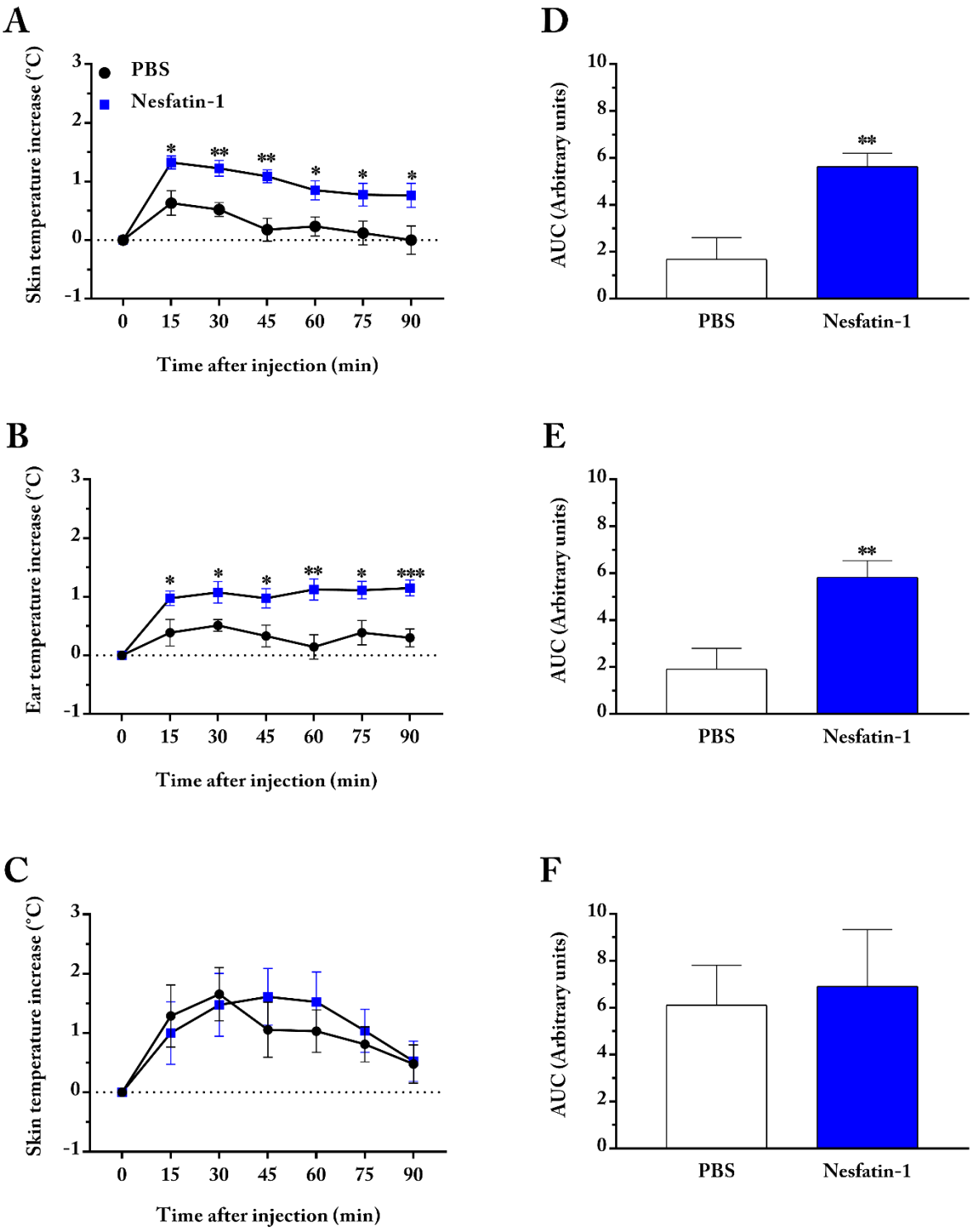

Figure 2.3.: Intra-PVN nesfatin-1 on light phase iBAT thermogenesis.

Effect of intra-PVN administration of nesfatin-1 (50 pmol/rat) or PBS as a control solution on light phase iBAT thermogenesis on *ad libitum* fed rats (8-9/group) measured over 90 minutes.

A) iBAT. B) Ear canal. C) Tail temperature, and respective AUC D-F). 2-way ANOVA, *P < 0.05, **P < 0.01, ***P < 0.001 (Student's *t*-test). All data are represented as mean ± SEM.

Experiment IId: changes in gene expression after intra-PVN nesfatin-1

In animals from experiment IIc, after a final intra-PVN injection of nesfatin-1, changes in gene expression in the hypothalamus, brainstem, and iBAT were studied at four hours post-injection. In the hypothalamus (Figure 2.4A-G), intra-PVN treatment with nesfatin-1 resulted in a significant decrease in *Nucb2* gene expression (p=0.0040), with a negative trend approaching significance for *Pomc* (p=0.0729), and a positive trend approaching significance for *Agrp* (p=0.0634). No change in gene expression could be found for *Npy* (p=0.2555), *Crf* (p=0.3468), *Cart* (p=0.3672) and *Oxytocin* (p=0.1850).

In the brainstem (Figure 2.5A-E), intra-PVN treatment with nesfatin-1 resulted in a significant increase in *Npy* (p=0.0450) and *Cart* (p=0.0460) gene expression, with a positive trend approaching significance for *Th* (p=0.0609). No change in gene expression could be found for *Nucb2* (p=0.4441) and *Pomc* (p=0.3011).

In the iBAT (Figure 2.6A-D), intra-PVN treatment with nesfatin-1 resulted in a negative trend for *Pgc1a* (p=0.0958), while a positive trend approaching significance could be found for *Dio2* (p=0.0626). Expression of *Cidea* (p=0.1773) and *Pparg* (p=0.2594) was unchanged. Notably, while the expression of *Ucp-1* showed only a positive trend towards increased expression (Figure 2.6E; p=0.1016), a strong correlation between *Ucp-1* expression and iBAT temperature increase at sacrifice could be found for nesfatin-1 treated animals (Figure 2.6F; r=0.9777, p=0.0002), but not in control-treated animals (Figure 2.6E; r=0.0015, p=0.9329).

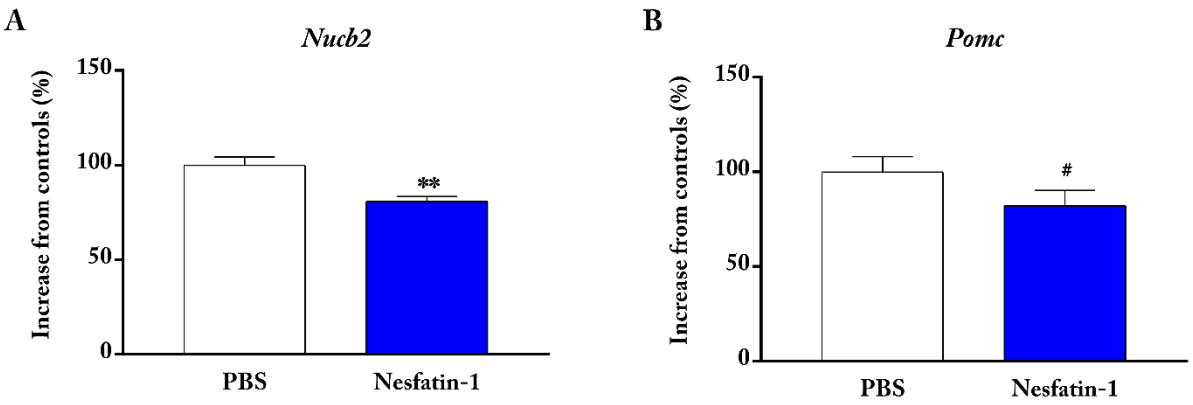

Figure 2.4.: Intra-PVN nesfatin-1 and hypothalamic gene expression.
Effect of intra-PVN administration of nesfatin-1 (50 pmol/rat) or PBS as a control solution on hypothalamic gene expression (5-8/group) 4 hours after the injection.
#P < 0.01, **P < 0.01 (Student's *t*-test). All data are represented as mean ± SEM

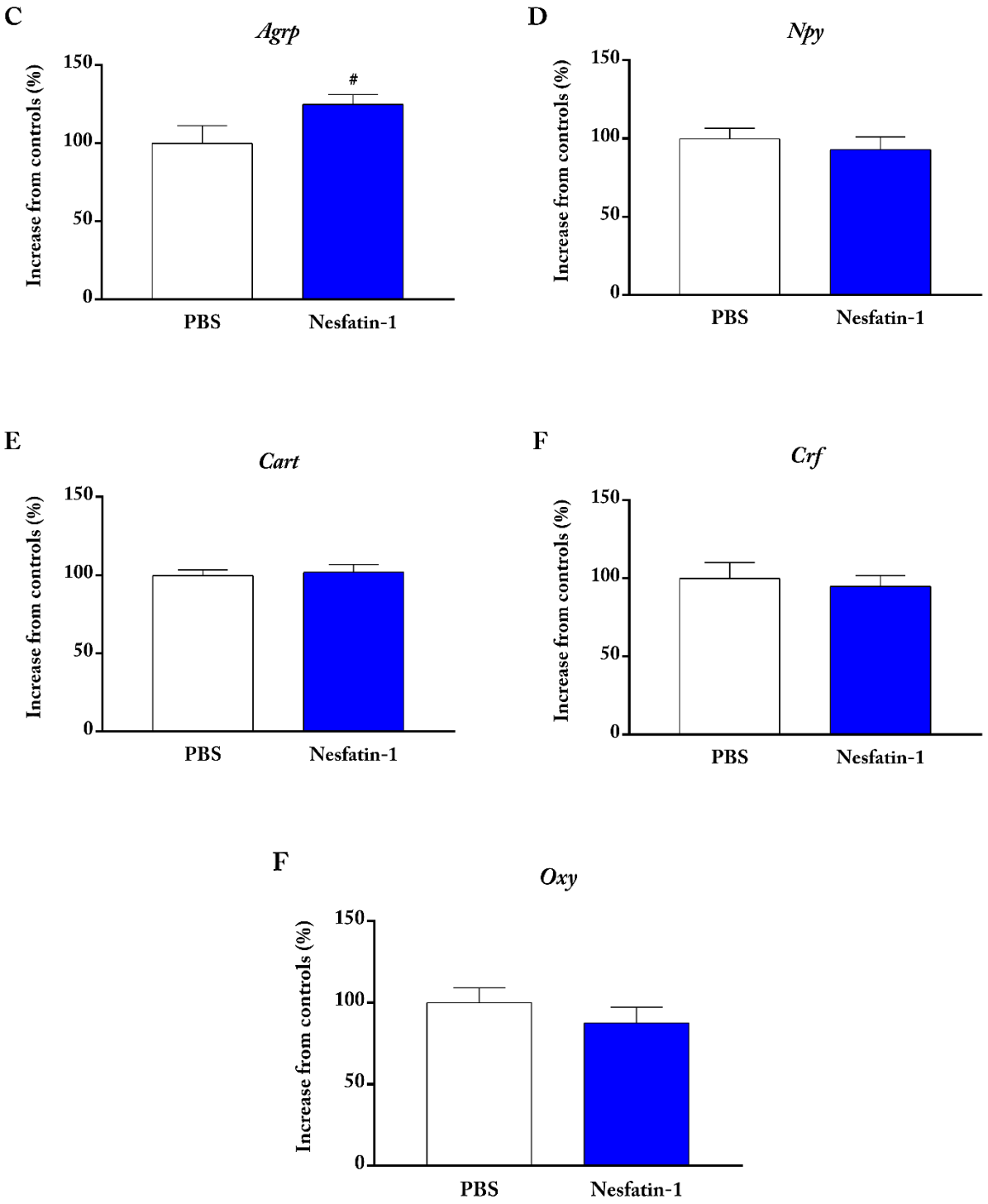

Figure 2.4. (continuation): Intra-PVN nesfatin-1 and hypothalamic gene expression.

Effect of intra-PVN administration of nesfatin-1 (50 pmol/rat) or PBS as a control solution on hypothalamic gene expression (5-8/group) 4 hours after the injection.

#P < 0.01, **P < 0.01 (Student's *t*-test). All data are represented as mean ± SEM.

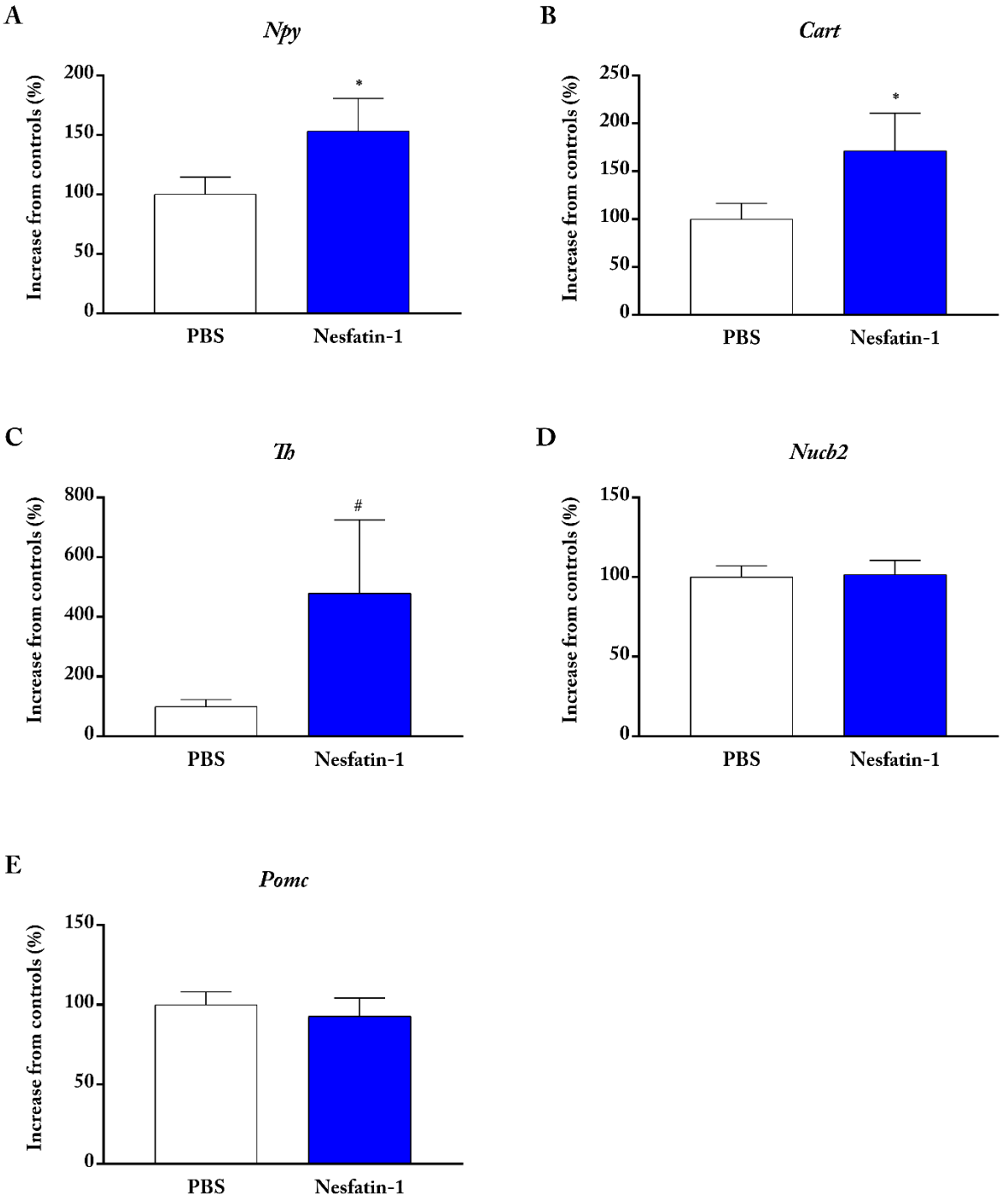

Figure 2.5.: Intra-PVN nesfatin-1 and brainstem gene expression.

Effect of intra-PVN administration of nesfatin-1 (50 pmol/rat) or PBS as a control solution on brainstem gene expression (5-8/group) 4 hours after the injection.

#P < 0.01, *P < 0.05 (Student's *t*-test). All data are represented as mean ± SEM.

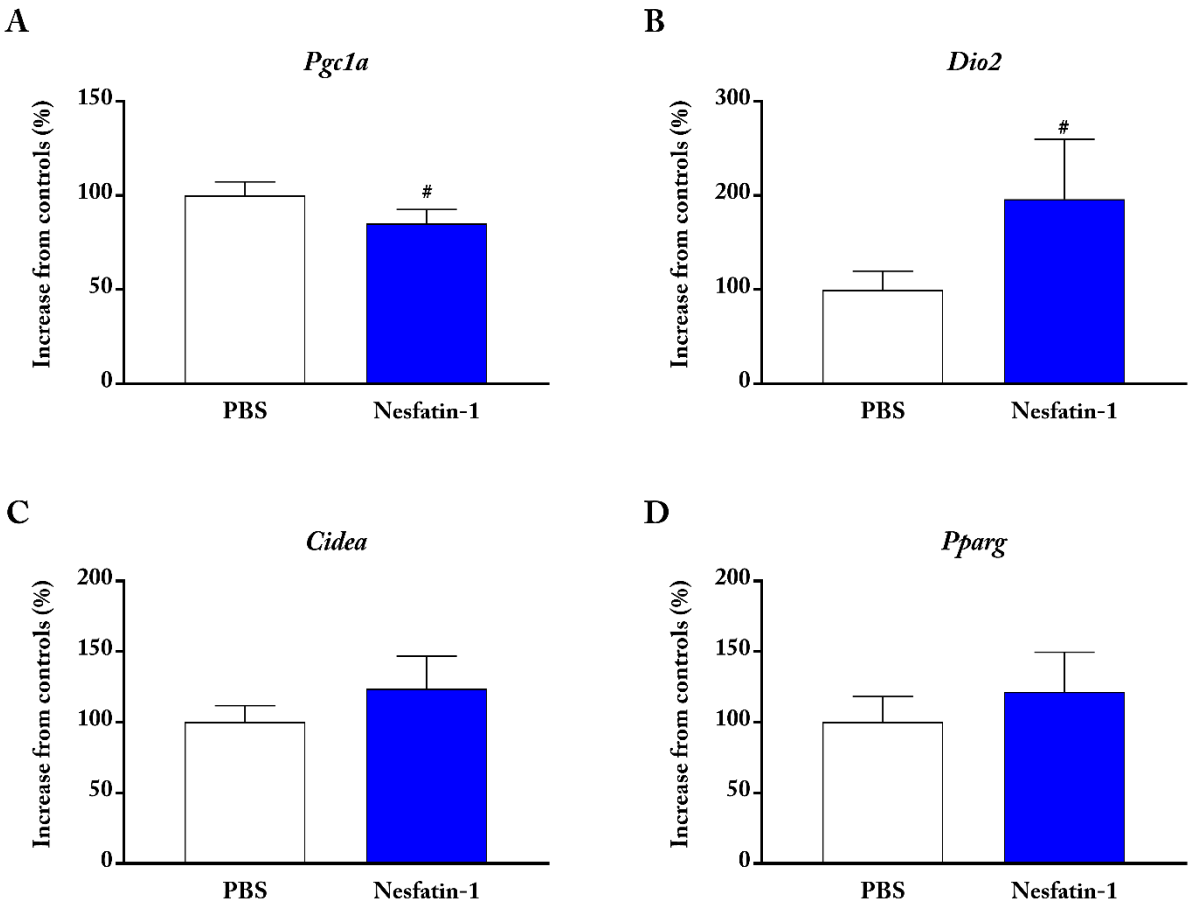

Figure 2.6.: Intra-PVN nesfatin-1 and iBAT gene expression.

Effect of intra-PVN administration of nesfatin-1 (50 pmol/rat) or PBS as a control solution on iBAT gene expression (5-8/group) 4 hours after the injection and correlation analysis (Spearman´s coefficient) between skin temperature increase from baseline at sacrifice and *Ucp1* mRNA expression for F) nesfatin-1. And G) PBS. #P < 0.1 (Student's *t*-test). All data are represented as mean ± SEM.

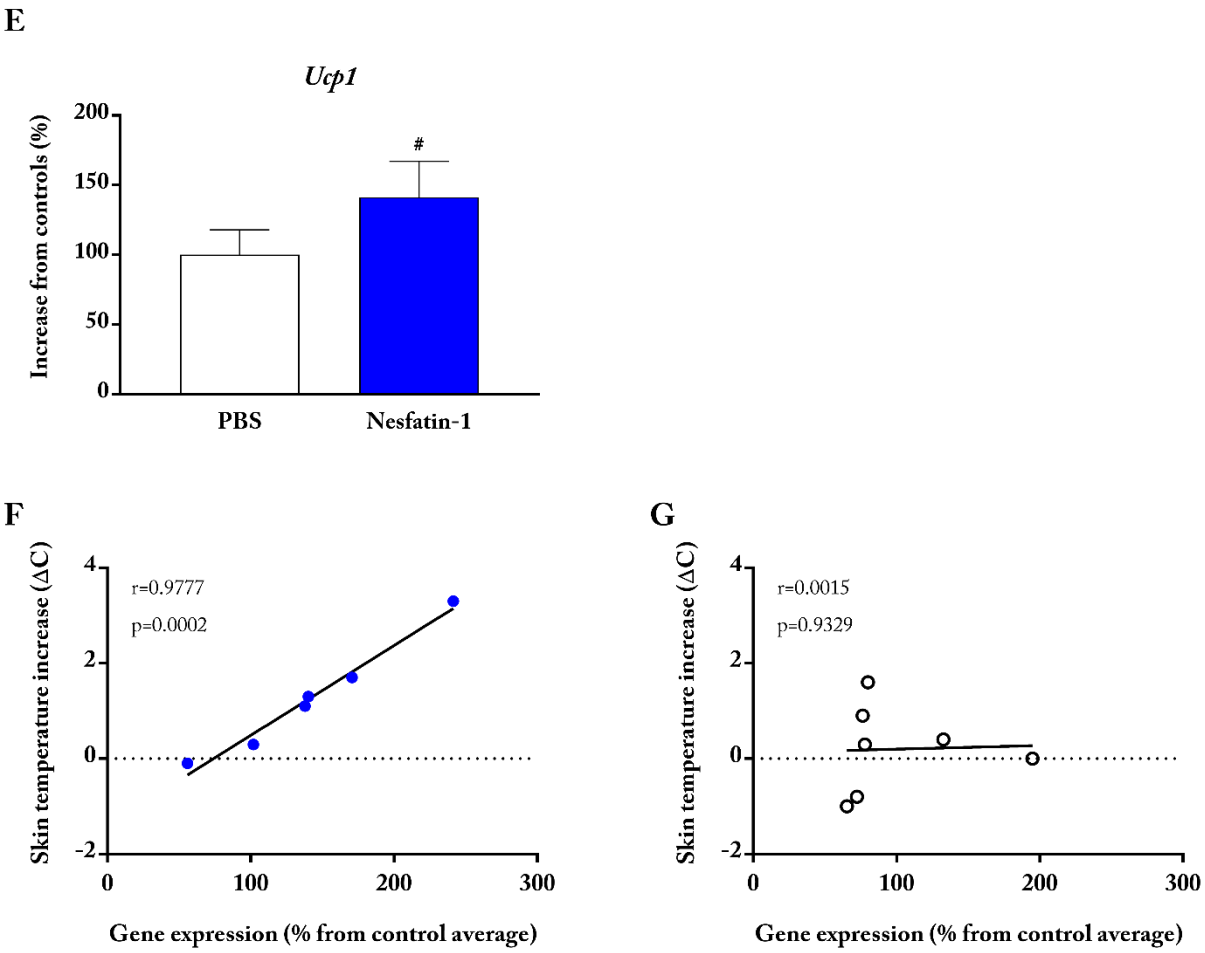

Figure 2.6. (continuation): Intra-PVN nesfatin-1 and iBAT gene expression.

Effect of intra-PVN administration of nesfatin-1 (50 pmol/rat) or PBS as a control solution on iBAT gene expression (5-8/group) 4 hours after the injection and correlation analysis (Spearman´s coefficient) between skin temperature increase from baseline at sacrifice and *Ucp1* mRNA expression for F) nesfatin-1. And G) PBS. #P < 0.1 (Student's *t*-test). All data are represented as mean ± SEM.

Experiment IIe: short-term effects of intra-PVN nesfatin-1

In animals from experiment IIa/b, the effects of intra-PVN nesfatin-1 were studied 35 minutes after its injection. An increase in iBAT temperature after intra-PVN nesfatin-1 (Figure 2.7A; p=0.0006) was measured as a control parameter. After 35 minutes, intra-PVN injection of nesfatin-1 significantly increased plasma CTS (Figure 2.7B; p=0.0106) and *c-fos* S expression in both the NTS (Figure 2.7C; p=0.0106) and PVN (Figure 2.7E; p=0.0028) compared to control animals. In addition, a significant correlation between the increase in iBAT temperature and *c-fos* increase expression was found in the NTS

(Figure 2.7D; r=0.3767; p=0.0106) but not in the PVN (Figure 2.7F; r=0.0749; p=0.3894) when analyzing nesfatin-1 and PBS treated animals together. Lastly, a trend for a correlation between plasma corticosterone and increase in iBAT temperature (r=0.2475; p=0.0702) was found (Figure A.2.2).

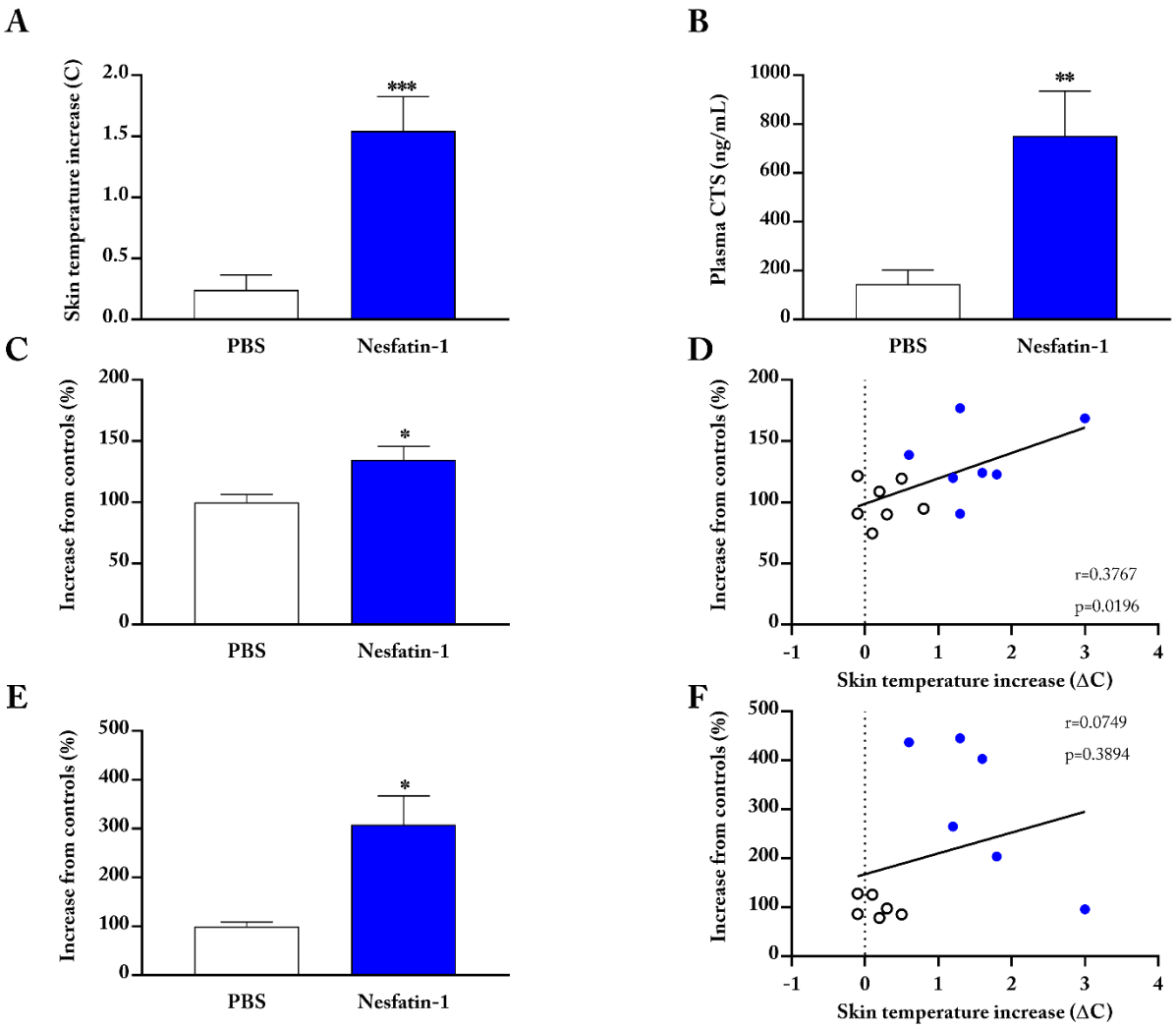

Figure 2.7.: Intra-PVN nesfatin-1 effects on cFOS expression and plasma corticosterone levels.
Effect of intra-PVN administration of nesfatin-1 (50 pmol/rat) or PBS as a control solution on iBAT thermogenesis, plasma CTS levels, and cFOS expression in the PVN and NTS (6-7/group) 35 minutes after the injection. A) iBAT temperature increase. B) plasma corticosterone levels. C) cFOS expression in the NTS. E) and in the PVN. Correlation analysis (Spearman´s coefficient) between skin temperature increase from baseline at sacrifice and cFOS expression D) in the NTS. F) and in the PVN.
*P < 0.05, **P < 0.01, ***P < 0.001 (Student's *t*-test). All data are represented as mean ± SEM.

In the brainstem, intra-PVN injection of nesfatin-1 resulted in a significant increase of *Th* (Figure 2.8A; p=0.0425) and a trend towards increased *Nucb2* (Figure 2.8B; p=0.0793) and *Cart* (Figure 2.8C; p=0.1016) mRNA expression. No difference in expression of *Oxytocin* (p=0.2402), *Npy* (p=0.4147), *Pomc* (p=0.3753) could be found (Figures 2.8D-F).

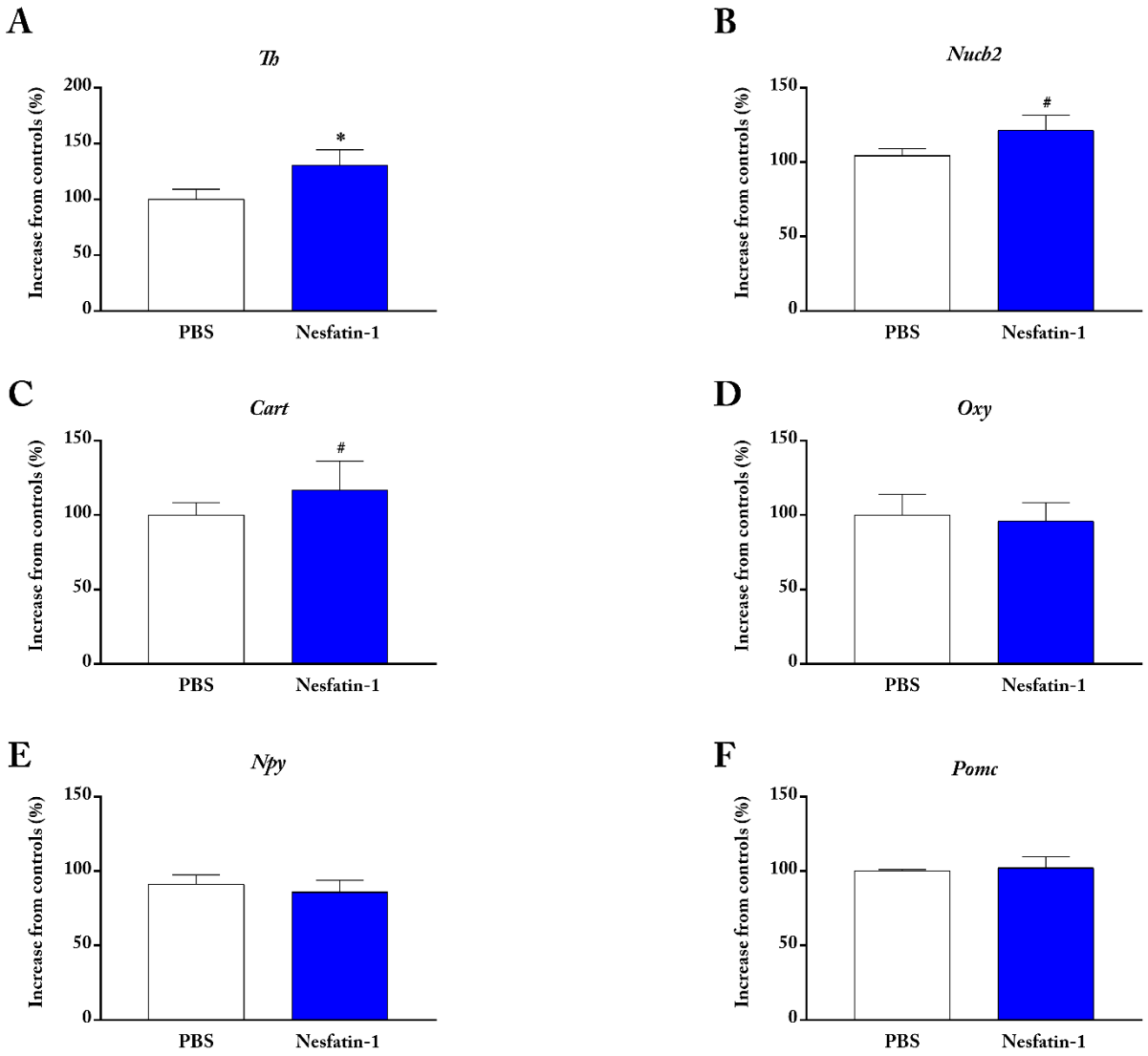

Figure 2.8.: Intra-PVN nesfatin-1 effects on brainstem gene expression.

Effect of intra-PVN administration of nesfatin-1 (50 pmol/rat) or PBS as a control solution on brainstem gene expression (6-7/group) 35 minutes after the injection.

#P < 0.01, *P < 0.05 (Student's *t*-test). All data are represented as mean ± SEM.

Experiment III: effects of ERK1/2 system inhibition on intra-PVN nesfatin-1 effects on energy homeostasis

Experiment IIIa: effects of intra-PVN U0126 on intra-PVN nesfatin-1 induced dark phase anorexia

As in experiment IIa, dark phase food intake was studied in animals fed *ad libitum* injected intra-PVN with U0126 (an ERK1/2 inhibitor) or control solution (DMSO:PBS) 30 minutes before intra-PVN treatment with nesfatin-1 at the onset of the dark phase. Similar to experiment IIa, intra-PVN treatment with nesfatin-1 significantly reduced cumulative food intake over six hours (Figure 3.1A) compared to its control group, as indicated by the effect of nesfatin-1 ($p=0.002$), time ($p<0.0001$) and time × nesfatin-1 ($p<0.0001$). Intra-PVN nesfatin-1 treated animals showed a significant reduction in food intake at hour three ($p=0.0332$) and hour six ($p=0.0004$). Intra-PVN pretreatment with U0126 30 minutes prior to nesfatin-1's intra-PVN injections completely blocked the anorexigenic effects of nesfatin-1 as indicated by the effect of U0126 ($p=0.0037$), time × nesfatin-1 × U0126 ($p<0.0057$), and a trend approaching significance for time × U0126 ($p=0.0721$).

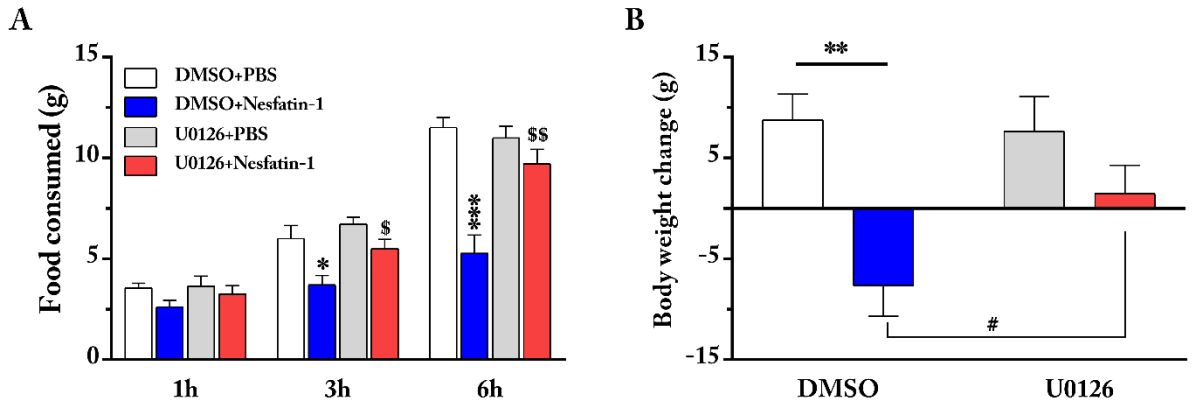

Figure 3.1.: Erk1/2 antagonism of intra-PVN nesfatin-1 effects on dark phase food intake.
Effect of pretreatment with U0126 (25ng/rat) on intra-PVN administration of nesfatin-1 (50 pmol/rat) or PBS as a control solution on dark phase food intake on *ad libitum* fed rats (12/group). A) Cumulative food intake. B) Bodyweight change after 6 hours. 2-way ANOVA, #P < 0.1, *P < 0.05, *P < 0.01 (Sidak's multiple comparison test). All data are represented as mean ± SEM.

Intra-PVN pretreatment with U0126 did not affect food intake *per se* at any time point compared to the control-treated group but significantly increased food intake when injected before nesfatin-1 at hour three ($p=0.0156$) and hour six ($p=0.0012$).

Pretreatment with intra-PVN U0126 also blocked intra-PVN nesfatin-1's effect on body weight over six hours (Figure 3.1B) as indicated by an effect of nesfatin-1 ($p=0.0047$), no effect of U0126 ($p=0.1770$), but a trend for nesfatin-1 × U0126 ($p=0.0933$). More in-depth, while the intra-PVN nesfatin-1 treated group showed a significant decrease in body weight over six hours when compared to its control group ($p=0.0016$), the group treated with intra-PVN U0126 before intra-PVN nesfatin-1 showed a non-significant reduction in body weight compared to its control group (U0126) ($p=0.2865$) and a trend towards less body weight loss ($p=0.0811$) when compared to the intra-PVN nesfatin-1 group.

Experiment IIIb: effects of intra-PVN U0126 on intra-PVN nesfatin-1 induced light phase iBAT thermogenesis

As in experiment IIc, thermal imaging of the iBAT, ear canal, and tail was performed every 15 minutes for a total of 90 minutes, during the light phase, in animals fed *ad libitum* injected intra-PVN with U0126 or control solution (DMSO:PBS) 30 minutes before intra-PVN treatment with nesfatin-1. To account for confounding factors (such as stress-induced iBAT thermogenesis) as two intra-PVN injections are here required, animals were monitored for their iBAT skin temperature before the first and the second injection. While a small temperature rise could be registered after 30 minutes from the first injection (Figure A.3.2C) the temperature across the four groups remained matched (Figure A.3.2A-B).

Similar to experiment IIc, treatment with nesfatin-1 elicited a strong increase in iBAT thermogenesis compared to control animals (Figure 3.2A), as indicated by the effect of nesfatin-1 ($p=0.0009$), time ($p<0.0001$) but lack of interaction of nesfatin-1 × time ($p=0.6744$). Analysis of the single time points showed a significantly increased iBAT thermogenesis at 15 minutes ($p=0.0368$), 30 minutes ($p=0.0008$),

45 minutes (p=0.0048) 60 minutes (p=0.0055), and 75 minutes (p=0.0233). Intra-PVN pretreatment with U0126 30 minutes prior to nesfatin-1's intra-PVN injection completely blocked the thermogenic effects of nesfatin-1 as indicated by a trend for the effect of U0126 (p=0.0963), and a trend approaching significance for nesfatin-1 × U0126 (p=0.0534). Notably, intra-PVN pretreatment with U0126 did not affect iBAT thermogenesis *per se* at any time point compared to the control-treated group but blocked the nesfatin-1 induced increase in iBAT thermogenesis at 30 minutes (p=0.0137), 45 minutes (p=0.0058), and 75 minutes (p=0.0360), with a trend approaching significance at 60 minutes (p=0.0547). Analysis of the AUC, expressed as before as net AUC, (Figure 3.2B) further shows a strong effect of intra-PVN nesfatin-1 induced increase in iBAT thermogenesis (p=0.0007), a trend for U0126 (p=0.0877), and interaction for nesfatin-1 × U0126 (p=0.0394). More in-depth, while the intra-PVN nesfatin-1 treated group showed a significant increase in iBAT thermogenesis compared to its control group (p=0.0003) and the group treated with intra-PVN U0126 before intra-PVN nesfatin-1 (p=0.0320), the latter showed no difference in iBAT thermogenesis compared to its control group (U0126) (p>0.9999). Similarly, treatment with intra-PVN nesfatin-1 elicited a strong increase in the core body temperature compared to the control group (Figure 3.2C), as indicated by the effect of nesfatin-1 (p=0.0433), but no effect of time (p=0.3796) or interaction of nesfatin-1 × time (p=0.7192). Additionally, intra-PVN pretreatment with U0126 did not affect the core body temperature, as suggested by the effect of U0126 (p=0.1651) and U0126 × time (p=0.3307), but showed a trend towards interaction with nesfatin-1 (nesfatin-1 × U0126; p=0.0829). Similarly, analysis of

the AUC (Figure 3.2D) showed an effect of intra-PVN nesfatin-1 (p=0.0393), no effect of U0126 (p=0.1678), and a trend towards interaction of nesfatin-1 × U0126 (p=0.0665).

Lastly, treatment with intra-PVN nesfatin-1 did not affect heat dissipation through the tail (Figure 3.2E) as suggested by a lack of effect of intra-PVN nesfatin-1 injections (p=0.1522). Pretreatment with U0126 also did not affect heat dissipation, as suggested by a lack of effect of U0126 pretreatment (p=0.7741); a weak trend towards interaction of nesfatin-1 × U0126 (p=0.1001) could be seen. Analysis of the AUC (Figure 3.2F) similarly showed no effect of nesfatin-1 (p=0.1686), no effect of U126 (p=0.7859), and a weak trend for nesfatin-1 × U0126 (p=0.1074).

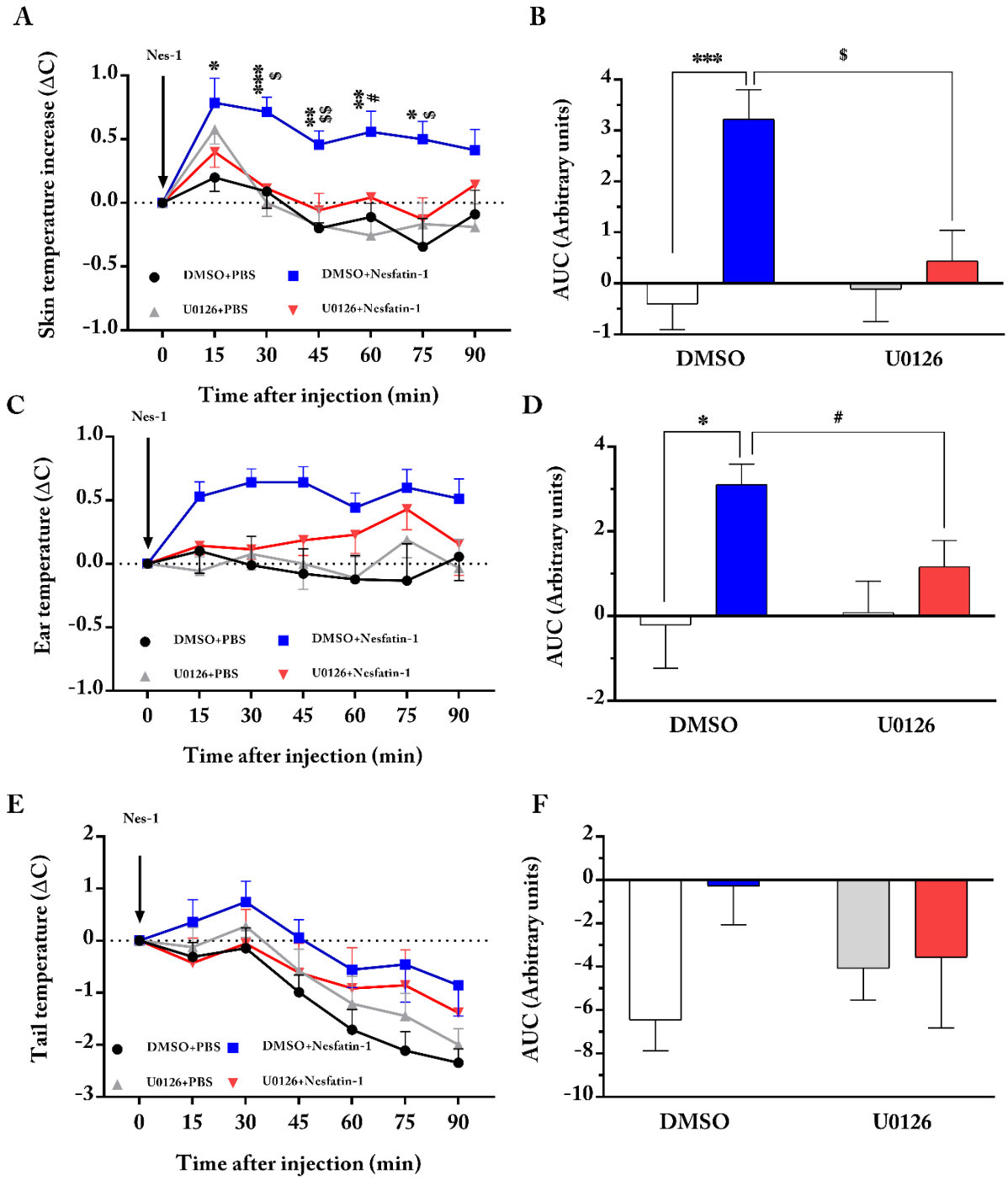

Figure 3.2.: Erk1/2 antagonism of intra-PVN nesfatin-1 effects on light phase iBAT thermogenesis.
Effect of pretreatment with U0126 (25ng/rat) on intra-PVN administration of nesfatin-1 (50 pmol/rat) or PBS as a control solution on light phase iBAT thermogenesis on *ad libitum* fed rats (7-9/group) measured over 90 minutes. A) iBAT. C) Ear canal. E) Tail temperature. 3-way ANOVA, *P < 0.05, **P < 0.01, ***P < 0.001 vs DMSO+PBS; #P < 0.1, $P < 0.05, $$P < 0.01 against U0126+nesfatin-1. (Newman–Keuls test) and respective AUC B, D, F). 2-way ANOVA, #P < 0.1, *P < 0.05, *P < 0.01 (Sidak's multiple comparison test). All data are represented as mean ± SEM.

Experiment IV: effects of viral knockdown of melanocortin type 4 receptors (MC4R) on intra-PVN nesfatin-1 induced effects on energy homeostasis.

Experiment IVa: model characterization

The involvement of MC4R in the NTS with regards to intra-PVN nesfatin-1 effects was studied in a knockdown model for these receptors. Male animals were injected intra-NTS with an AAV carrying an shRNA sequence against the MC4R in the NTS (or a scramble shRNA sequence used as control) and their phenotype was monitored for six weeks. Intra-NTS knockdown of MC4R resulted in a subtle but overall significant reduction of body weight (Figure 4.1A) as indicated by a significant effect of the knockdown ($p=0.023$) and time ($p<0.0001$). No interaction knockdown × time was found ($p=0.99$). Intra-NTS knockdown of MC4R also resulted in overall significantly higher food intake when normalized for body weight (Figure 4.1B), as indicated by a significant effect of the knockdown ($p=0.0412$) and time ($p<0.0001$). No interaction knockdown × time was found ($p=0.4619$). No difference in body fat percentage could be found at any time point measured (Figure 4.1C), as indicated by a lack of effect of the knockdown ($p=0.9035$). Finally, intra-NTS knockdown of MC4R did not affect basal iBAT thermogenesis (Figure 4.1D) in week four after knockdown as indicated by the lack of effect of the knockdown ($p=0.6560$) and dry heat loss measured during the light phase ($p=0.51$) (week six) (Figure 4.1E). Notably, in this latter experiment a significant interaction knockdown × time was found ($p=0.0019$).

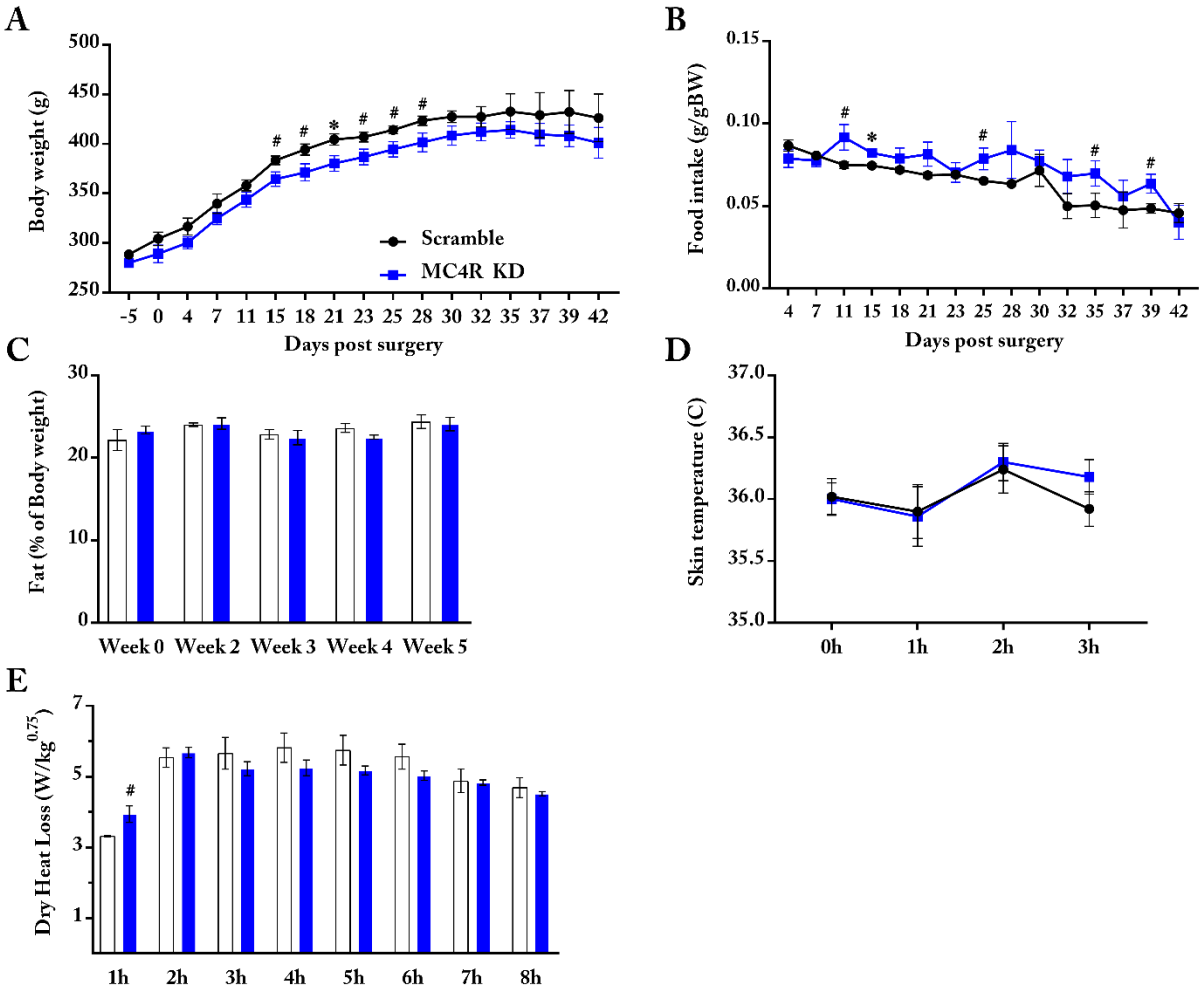

Figure 4.1.: Phenotyping of the mNTS MC4R knockdown model.

Animals (7-9/group) were monitored over 6 weeks following surgery. A) Bodyweight development. B) Food intake normalized per body mass. C) Fat mass. D) Light phase iBAT temperature. E) Dry heat loss during direct calorimetry. 2-way ANOVA, #P < 0.1 *P < 0.05, (Student's *t*-test). All data are represented as mean ± SEM.

Experiment IVb: effects of intra-NTS MC4R on intra-PVN nesfatin-1 induced iBAT thermogenesis

As in experiment IIc and IIIb, thermal imaging of the iBAT, ear canal, and tail was performed every 15 minutes for a total of 90 minutes, during the light phase, in animals fed *ad libitum* after injection of intra-PVN or nesfatin-1 or PBS as a control solution. In intra-NTS scramble animals, similarly to previous experiments intra-PVN treatment with nesfatin-1, nesfatin-1 induced a strong increase in iBAT thermogenesis compared to control animals (Figure 4.2A) as indicated by the effect of nesfatin-1

(p=0.0028), time (p<0.0001) but lack of interaction of nesfatin-1 × time (p=0.3223). Analysis of the single time points showed a significantly increased iBAT thermogenesis at 15 minutes (p=0.0351), 45 minutes (p=0.0050), and 60 minutes (p=0.0073), with a trend approaching significance at 30 minutes (p=0.0650). While intra-NTS MC4R did not affect iBAT thermogenesis (p=0.1490) a trend approaching significance for an interaction nesfatin-1 × knockdown was found (p=0.0681). Accordingly, in MC4R knockdown animals, intra-PVN administration of nesfatin-1 failed to elevate iBAT thermogenesis at every time point except for the 45 minutes timepoint, where a trend approaching significance could be spotted (p=0.0569). Furthermore, scramble animals treated with intra-PVN nesfatin-1 showed higher iBAT thermogenesis than MC4R knockdown animals treated with intra-PVN nesfatin-1 at 45 minutes (p=0.0300) and 60 minutes (p=0.0114). Analysis of the AUC (Figure 4.2B) confirms these results, highlighting a strong effect of intra-PVN nesfatin-1 in increasing iBAT thermogenesis (p=0.0033), and an interaction nesfatin-1 × knockdown was found (p=0.0614) despite no significant effect of the knockdown *per se* (p=0.1138). Further analysis showed how intra-PVN nesfatin-1 in scramble animals significantly increased iBAT thermogenesis both when compared to their controls (p=0.0420) and when compared to intra-PVN nesfatin-1 in MC4R knockdown animals (p=0.0258). Additionally, no difference between intra-PVN PBS and intra-PVN nesfatin-1 was found in MC4R knockdown animals (p=0.3679).

Mirroring the iBAT, intra-PVN treatment with nesfatin-1 induced a strong increase in core body temperature compared to control animals (Figure 4.2C) as indicated by a significant effect of nesfatin-1 (p=0.0165), time (p<0.0001) but lack of interaction of nesfatin-1 × time (p=0.1649). The single time-point analysis revealed a significant increase at 15 minutes (p=0.0016) and 60 minutes (p=0.0160) with a trend approaching significance at 45 minutes (p=0.0917). Once again, while intra-NTS MC4R did not affect also core body temperature (p=0.2514) a strong interaction nesfatin-1 × knockdown was present (p=0.0073). Accordingly, intra-PVN nesfatin-1 in MC4R knockdown animals failed to elevate core body temperature at every time point; additionally, they also displayed a significantly lower core body temperature compared to intra-PVN nesfatin-1 in scramble animals at 15 minutes (p=0.0193), with a trend approaching

significance at 45 minutes (p=0.0569) and 60 minutes (p=0.0776). Analysis of the AUC (Figure 4.2D) confirmed this result, showing a strong effect of intra-PVN nesfatin-1 in elevating core body temperature (p=0.0183) and an interaction nesfatin-1 × knockdown (p=0.0090) with no significant effect of the knockdown (p=0.2097). Once, again, intra-PVN nesfatin-1 in scramble animals significantly increased core body temperature both when compared to their controls (p=0.0039) and when compared to intra-PVN nesfatin-1 in MC4R knockdown animals (p=0.0263). No difference between intra-PVN PBS and intra-PVN nesfatin-1 was found in MC4R knockdown animals (p=0.9362).

Lastly, intra-PVN nesfatin-1 did not affect heat dissipation through the tail (Figure 4.2E) as suggested by a lack of effect of intra-PVN nesfatin-1 (p=0.594). Intra-NTS MC4R knockdown also did not affect heat dissipation via the tail (p=0.5139); no interaction nesfatin-1 × knockdown was found (p=0.5462). Analysis of the AUC (Figure 4.2F) similarly showed no effect of nesfatin-1 (p=0.5432), MC4R knockdown (p=0.5139) or interaction nesfatin-1 × knockdown (p=0.5059).

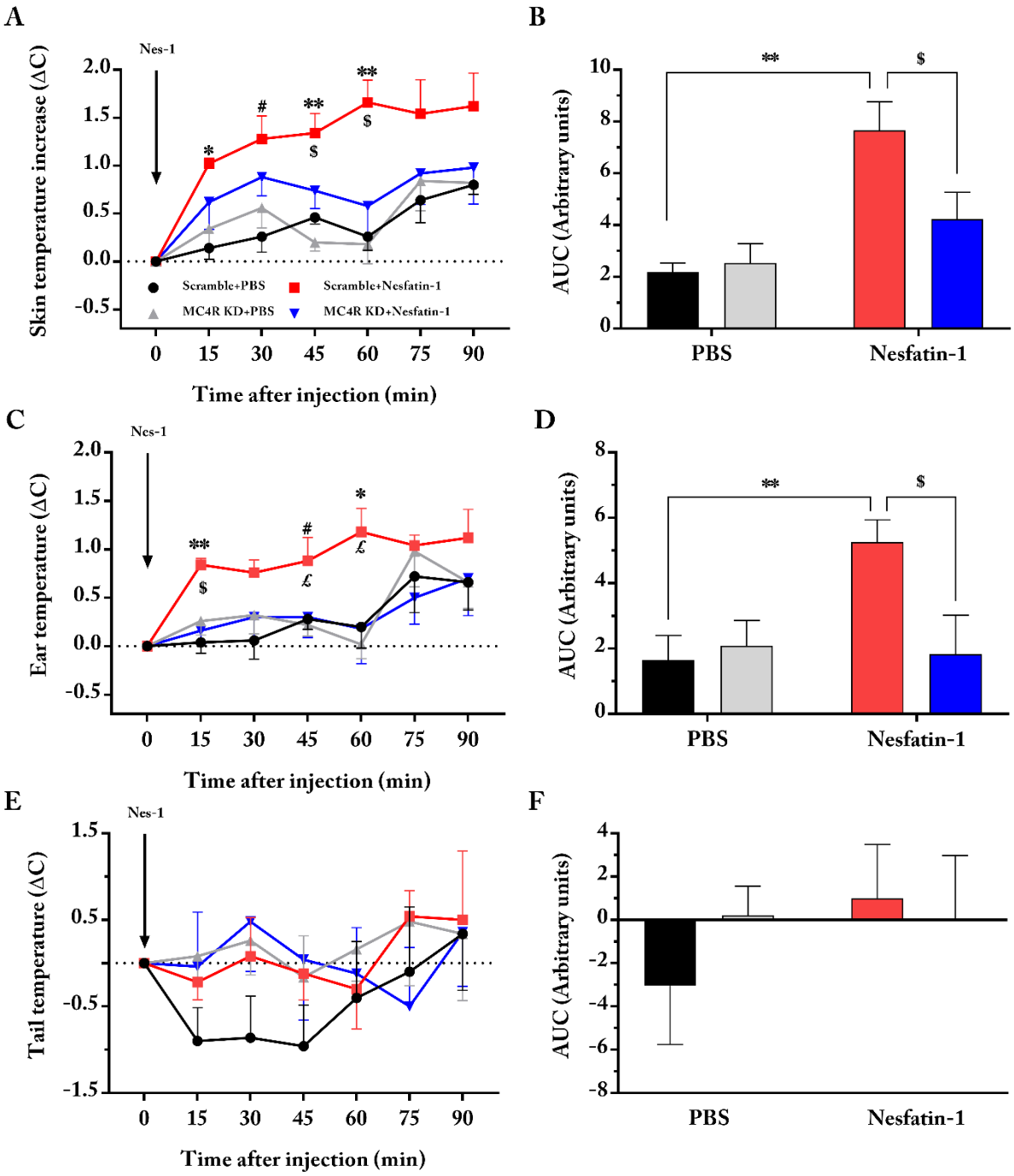

Figure 4.2.: MC4R knockdown effects on intra-PVN nesfatin-1 light phase iBAT thermogenesis.
Effect of MC4R knockdown on intra-PVN administration of nesfatin-1 (50 pmol/rat) or PBS as a control solution on light phase iBAT thermogenesis on *ad libitum* fed rats (5/group) measured over 90 minutes. A) iBAT. C) Ear canal. E) Tail temperature. 3-way ANOVA, #P < 0.1, *P < 0.05, **P < 0.01, ***P < 0.001 vs Scramble+PBS; £P < 0.1, $P < 0.05, $$P < 0.01 against MC4R Knockdown+nesfatin-1. (Newman–Keuls test); and corrispetive AUC B, D, F). 2-way ANOVA, $P < 0.05 against MC4R Knockdown+nesfatin-1; *P < 0.05, *P < 0.01 vs Scramble+PBS (Sidak's multiple comparison test).
All data are represented as mean ± SEM.

Experiment V: role of NTS GLP-1 system on hedonic and homeostatic feeding behavior, and interaction with the NTS nesfatin-1 system

Experiment Va: effects of the blockade of NTS endogenous nesfatin-1 on hedonic feeding behavior, and interactions with the NTS GLP-1 system

The role of NTS endogenous nesfatin-1 in hedonic food intake and its interaction with the NTS GLP-1 system was studied in a progressive ratio schedule of reinforcement task (PR) during the light phase. Both male and female animals fed *ad libitum* were injected intra-NTS with Nes-1 Ab or rabbit IgG (as a control solution) 30 minutes before intra-NTS treatment with Ex4 or artificial cerebrospinal fluid (aCSF) as a control solution. In male animals (Figure 5.1A), treatment with intra-NTS Ex4 elicited a reduction in the number of pellets earned during the PR task ($p=0.0337$), while no effect of the pretreatment with intra-NTS Nes-1 Ab ($p=0.9268$) or interaction Ex4 × Nes-1 Ab ($p=0.6469$) was found. Treatment with intra-NTS Ex4 also showed a trend approaching significance ($p=0.067$) in reducing the breakpoint (Figure 5.1B; as in, the last completed series of presses to obtain a reward). While no effect of the pretreatment with intra-NTS Nes-1 Ab could be found ($p=0.7946$), the interaction Ex4 × Nes-1 Ab also showed a trend approaching significance ($p=0.0754$). Post hoc comparison shows a significant difference for Ex4 in reducing the breakpoint in the group pretreated with control IgG ($p=0.0446$) but not in the group pretreated with intra-NTS Nes-1 Ab ($p=0.3235$). Similarly, treatment with intra-NTS Ex4 (Figure 5.1C) also showed a trend ($p=0.09268$) in reducing active lever presses (as in, the lever coupled with the release of a pellet), while no effect of Nes-1 Ab ($p=0.7571$) or interaction Ex4 × Nes-1 Ab ($p=0.2300$) could be found.

Treatment with intra-NTS Ex4 (Figure 5.1D) did not affect inactive lever presses ($p=0.09268$; as in, the lever whose press was not coupled with the release of a pellet), but a trend approaching significance ($p=0.0652$) for Nes-1 Ab as well as a trend for the interaction Ex4 × Nes-1 Ab ($p=0.0911$) could be found. Post hoc comparison shows a significant difference for Ex4 in reducing inactive lever presses in the group

pretreated with intra-NTS Nes-1 Ab (p=0.0446) but not in the group pretreated with control IgG (p=0.3235).

Treatment with intra-NTS Ex4 elicited a reduction in horizontal (locomotory) activity (Figure 5.1E; p=0.0337), while no effect of the pretreatment with intra-NTS Nes-1 Ab (p=0.1758) or interaction EX4 × Nes-1 Ab (p=0.4980) was found. The post-hoc comparison shows a trend approaching significance for Ex4 in horizontal activity in the group pretreated with intra-NTS Nes-1 Ab (p=0.0794) but not in the group pretreated with control IgG (p=0.3797). Lastly, neither treatment with intra-NTS Ex4 (p=0.4540), nor intra-NTS Nes-1 Ab (p=0.2204) affected head entries (Figure 5.1F; as an index of food-seeking behavior), and no interaction EX4 × Nes-1 Ab (p=0.5886) could be found.

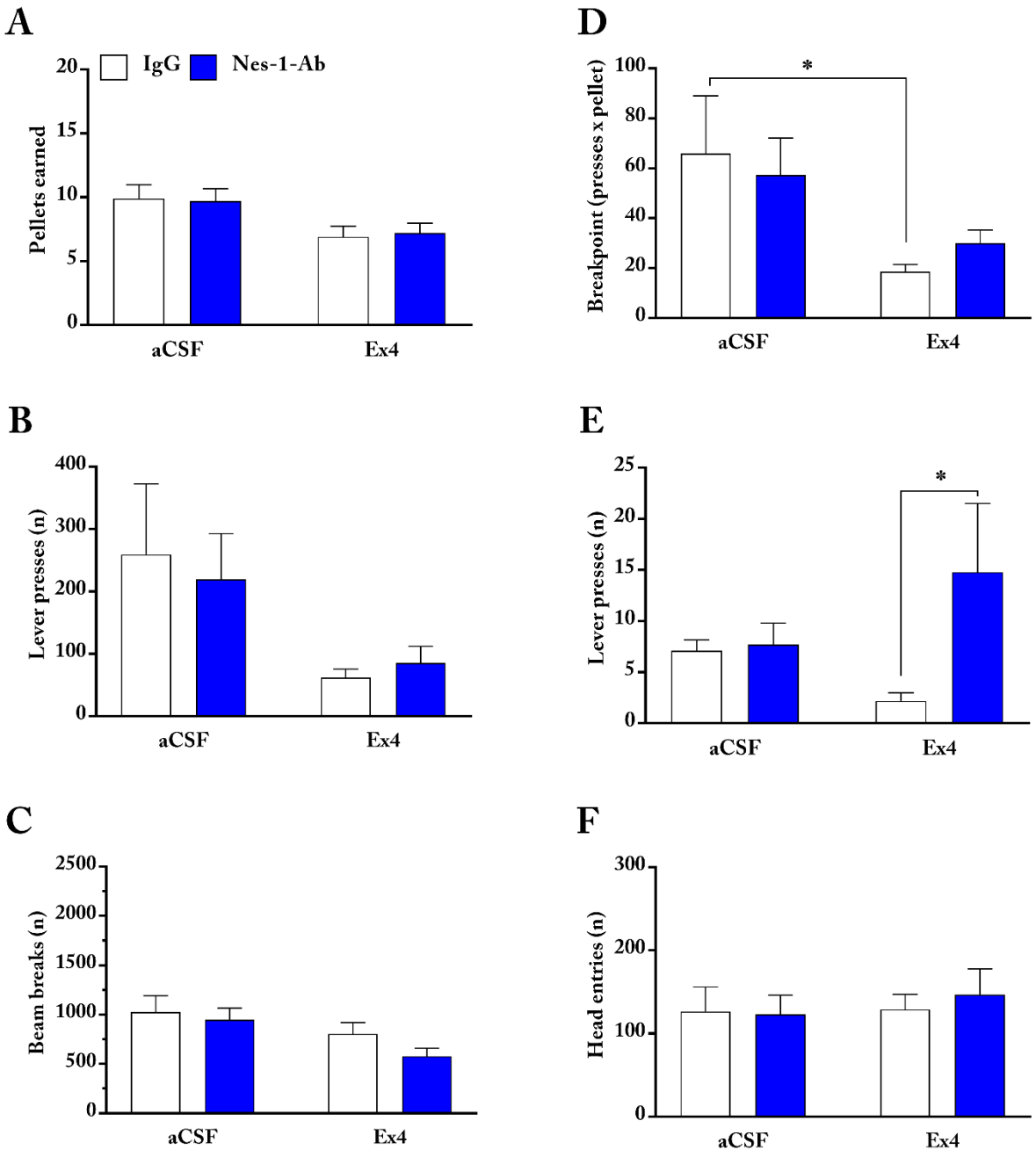

Figure 5.1.: Role of endogenous NUCB2/nesfatin-1 in the NTS on hedonic food behavior and interaction with the GLP-1 system in male animals.

Effect of the administration of NUBC2/nesfatin-1 directed antibodies (0.1µg) or IgG as a control solution (0.1µg), and of the pretreatment with Exendin-4 (0.1µg) on the number of levers presses A) rewards earned. B) breakpoint. C) active lever presses. D) inactive lever presses. E) horizontal activity. And F) head entries in *ad libitum* fed male rats in the progressive ratio schedule of reinforcement (9-10/group). 2-way ANOVA, *P < 0.05 (Sidak's multiple comparison test). All data are represented as mean ± SEM.

In female animals (Figure 5.2A), treatment with intra-NTS Ex4 elicited a reduction in the number of pellets earned during the PR task ($p=0.0027$), while no effect of the pretreatment with intra-NTS Nes-1 Ab ($p=0.9353$) or interaction Ex4 × Nes-1 Ab ($p=0.5871$) was found. Treatment with intra-NTS Ex4 also significantly reduced the breakpoint (Figure 5.2B; $p=0.0016$), while no effect of the pretreatment with intra-NTS Nes-1 Ab ($p=0.7786$) or interaction EX4 × Nes-1 Ab ($p=0.9521$) could be found. Similarly, treatment with intra-NTS Ex4 (Figure 5.2C) also reduced active lever presses ($p=0.0068$), while no effect of Nes-1 Ab ($p=0.9871$) or interaction EX4 × Nes-1 Ab ($p=0.5681$) could be found.

Treatment with intra-NTS Ex4 (Figure 5.2D) strongly reduced inactive lever presses ($p=0.0097$) while no effect of Nes-1 Ab ($p=0.2286$) or interaction Ex4 × Nes-1 Ab ($p=0.1726$) could be found.

Both treatment with intra-NTS Ex4 (Figure 5.2E; $p=0.0061$) and pretreatment with intra-NTS Nes-1 Ab ($p=0.0251$) strongly reduced horizontal (locomotory) activity and a trend approaching significance for the interaction EX4 × Nes-1 Ab ($p=0.0693$) was found. Post-hoc comparison shows a significant effect for Ex4 in reducing active lever presses during the PR task in the group pretreated with control IgG ($p=0.0017$) but not in the group pretreated with intra-NTS Nes-1 Ab ($p=0.1146$). Furthermore, pretreatment with intra-NTS Nes-1 Ab significantly reduced *per se* horizontal activity compared to control IgG ($p=0.0106$).

Lastly, treatment with intra-NTS Ex4 also significantly reduced head entries (Figure 5.2F; $p=0.0137$), while intra-NTS Nes-1 Ab had no effect ($p=0.2929$). No interaction EX4 × Nes-1 Ab ($p=0.7906$) could be found.

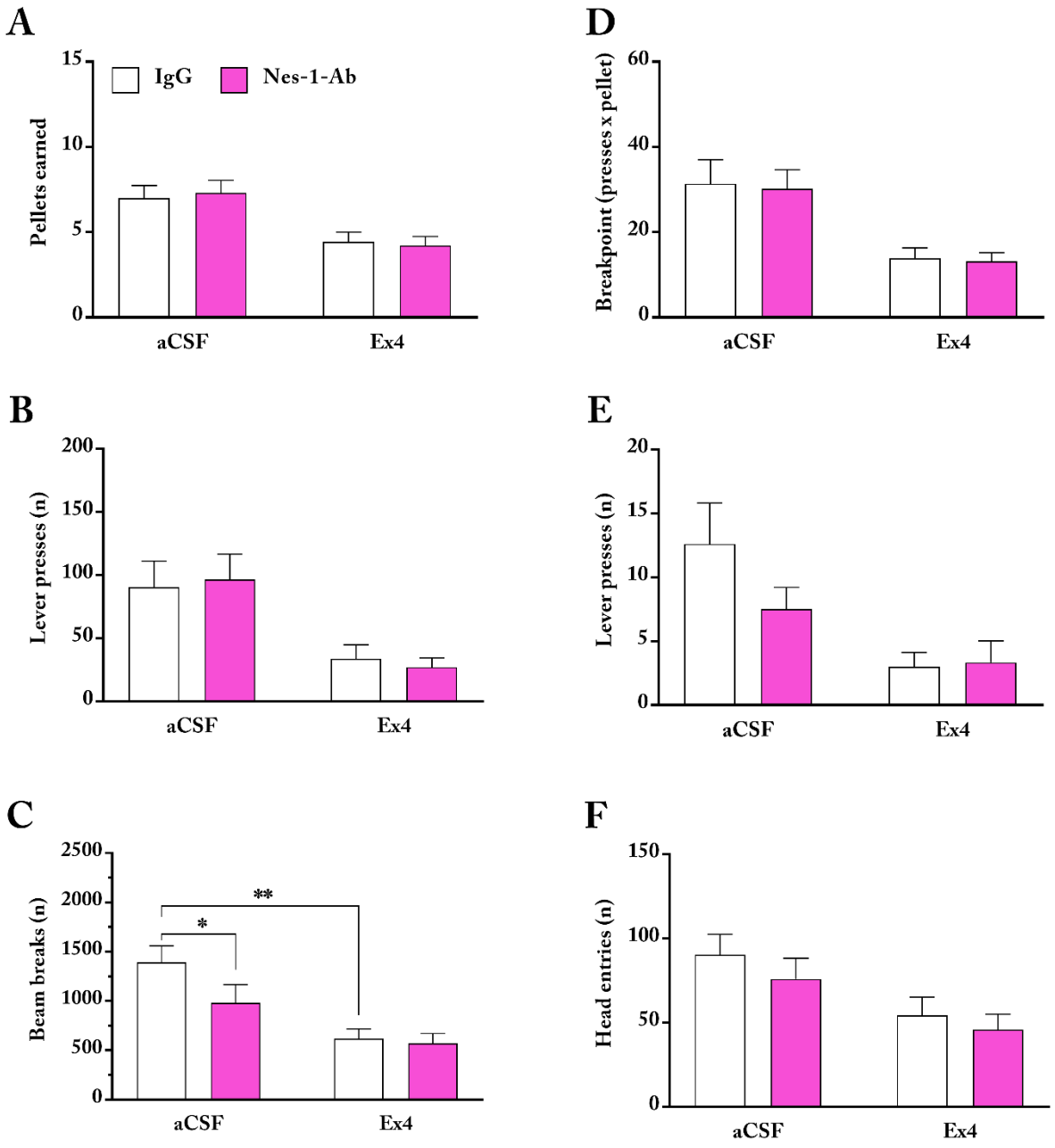

Figure 5.2.: Role of endogenous NUCB2/nesfatin-1 in the NTS on hedonic food behavior and interaction with the GLP-1 system in female animals.

Effect of the administration of NUBC2/nesfatin-1 directed antibodies (0.1µg) or IgG as a control solution (0.1µg), and of the pretreatment with Exendin-4 (0.1µg) on the number of levers presses A) rewards earned. B) breakpoint. C) active lever presses. D) inactive lever presses. E) horizontal activity. And F) head entries in *ad libitum* fed female rats in the progressive ratio schedule of reinforcement (9-10/group). 2-way ANOVA, *P < 0.05, **P < 0.01 (Sidak's multiple comparison test). All data are represented as mean ± SEM.

Experiment Vb: effects of the blockade of NTS endogenous nesfatin-1 on homeostatic feeding behavior, and interactions with the NTS GLP-1 system

Parallel to experiment IVa, homeostatic food intake was studied over 24h in both male and female animals fed *ad libitum,* after being injected intra-NTS with Nes-1 Ab or rabbit IgG (as a control solution) 30 minutes before intra-NTS treatment with Ex4 or aCSF (as a control solution).

In male animals (Figure 5.3A), treatment with intra-NTS Ex4, the treatment induced a strong reduction in food intake over 24 hours after its injection ($p=0.0020$). Pretreatment with intra-NTS Nes-1 Ab blocked this effect, as indicated by the effect of the Nes-1 Ab ($p=0.0005$) and the interaction EX4 × Nes-1 Ab ($p=0.0020$). Post hoc comparison showed no effect *per se* of the Nes-1 Ab on food intake, compared to the control IgG treated group ($p=0.8973$). Additionally, in animals pretreated with control IgG, intra-NTS treatment with Ex4 induced a strong reduction in food intake compared to the aCSF treated animals ($p<0.0001$), but only a trend approaching significance in reducing food intake could be found in the group pretreated with intra-NTS Nes-1 Ab ($p=0.0576$).

Bodyweight change over 24 hours was also monitored (Figure 5.3B). Animals treated with intra-NTS Ex4 showed a strong reduction in body weight 24 hours after the injection ($p<0.0001$). Pretreatment with intra-NTS Nes-1 Ab blocked this effect, as indicated by the effect of the Nes-1 Ab ($p<0.0001$) and the interaction EX4 × Nes-1 Ab ($p=0.0002$). Post hoc comparison showed no effect *per se* of the Nes-1 Ab on body weight change, compared to the control IgG treated group ($p=0.9491$). Additionally, in animals pretreated with control IgG, intra-NTS treatment with Ex4 induced a strong reduction in body weight compared to the aCSF treated animals ($p<0.0001$), but this effect was completely blocked in the group pretreated with intra-NTS Nes-1 Ab ($p=0.1658$).

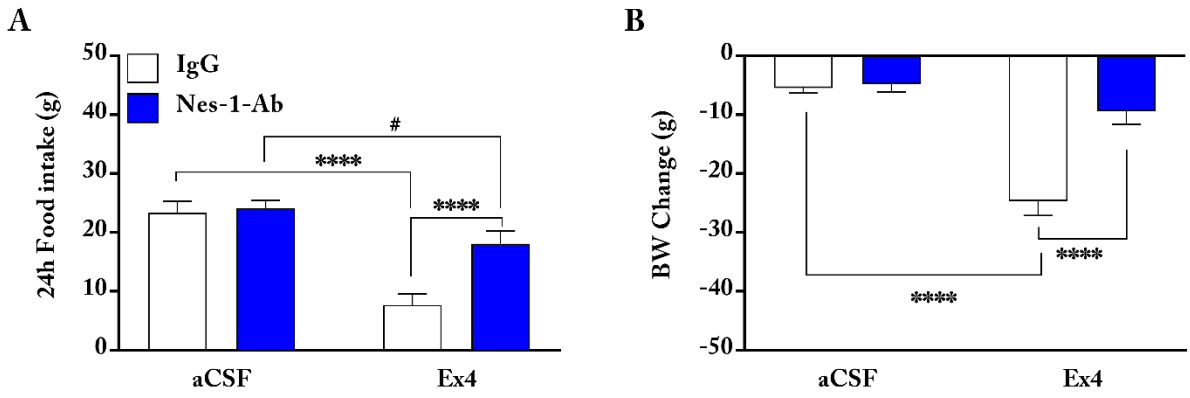

Figure 5.3.: Role of endogenous NUCB2/nesfatin-1 in the NTS on homeostatic food behavior and interaction with the GLP-1 system.

Effect of the administration of NUBC2/nesfatin-1 directed antibodies (0.1µg) or IgG as a control solution (0.1µg), and of the pretreatment with Exendin-4 (0.1µg) on A) 24 hours food intake; B) 24 hours body weight change; in *ad libitum* fed male rats (10/group). 2-way ANOVA, #P < 0.1 ****P < 0.0001 (Sidak's multiple comparison test). All data are represented as mean ± SEM.

In female animals (Figure 5.4A), treatment with intra-NTS Ex4 induced a strong reduction in food intake over 24 hours after its injection ($p<0.0001$). This time, pretreatment with intra-NTS Nes-1 Ab did not block this effect, as suggested by the lack of effect of the Nes-1 Ab ($p=0.4176$) and interaction EX4 × Nes-1 Ab ($p=0.6698$).

Bodyweight change over 24 hours was also monitored (Figure 5.4B). Animals treated with intra-NTS Ex4 showed a strong reduction in body weight 24 hours after the injection ($p<0.0001$). Similar to the food intake experiment, pretreatment with intra-NTS Nes-1 Ab did not block this effect, as indicated by a trend of the Nes-1 Ab ($p=0.0968$) and the lack of interaction EX4 × Nes-1 Ab ($p=0.6972$). Post hoc comparison showed intra-NTS treatment with Ex4 induced a strong reduction in body weight over 24 hours compared to aCSF in the control IgG pretreated group ($p=0.0035$) and the group pretreated with intra-NTS Nes-1 Ab ($p=0.0184$).

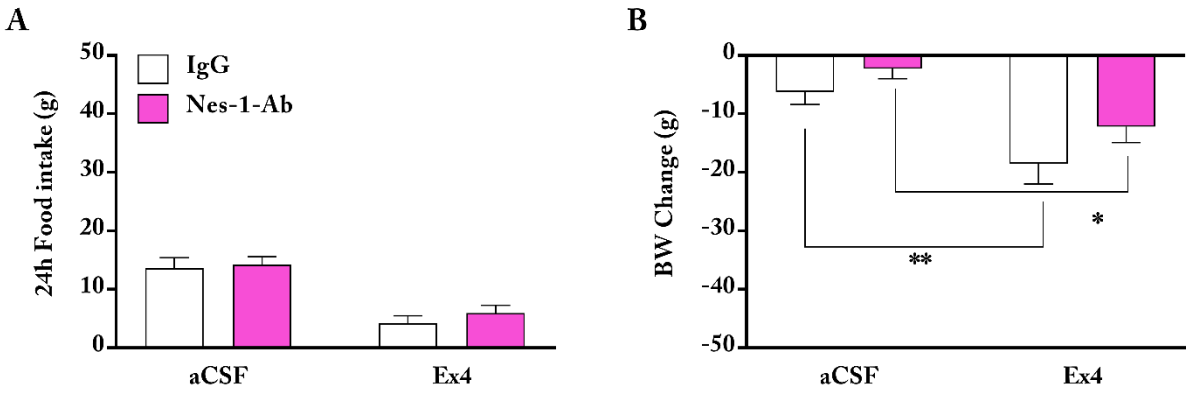

Figure 5.4.: Role of endogenous NUCB2/nesfatin-1 in the NTS on homeostatic food behavior and interaction with the GLP-1 system

Effect of the administration of NUBC2/nesfatin-1 directed antibodies (0.1µg) or IgG as a control solution (0.1µg), and of the pretreatment with Exendin-4 (0.1µg) on A) 24 hours food intake; B) 24 hours body weight change; in *ad libitum* fed female rats (9-10/group). 2-way ANOVA, *P < 0.5 **P < 0.01, ***P < 0.001 (Sidak's multiple comparison test). All data are represented as mean ± SEM.

Experiment Vc: effects of NTS endogenous nesfatin-1 on dark phase homeostatic feeding behavior, and interactions with the NTS GLP-1 system

Lastly, a short term (3 hours) food intake experiment was conducted in the same cohort of male animals from experiment IVa and IVb, at the onset of the dark phase (Figure 5.5A). Treatment with intra-NTS Ex4 induced a trend towards reduced food intake over 3 hours after its injection (p=0.0799). Pretreatment with intra-NTS Nes-1 Ab did not block this effect (p=0.5092) but a significant interaction EX4 × Nes-1 Ab (p=0.0383) could be found. Post hoc comparison showed intra-NTS treatment with Ex4 induced a reduction in food intake over 3 hours compared to aCSF in the group pretreated with intra-NTS Nes-1 Ab (p=0.0220) but not in the control IgG pretreated group (p=0.7916).

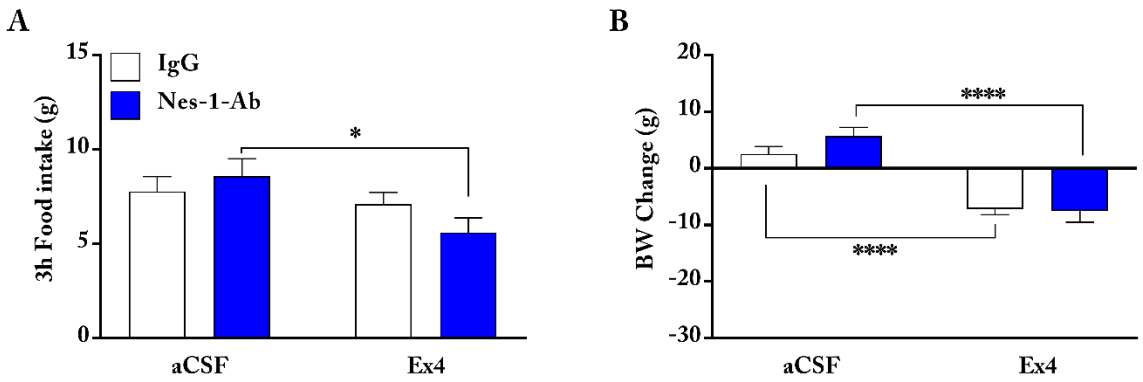

Figure 5.5.: Role of endogenous NUCB2/nesfatin-1 in the NTS on homeostatic food behavior and interaction with the GLP-1 system.

Effect of the administration of NUBC2/nesfatin-1 directed antibodies (0.1µg) or IgG as a control solution (0.1µg), and of the pretreatment with Exendin-4 (0.1µg) on A) 3 hours dark phase food intake; B) 3 hours body weight change; in *ad libitum* fed male rats (10/group). 2-way ANOVA, *P < 0.05 ****P < 0.0001 (Sidak's multiple comparison test). All data are represented as mean ± SEM.

Bodyweight change over 3 hours was also monitored (Figure 5.5B). Animals treated with intra-NTS Ex4 showed a strong reduction in body weight 3 hours after the injection ($p<0.0001$). Pretreatment with intra-NTS Nes-1 Ab did not block this effect, as suggested by the lack of effect of the Nes-1 Ab ($p=0.2556$) and interaction EX4 × Nes-1 Ab ($p=0.1572$). Post hoc comparison showed intra-NTS treatment with Ex4 induced a strong reduction in body weight over 3 hours compared to aCSF in both the control IgG pretreated group ($p<0.0001$) and in the group pretreated with intra-NTS Nes-1 Ab ($p<0.0001$). Lastly, treatment with intra-NTS Ex4 two hours before the sacrifice did not alter NTS NUCB2 expression in both males (Figure 5.6A; $p=0.4521$) and females (Figure 5.6B; $p=0.4115$).

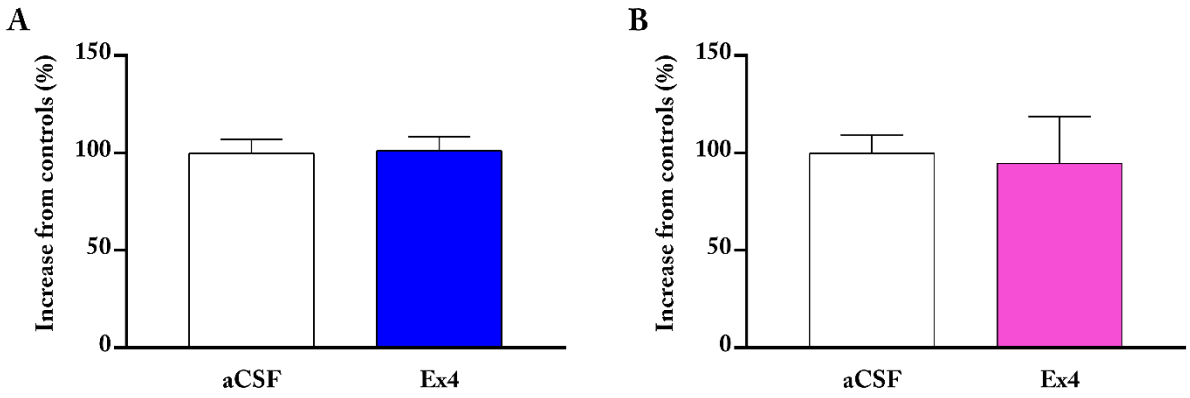

Figure 5.6.: Nucb2 mRNA expression in the NTS after Exendin-4 injection.
Effect of intra-NTS administration of Exendin-4 (0.1µg) or aCSF as a control solution on NTS Nucb2 mRNA expression (9-10/group) 2 hours after the injection. All data are represented as mean ± SEM.

Discussion

NUCB2/Nesfatin-1 is a peptide that has been associated with the physiological regulation of various aspects of energy metabolism but mainly characterized as an anorexigenic peptide (Oh-I et al., 2006) and promoter of energy expenditure (Dore, Levata, Gachkar, et al., 2017; K. Könczöl et al., 2012; Wernecke et al., 2014). Coherently with its proposed role, NUCB2/nesfatin-1 expression is well represented in both the periphery and central nervous system in areas involved in the regulation of energy homeostasis.

While nesfatin-1 (and its precursor NUCB2) participate in the regulation of feeding state and energy metabolism, the feeding state, in turn, affects the expression of NUCB2/nesfatin-1: endogenous levels of NUCB2/nesfatin-1 are reduced before a meal or by food deprivation and restored by refeeding, both in the brain (Garcia-Galiano et al., 2010; Kohno et al., 2008; Oh-I et al., 2006) and peripherally (Ramanjaneya et al., 2010; Stengel, et al., 2009) in the plasma and adipose tissue.

In the regulation of energy expenditure, nesfatin-1 promotes increased energy expenditure likely by increasing sympathetic nervous activity, as central nesfatin-1 application increases plasma catecholamines, mean arterial pressure, and renal sympathetic tone (Tanida & Mori, 2011; Yilmaz et al., 2015; Gina L. C.

Yosten & Samson, 2009) following both i.c.v. or intra-PVN administrations (Tanida et al., 2015; Tanida & Mori, 2011). In support of this hypothesis, the presence of NUCB2/nesfatin-1 is found in both sympathetic and parasympathetic preganglionic neurons, in the nucleus ambiguus, and Edinger-Westphal nucleus (K. S. Foo et al., 2008; Goebel-Stengel et al., 2011; Goebel et al., 2009), and site-specific injections of nesfatin-1 into the medial NTS (Mimee et al., 2012) or nucleus ambiguus (Brailoiu et al., 2013) have been reported to regulate cardiovascular functions, thus providing a link between nesfatin-1 and regulation of autonomic functions.

Accordingly, central administration of nesfatin-1 results in an increase in core body temperature (K. Könczöl et al., 2012), dry heat loss (Wernecke et al., 2014), and iBAT temperature (Dore, Levata, Gachkar, et al., 2017; Levata et al., 2019). These effects are due to an increased sympathetic outflow to the iBAT, likely mediated by the recruitment of downstream effectors like the central melanocortin system (among others). Accordingly, blockade of the central melanocortin receptors with i.c.v. injections of SHU9119 (a melanocortin receptor 3/4 antagonist) reduces the ability of i.c.v. nesfatin-1 to increase dry heat loss and iBAT temperature (Dore, Levata, Gachkar, et al., 2017), and β_3-adrenergic receptors blockade obtained with peripheral administration of SR 59230 A (a selective β_3-adrenergic receptors antagonist) blocks the ability of i.c.v. nesfatin-1 to increase iBAT temperature and weight loss (Levata et al., 2019).

However, a clear understanding of the underlying mechanisms of action of nesfatin-1 is still missing. Despite reports of interactions with $G_{i/o}$-protein-coupled receptors (Brailoiu et al., 2007, 2013; Suzuki et al., 2012), potassium (Dore et al., 2020; Maejima et al., 2017; Christopher J Price et al., 2008), and calcium channels (Brailoiu et al., 2007, 2013) a receptor for nesfatin-1 has yet to be identified. In addition, while several studies have reported interactions with the oxytocin (Maejima et al., 2009; Gina L C Yosten & Samson, 2010), CRH (Stengel et al., 2009), and serotoninergic (Nonogaki et al., 2008), in addition to the melanocortin system (Maejima et al., 2009) to be crucial for the anorectic effect of nesfatin-1, their involvement in mediating nesfatin-1's effect on energy expenditure is far less explored.

Experiment I: effect of feeding state on nesfatin-1 induced increase in energy expenditure in the light phase

In experiment I, direct calorimetry was employed to study the effect of feeding status on NUCB2/nesfatin-1-induced energy expenditure. *Ad libitum* fed or 24 hours food-deprived animals were injected with either nesfatin-1 or PBS (as a control solution) prior to an 8 hours direct calorimetry session. The i.c.v. application of nesfatin-1 in 24 hours food-deprived animals significantly increased dry heat loss (as a measure of energy expenditure) over 8 hours compared to i.c.v. PBS-treated animals, reaching its maximum effect at hour 4, confirming previous reports (Dore, Levata, Gachkar, et al., 2017; Wernecke et al., 2014). In a similar way, i.c.v. application of nesfatin-1 significantly increased dry heat loss over 8 hours compared to PBS-treated animals in *ad libitum* fed animals as well, reaching its maximum at hour 3 (Figures 1.1A). Although i.c.v. application of nesfatin-1 was unable to significantly affect body weight loss measured at the end of the direct calorimetry session (Figure A.1), a strong correlation between body weight loss and dry heat loss produced could be found in the nesfatin-1 treated groups (Figure 1.3A) but not in the control-treated groups (Figure 1.3B). As all the groups were weight-matched before undergoing direct-calorimetry, these results confirm that the bodyweight change is driven by nesfatin-1's action, likely this as a result of increased iBAT activity. Although alterations in locomotor activity could not be measured, this is unlikely to have played a role: previous experiments have shown that i.c.v. injection of nesfatin-1 (albeit at a smaller dose of 25 pmol) does not alter locomotor activity during the light or dark phase (K. Könczöl et al., 2012). Interestingly, analysis of the *ad libitum* fed and 24 hours food-deprived group separately showed a trend towards significance only in the latter group, with no correlation in the former group. As *ad libitum* fed animals had access to food until the very start of the direct calorimetry session, this discrepancy is likely to be caused by differences in meal consumption and consequent postprandial thermogenesis added over the thermogenic effects of nesfatin-1.

Lastly, i.c.v. treatment with nesfatin-1-induced a significantly higher increase in energy expenditure during the first 4 hours in *ad libitum* fed animals compared to i.c.v. nesfatin-1 treated 24 hours food-deprived animals. Notably, the dry heat loss in the *ad libitum* fed group remained (albeit not significantly) constantly above the dry heat loss of the 24 hours fasted group, ultimately resulting in an overall significantly higher dry heat loss (Figure 1.1B).

Considering only the nesfatin-1 treated groups of Experiment I, no significant difference could be found in terms of peak dry heat loss between *ad libitum* fed animals and 24 hours fasted animals when said peak was measured at any given time during the 8 hours session (Figure 1.2A). However, *ad libitum* fed animals showed a significantly quicker response to i.c.v. nesfatin-1 expressed as the time to reach 50% of their peak dry heat loss (Figure 1.2B) along with a trend in reaching their peak dry heat loss faster (Figure 1.2C).

This quicker onset in *ad libitum* fed animals could be linked to more readily available action of the putative downstream effectors of nesfatin-1. As mentioned, nesfatin-1-induced increase in energy expenditure has been primarily linked to the recruitment of the central melanocortin system, as co-administration of SHU9119 – an antagonist of the MC3/4 receptors – is able to fully block nesfatin-1's effect on dry heat loss (Dore, Levata, Gachkar, et al., 2017). The central melanocortin system is a well-established regulator of energy homeostasis that modulates both feeding behavior and energy expenditure (Ellacott & Cone, 2006; Jeong et al., 2014), and its close interaction with nesfatin-1, also in regard to other physiological systems, has been suggested by several studies. First, NUCB2/nesfatin-1 abundantly co-localizes with POMC in arcuate nucleus neurons (K. S. Foo et al., 2008); secondly, antagonism of the MC3/4 receptors via SHU9119 has been able to attenuate or block nesfatin-1 effects on food intake (Oh-I et al., 2006; Gina L. C. Yosten & Samson, 2009; Yuan et al., 2017), gastric motility (Z. L. Li et al., 2013; Wang et al., 2014; Luo Xu et al., 2015), sympathetic nerve outflow (Tanida & Mori, 2011), mean arterial pressure (Tanida & Mori, 2011; Yilmaz et al., 2015; Gina L. C. Yosten & Samson, 2009), and energy expenditure (Dore, Levata, Gachkar, et al., 2017). Importantly, in the same fashion as described before for nesfatin-1, also the

melanocortin system is influenced by changes in the metabolic state: fasting leads to a reduction in *Pomc* mRNA (Mizuno et al., 1998; Schwartz et al., 1997; Swart et al., 2002) – which serves as precursor for α-MSH and ACTH, physiological ligands for the melanocortin receptors – while at the same time upregulating prolylcarboxypeptidase (*Prcp*) mRNA, a protease which is degrading central α-MSH – that physiologically serves as an agonist of the MC3/4 receptors – and therefore decreases melanocortin receptor signaling (Kwon Jeong et al., 2013; Wallingford et al., 2009). Following the opposite pattern, levels of AgRP – which conversely serves as an inverse agonist of the MC3/4 receptors – are increased before a meal and during acute and chronic fasting to promote food intake and are lowered upon feeding (Mizuno et al., 1998, 1999). In addition, most of the brain areas that express melanocortin receptor are reached by both stimulatory POMC and inhibitory AgRP inputs (Bagnol et al., 1999; Haskell-Luevano et al., 1999), and these synapses show a high degree of plasticity in response to fasting and feeding (T. Liu et al., 2012; Yang et al., 2011). Finally, pharmacological agonism of the MC4 receptors in the brainstem and spinal cord has been shown to inhibit parasympathetic and stimulate sympathetic preganglionic neurons respectively. The resulting regulation of the sympathetic outflow to the periphery ultimately affects functions such as glucose homeostasis, energy expenditure, and thermogenesis (Sohn et al., 2013). In addition, retrograde transsynaptic tracing with a pseudo-rabies virus has identified specific MC4 receptors-expressing neurons in multiple nuclei of the central nervous system known to regulate the sympathetic outflow – such as the PVN, intermediolateral cell column (ILM), raphe pallidus (RPa), and dorsomedial hypothalamic nucleus (DMH) - to be connected to the iBAT (Voss-Andreae et al., 2007) providing both a functional and anatomical link between activation of the melanocortin and the sympathetic nervous system. Overall, a more responsive central melanocortin system during fed states could mediate the effects of nesfatin-1 in a quicker way compared to food deprived states.

A final consideration should go to the adaptation of the sympathetic nervous system activity in response to changes in metabolic state. Two days of fasting has been shown to markedly suppress sympathetic activity in the heart (James B. Young & Landsberg, 1977), pancreas, and liver (James B Young & Landsberg, 1979)

with a complete reversal of this effect upon refeeding. Conversely, three days of sucrose exposure (Young & Landsberg, 1977) markedly increases sympathetic activity in the heart. Interestingly, the impact of the metabolic state on sympathetic nervous system activity in the heart is nicely paralleled in the iBAT (J B Young et al., 1982). Such findings could be explained by a mechanism by which the body tries to conserve energy during fasting and to burn excess energy in response to overfeeding. Furthermore, the reduction in iBAT activity during fasting is unlikely to be due to a shortage of lipid substrate. Unlike what has just been described for heart, pancreas, liver, and iBAT, fasting can induce increased sympathetic activity in the adrenal medulla (J. B. Young et al., 1984), epididymal, and retroperitoneal white adipose tissue (James B. Young, 2003). This fasting-induced activation leads to an increased adrenaline secretion from the medulla and enhanced lipolysis, increasing substrate availability for the iBAT.

Therefore, the delayed onset of nesfatin-1's effects in increasing energy expenditure observed here in 24h food-deprived animals compared to *ad libitum* fed animals could be explained by the effects of fasting on both the central melanocortin system as well as the sympathetic nervous system. Nesfatin-1 relies on noradrenergic stimulation (Levata et al., 2019) and recruitment of the central melanocortin system (Dore, Levata, Gachkar, et al., 2017) to activate the iBAT and increase thermogenesis and energy expenditure. The fasting-induced diminished stimulatory activity of the central melanocortin system could ultimately result in reduced sympathetic outflow towards the periphery; along with reduced sympathetic activity in the iBAT, this could cause a delayed (Figure 1.2B) and less potent (Figure 1.1B) activation of the iBAT itself by i.c.v. administration of nesfatin-1.

Experiment II & III: effect of intra-PVN nesfatin-1 injections on energy homeostasis and role of the ERK1/2 system.

The central nervous system orchestrates the regulation of energy homeostasis. Within its structures, the hypothalamus is perhaps the best and most studied important in the central regulation of feeding and energy expenditure. Cues coming from relevant organs in the periphery (e.g. pancreas, liver, white adipose tissue)

inform the hypothalamus about the body's metabolic status, modulating feeding behavior accordingly. In this sense, the PVN is one of the most important nuclei: classically defined as "satiety center", its lesion leads to sustained overeating and consequently obesity (Leibowitz et al., 1981; Sims & Lorden, 1986), and thanks to the various peptides and hormone that it releases in the periphery are able to control processes such as stress response, thyroid and cardiovascular functions among others.

As the "main hub" of central energy homeostasis regulation, all signals which carry energy-related information converge here from both the periphery and other brain areas; once these signals are integrated, an appropriate response is generated - mainly by involving the autonomous nervous system – that ultimately regulates feeding behavior and energy expenditure (Roh et al., 2016). For example, both NPY/AgRP and POMC neurons from the arcuate nucleus send strong projections to the PVN, involving this area in both acute and long-term regulation of feeding responses, respectively (Atasoy et al., 2012; Fenselau et al., 2017). Additionally, the PVN is connected to various autonomic areas within the brain (namely the Edinger-Westphal nucleus, NTS, the dorsal motor nucleus of the vagus (DMX) and ILM) (Geerling et al., 2010; C.B. Saper et al., 1976; Swanson, 1977; Swanson et al., 1980), and to various organs in the periphery as well such as the pancreas (Jansen et al., 1997), liver (Stanley et al., 2010), white (Maryam Bamshad et al., 1998; Stanley et al., 2010), and brown adipose tissue (Song et al., 2008).

The PVN is also a site of utmost importance for nesfatin-1. Together with the lateral hypothalamic area, and the NTS, the PVN possesses the highest number of nesfatin-1 positive cells in both its magnocellular and parvocellular neuronal populations (Brailoiu et al., 2007; K. S. Foo et al., 2008; Oh-I et al., 2006). Here, nesfatin-1 can influence the excitability of PVN neurons by having both depolarizing and hyperpolarizing effects in nearly all of the subtypes of PVN neurons (C. J. Price et al., 2008). As nesfatin-1 is thought to be released mainly in a paracrine or autocrine fashion (Maejima et al., 2009) this suggests that nesfatin-1 release in the PVN is tightly regulated to allow control over the many functions that this peptide regulates.

Given the importance of the PVN for nesfatin-1's effects, in Experiment II we sought to expand the findings of Experiment I and investigate if the PVN would participate in mediating the effects of nesfatin-1 on food intake, energy expenditure, and iBAT thermogenesis. For this reason, in Experiment II, site-specific, intra-PVN injections of nesfatin-1 were employed exclusively in *ad libitum* fed animals. In addition, the role of the ERK1/2 system was also investigated.

Using the same experimental setup as in Experiment I, in Experiment IIb nesfatin-1 administered intra-PVN was able to significantly increase dry heat loss over 8 h compared to intra-PVN PBS-treated animals (Figure 2.2A) further supporting the hypothesis that the PVN is critical for the mediation of nesfatin-1's effect on energy expenditure, as its specific stimulation can fully replicate nesfatin-1's i.c.v. effect. This is in accordance with other studies in which microinjections of nesfatin-1 in the PVN mimicked the effects of i.c.v. application of nesfatin-1, reducing food intake (X. Chen et al., 2012; Maejima et al., 2009), and increasing sympathetic nerve activity (Tanida et al., 2015). Notably, no discernible differences in the increase in energy expenditure could be found between intra-PVN treated animals from Experiment IIb and i.c.v. treated animals from Experiment I in both in absolute values (i.c.v. ~5.89 $W/Kg^{0.75}$; intra-PVN ~5.73 $W/Kg^{0.75}$) or in magnitude (i.c.v. ~+17% over respective controls; intra-PVN ~+12.6% over respective controls). While the results from this study are the first to allow a direct comparison of PVN v.s. i.c.v. application with regards to energy expenditure, other aspects of sympathetic nerve activation have been studied before. In Tanida et al (Tanida et al., 2015), stimulation of the PVN with nesfatin-1 would elicit an increase in renal sympathetic nerve activity of lower magnitude compared to the same experimental setup carried over with i.c.v. injection of nesfatin-1 (Tanida & Mori, 2011). Despite a difference in the dose used (100 pmol in this study 200 pmol in Tanida's for i.c.v. stimulation, and 50 pmol in both studies for PVN stimulation), as in our study, only one PVN was pharmacologically stimulated as opposite to Tanida's stimulation of both PVNs, it is even more unexpected that the stimulation of additional brain areas that are likely reached by nesfatin-1 via the ventricular system did not yield larger effects on dry heat loss compared to the stimulation of the PVN alone.

For example, the medial NTS is a plausible target for mediating a nesfatin-1-driven modulation of sympathetic nerve activity. Similar to its applications to the PVN, stimulation with nesfatin-1 in the NTS can both depolarize and hyperpolarize its neurons (Mimee et al., 2012), ultimately leading to an increase in blood pressure and heart rate in urethane anesthetized rats (Mimee et al., 2012).

It could also be hypothesized that in both i.c.v. and intra-PVN injections, nesfatin-1 was able to push the thermogenic capacity of the animals to their physiological limit, either saturating downstream signaling pathways or the iBAT thermogenic capabilities. Notably, the existence of a thermogenic "ceiling" has been shown in mice exposed to severe cold (Hammond et al., 1994; Zhao et al., 2010). In these studies, mice were able to increase their thermogenic output in response to ever-decreasing temperature by increasing their food intake and – in the long term – iBAT mass. However, this increase was not infinite, and in response to harsh cold the mice thermogenic output was unable to compensate for the heat loss, finally resulting in body weight loss. In accordance with this hypothesis, co-administration of i.c.v. nesfatin-1 and leptin was unable to elevate thermogenesis compared to i.c.v. administration of nesfatin-1 or leptin alone in direct calorimetry experiments (Wernecke et al., 2014). In this study, due to the acute nature of the stimulation, it is tempting to speculate that a single injection of nesfatin-1 could push the iBAT to its thermogenic limit, as an increase in iBAT mass is not to be expected in an acute experiment. However, as cold exposure was not employed in this study, nor different doses of nesfatin-1 were tested, further experiments are necessary to validate this hypothesis.

Lastly, while the same dose (50 pmol) was used in both Tanida et al. (Tanida et al., 2015) and our study to stimulate the PVN, another difference lies in the i.c.v. one (100 pmol i.c.v. in this study; 200 pmol i.c.v. in Tanida et al). In addition, sympathetic nerve activity was not measured in our studies. Therefore, adding to what discussed above, the lack of difference between i.c.v. and PVN stimulation seen in this study could be due to technical limitation of our apparatus (e.g. not sensible enough) or because our measured parameter is not as affected by the site of stimulation as renal sympathetic nerve activity is instead.

In Experiment IIa, dark phase food intake was measured. Intra-PVN microinjection of nesfatin-1 was able to reduce cumulative food intake over 6 hours compared to intra-PVN PBS-treated animals (Figure 2.1A), with the effect reaching its peak already at the third hour (Figure 2.1B). Intra-PVN nesfatin-1 also prevented an increase in body weight compared to PBS-treated animals.

While this experiment is in agreement with previous observations (Maejima et al., 2009), more experiments are needed to shed light on the mechanism by which nesfatin-1 regulates food intake. As of date, a putative receptor for nesfatin-1 has still to be identified although the involvement of a G_i-protein coupled receptor as a downstream mediator is generally accepted. In fact, pretreatment with pertussis toxin abolishes the nesfatin-1 induced depolarization and Ca^{2+} influx in the cell (Brailoiu et al., 2007, 2013; Ozcan et al., 2016). Nesfatin-1 is also able to modulate Ca^{2+} influx through L- (Brailoiu et al., 2007; Ishida et al., 2012; Nakata et al., 2011) P/Q- (Brailoiu et al., 2007, 2013) N- (Iwasaki et al., 2009) type Ca^{2+} channels.

Following up the findings of Experiment IIa, we sought to investigate possible downstream mediators of nesfatin-1's effects, by investigating the participation of the extracellular signal-regulated kinase 1/2 (ERK1/2) in the central effects of nesfatin-1. The rationale for this is that the ERK1/2 system has been shown to participate in the regulation of feeding behavior. Similar to nesfatin-1, ERK1/2 is responsive to the nutritional status, as fasting has been shown to decrease pERK1/2 levels in the PVN (Morikawa et al., 2004) with refeeding reversing this effect (Ueyama et al., 2004). Glucose application to primary hypothalamic neurons dose-dependently increases pERK1/2 and increases *Pomc* expression in a pERK-dependent manner (Zhang et al., 2015). ERK1/2 is also part of the downstream signaling of the leptin receptor (Villanueva & Myers, 2008) and hypothalamic pERK1/2 mediates the anorectic effect of peripherally-administered leptin (Rahmouni et al., 2009). Finally, ERK1/2 is potently activated in the ARC and PVN after amphetamine treatment in rats (Yu et al., 2018).

ERK1/2 belongs to the mitogen-activated protein kinase (MAPK) family and its role is to transduce external cellular stimuli into appropriate intracellular response that regulate functions from cellular

proliferation and differentiation to senescence (Lake et al., 2016), and more. In brief, in response to external stimuli, a process of signal transduction is often initiated by receptor tyrosine kinases. This starts a series of intracellular processes (see (Lake et al., 2016; McKay & Morrison, 2007) for a detailed review on the mechanisms) that culminates in the phosphorylation of MAPK (pMAPK), activating it. In this active form, pMAPK targets and phosphorylates ERK1/2 into pERK1/2. Finally, pERK1/2 phosphorylates a large array of downstream targets (e.g. transcription factors), determining an appropriate intracellular response to the initiating signal.

Based on these evidences, we hypothesized a role for hypothalamic ERK1/2 as a downstream effector of intra-PVN nesfatin-1 effects on energy balance. In support of this hypothesis, i.c.v. administration of nesfatin-1 has been shown to increase levels of hypothalamic pERK1/2 in a dose and time-dependent manner (Tanida et al., 2015), suggesting that stimulation with nesfatin-1 can recruit the ERK1/2 either directly via its putative receptor or through a convergence of intracellular signaling pathways.

In experiment IIIa dark-phase food intake was studied in *ad libitum* fed rats treated using a similar experimental setup as in experiment IIa, with intra-PVN U0126 (a specific ERK1/2 inhibitor) administered prior to intra-PVN injections of nesfatin-1. Confirming our previous results, intra-PVN administration of nesfatin-1 potently reduced food intake over 6 hours and reduced body weight gain compared to control-treated animals (Figure 3.1A). Remarkably, while pretreatment with U0126 was unable to alter food intake or bodyweight change *per se*, it almost completely blocked the anorexigenic effect of nesfatin-1 (Figure 3.1A) and prevented nesfatin-1's induced loss in body weight (Figure 3.1B) with this effect lasting at the 24 hour time point (Figure A.3.1). The necessity of functional ERK1/2 signaling for the anorectic effects of nesfatin-1 seen in this experiment confirms previous *in vitro* findings showing a connection between NUCB2/nesfatin-1 and the ERK1/2 system. In fact, NUCB2/nesfatin-1 has been reported to enhance ERK phosphorylation (Z. Chen et al., 2018; Ishida et al., 2012; Tagaya et al., 2012; Yamada et al., 2010) while *Nucb2/nesfatin-1* mRNA is in concert stabilized in an ERK1/2-dependent way in HTB185 cells,

extending its half-life up to four times (Yamada et al., 2010). This effect was shown to be specific, as it could be blocked by pretreatment with PD98059, a specific ERK1/2 inhibitor. However, whether this implies direct phosphorylation as part of an intracellular signaling cascade of the putative nesfatin-1 receptor, or rather as a part of converging signaling events downstream of other systems recruited by nesfatin-1 (e.g. CRH, melanocortins, and more) remains to be clarified.

In support of the latter hypothesis, nesfatin-1 could recruit the ERK1/2 system in the hypothalamus through the activation of CRH neurons: treatment with nesfatin-1 upregulates the levels of pERK1/2 in a CRH-dependent way (Z. Chen et al., 2018), as this effect could be abolished by pretreatment with CP376395 – a CRH receptor type 1 antagonist. CRH receptors are G protein-coupled receptors, and their activation is linked to a number of signaling pathways including the activation of the MAPK-ERK1/2 system via an increase of intracellular cAMP and calcium. A similar mechanism has been proposed to recruit ERK1/2 in the NTS as a mediator of the effects of other anorectic factors such as cholecystokinin (CCK) (Sutton et al., 2004) and melanocortin receptor ligands (Sutton et al., 2005), following the activation of their respective receptors. Of note, CCK neurons in the NTS are also responsive to nesfatin-1, and nesfatin-1 itself is required for CCK's anorectic effect (Saito et al., 2016).

Finally, ERK1/2 in the arcuate nucleus has been shown to mediate leptin's effects in both feeding behavior and sympathetic activation of the iBAT (Rahmouni et al., 2009). However, the involvement of leptin as a downstream mediator of the effects of nesfatin-1 seen in this study is unlikely. First, nesfatin-1's effects have been proposed to be independent of leptin. For example, central nesfatin-1 can block food intake in Zucker fatty rats carrying a leptin receptor mutation (Oh-I et al., 2006), and intraperitoneal administration of nesfatin-1 does the same in db/db mice and mice fed a high-fat diet (Shimizu et al., 2009); similarly, the nesfatin-1-induced increase in sympathetic nerve activity and phosphorylation of ERK1/2 is preserved in both Zucker fatty rats and high-fat-diet fed mice (Tanida et al., 2015), suggesting that nesfatin-1 exerts its anorexigenic effects in a leptin-independent manner. Second, co-administration of leptin and nesfatin-1

fails to produce a larger effect on energy expenditure than nesfatin-1 or leptin administered alone, suggesting the possibility that the two molecules act through a common downstream signaling pathway (Wernecke et al., 2014). Third, it's rather the presence of hypothalamic nesfatin-1 that might be essential to the anorexigenic effect of leptin, as central administration of leptin failed to induce anorexia in PVN NUCB2/nesfatin-1 knockdown animals (Darambazar et al., 2015). In spite of this, antibodies directed against nesfatin-1 failed to suppress leptin-induced anorexia (Oh-I et al., 2006).

In summary, these results suggest that nesfatin-1 activates the ERK1/2 system to reduce food intake. Whether this happens either after activation of its putative receptor or as a downstream effector of other anorexigenic factors is an open question for future studies.

As previously mentioned, nesfatin-1 controls energy homeostasis not only by influencing feeding behavior but also by actively participating in the control of energy expenditure as well. I.c.v. injections of nesfatin-1 increase energy expenditure (K Könczöl et al., 2012; Wernecke et al., 2014), by increasing heat production from the iBAT (Dore, Levata, Gachkar, et al., 2017; Levata et al., 2019). Since in experiment IIa/b the effects of i.c.v. nesfatin-1 on energy expenditure and food intake could be fully recapitulated with intra-PVN stimulation, we hypothesized that the intra-PVN injections of nesfatin-1 would activate this area which would be sufficient to, in turn, recruit the iBAT and increase thermogenesis. Supporting this hypothesis, the PVN has been shown in multiple viral labeling studies to send extensive projections directed to BAT (M Bamshad et al., 1999; Cano et al., 2003; Madden & Morrison, 2009), placing the PVN in an ideal spot to modulate sympathetic outflow to this tissue.

In Experiment IIc intra-PVN microinjections of nesfatin-1 were employed to study a possible effect on iBAT activation. Intra-PVN application of nesfatin-1 led to a significant increase in iBAT temperature compared to PBS injected controls (Figure 2.3A, 2.3D) over 90 minutes. Similarly, also the temperature of the ear canal – measured as an index of core body temperature - was increased in nesfatin-1 treated animals compared to PBS injected controls (Figure 2.3B, 2.3E). Lastly, intra-PVN injection of nesfatin-1 did not

affect heat dissipation through the tail (Figure 2.3C, 2.3F) compared to PBS-injected controls, suggesting that the observed increase in core body temperature is due to an increased iBAT activity and not due to altered heat dissipation, in agreement with previous reports where no direct effect on the peripheral vascular system could be found (Dore, Levata, Gachkar, et al., 2017). These results complete those from experiment IIb, validating even further the role of the PVN as an essential mediator for nesfatin-1 effects. However, it should be noted that the relationship between stimulation of the PVN activation of the iBAT is unclear. On the one hand, the PVN sends projections to the iBAT either directly or through via the IML (François et al., 2019) or the Raphe pallidus, (where also nesfatin-1 is expressed) which are in turn targeting the iBAT; moreover, stimulation with glutamate in the PVN increases iBAT thermogenesis (Amir, 1990) and lesions of PVN attenuate fever (Caldeira et al., 1998), prompting to believe that activation of the PVN leads to activation of the iBAT. On the other hand, general activation of neurons in the PVN – either by treatment of the PVN with bicuculline (an antagonist of the $GABA_A$ receptors) or its stimulation with excitatory amino acids – has been shown to inhibit sympathetic outflow towards the BAT as well as BAT thermogenesis and febrile response (Madden & Morrison, 2009). In the PVN, nesfatin-1 has been shown to mediate both depolarization or hyperpolarization in nearly all neuronal subtypes (C. J. Price et al., 2008). As nesfatin-1 is thought to be released in an autocrine or paracrine fashion, this means that by either strictly localized release of nesfatin-1 to target single neuronal types, or by multiple receptors each exerting different responses. However, as a receptor for nesfatin-1 has not yet been discovered, it can only be speculated that in this study nesfatin-1 had a net inhibitory effect on the PVN neurons, allowing for the disinhibition of downstream targets.

Following the findings on food intake of Experiment II and IIIa, in Experiment IIIb the effects of nesfatin-1-induced iBAT activation were again investigated in rats treated with intra-PVN U0126 prior to intra-PVN nesfatin-1 (Figure 3.2A). Intriguingly, the iBAT activation over 90-minute induced by nesfatin-1 compared to controls was completely blocked by pretreatment with U0126 which by itself did not affect iBAT activation. Similar results were obtained also for the ear canal temperature (Figure 3.2C) where the

increase induced by nesfatin-1 was completely blocked by pretreatment with U0126. No differences could be found for the tail temperature (Figure 3.2E). These results show that the recruitment of ERK1/2 by hypothalamic nesfatin-1 is necessary not only for the reduction of food intake but also for the activation of the iBAT. I.c.v. administration of nesfatin-1 has been shown to mediate increase sympathetic outflow in kidneys (Tanida & Mori, 2011), liver, and WAT, in an ERK1/2-dependent way (Tanida et al., 2015). As proposed for the anorectic effects of nesfatin-1, ERK1/2 recruitment could happen via CRH neurons: in fact, blockade of CRH receptors with astressin 2B was able to abolish the increase in renal sympathetic outflow in response to i.c.v. nesfatin-1, although it was ineffective in modulating the nesfatin-1-induced increase in sympathetic outflow in the WAT.

Finally, given the anorexigenic and thermogenic effects of nesfatin-1, we investigated if its administration in the PVN would lead to changes in the expression of possible gene targets, in both the brain and the periphery. PVN, NTS, and iBAT target gene expression were analyzed at 4 hours after intra-PVN administration of nesfatin-1 as previously established (Dore, Levata, Gachkar, et al., 2017); an additional early time point (35 minutes post-intra-PVN nesfatin-1) was considered for the NTS and with regards to *c-fos* also for the PVN.

In line with our previous thermography results, iBAT temperature measured at 35 minutes post-treatment was significantly increased in the nesfatin-1 treated group compared to the control one (Figure 2.7A). This increase in iBAT temperature was associated with a significant increase of *c-fos* expression (an indirect marker for neuronal activity) in both the PVN (Figure 2.7E) and the NTS (Figure 2.7C) suggesting that PVN stimulation with nesfatin-1 leads to the activation of NTS neurons for the regulation of (at least) iBAT thermogenesis. These results are in agreement with previous observations that have shown increased *c-fos* expression in both the PVN and NTS following nesfatin-1 administration (Maejima et al., 2009). Additional studies (Blouet & Schwartz, 2012; Singru et al., 2012) have also shown that increase of *c-fos* in these two nuclei is also common after re-feeding, especially in the parvicellular PVN and medio-caudal

NTS, where nesfatin-1 immunoreactivity is well represented (Brailoiu et al., 2013; K. S. Foo et al., 2008). Interestingly, in this study, the increase in PVN and NTS *c-fos* and the increase of iBAT temperature 35 minutes following intra-PVN nesfatin-1 were strongly correlated in the NTS (Figure 2.7D) but not in the PVN (Figure 2.7F). One possible explanation for this result would be that the control of the sympathetic outflow towards the iBAT mediated by nesfatin-1 starts in the PVN and must pass through the NTS before reaching the periphery, rather than reaching the iBAT via the direct connections between this area and the PVN (M Bamshad et al., 1999; Cano et al., 2003; Madden & Morrison, 2009), as previously speculated. However, caution should be used when interpreting these results, and the involvement of the PVN in the matter explored with further studies: while extremely useful as a marker of neuronal activation, *c-fos* mRNA expression is sensitive to a wide array of stimuli that span from stress to intraparenchymal injection of substances, to mechanical injuries (Barros et al., 2015). Thus, it is plausible that the *c-fos* expression pattern seen in the PVN in this study might not be exclusively associated with nesfatin-1 effects alone.

In the periphery, plasma CTS after 35 minutes post-intra-PVN treatment with nesfatin-1 was significantly increased in the nesfatin-1 treated group compared to the control one (Figure 2.7B), possibly indicating the activation of the hypothalamus-pituitary-adrenal (HPA) axis as a consequence of the treatment. Peptides known to regulate food intake such as CRH, NPY, CCK, and others (Ueta et al., 2003) have been described to also participate in the regulation of stress-related and anxiety-related behaviors: for example, *Crf* expression is upregulated by both starvation (Harris et al., 2002) and obesity (Dallman et al., 2006), suggesting that the HPA axis activity and the metabolic state of the body deeply influence one another. Nesfatin-1 is no exception: its i.c.v. administration induces stress and anxiety-related behavior (Merali et al., 2008), and increases plasma levels of ACTH and CTS (Katalin Könczöl et al., 2010). In concert, plasma levels of nesfatin-1 are elevated in response to acute (but not chronic) stress (Y. Y. Xu et al., 2015). Furthermore, nesfatin-1 in the brainstem is co-expressed in the medullary A2 catecholamine cell group (Brailoiu et al., 2013; K. S. Foo et al., 2008), and in this area, intra-PVN nesfatin-1 led to increased expression of tyrosine hydroxylase (*Th*), the rate-limiting enzyme in the synthesis of catecholamines, both

at 35 minutes (Figure 2.8A) and 4 hours (Figure 2.5C) post-intra-PVN nesfatin-1 injection. Finally, NUCB2/nesfatin-1 neurons extensively co-localize with CRH neurons in the PVN (Brailoiu et al., 2013; K. S. Foo et al., 2008) and activate them (C. J. Price et al., 2008).

Stress-related stimuli cause the hypothalamus to release CRH, which in turn stimulates the pituitary to synthesize and release ACTH, ultimately increasing *Ucp1* mRNA expression and iBAT activity (Luijten et al., 2019; Van Den Beukel et al., 2014), offering a possible mechanism by which nesfatin-1 might be able to increase iBAT thermogenesis by increasing the activity of the HPA axis, at least in the short term.

In the NTS, intra-PVN nesfatin-1 was associated with increased expression of *Cart* at both 35 minutes (Figure 2.8C) and 4 hours (Figure 2.5B) post-injection, while its expression in the PVN was unchanged at 4 hours (Figure 2.4E). *Pomc* expression was unaltered in the NTS at both 35 minutes (Figure 2.8F) and 4 hours (Figure 2.5E) but showed a trend towards increased expression in the PVN at 4 hours (Figure 2.4B). In addition, *Npy* expression was increased in the NTS at 4 hours (Figure 2.5A) and unchanged in the PVN at the same time point (Figure 2.4D). These results are in contrast with previous reports that showed how nesfatin-1 would increase *Pomc* expression, decrease *Npy*, and leave *Cart* expression unchanged in the same areas examined here (Dore, Levata, Gachkar, et al., 2017; Wernecke et al., 2014). However, it should be considered that in these latter studies nesfatin-1 was delivered in the ventricular system, and had thus access to a wider variety of brain areas compared to the unilateral stimulation of the sole PVN used in this study. Therefore, the most parsimonious explanation for these differences would suggest that different brain nuclei respond differently to the presence of nesfatin-1 and that the effects on gene expression seen after ventricular delivery of nesfatin-1 are the net sum of these responses.

Lastly. While *Nucb2* mRNA was initially up-regulated in the NTS (albeit not significantly) at 35 minutes (Figure 2.8A), it was unchanged at 4 hours (Figure 2.5D) and significantly down-regulated in the PVN after 4 hours (Figure 2.4A). As this down-regulation happened at the site of injection, it is likely the consequence of a counter-regulatory mechanism in response to the administration of exogenous

nesfatin-1, while the early upregulation in the NTS is might be attributed to nesfatin-1 sensitive neurons in this area.

Administration of nesfatin-1 in the PVN led to an increase (albeit non-significant) in the iBAT of target genes involved in thermogenesis, Iodothyronine Deiodinase (*Dio2*), and Uncoupling-Protein 1 (*Ucp1*) (Figure 2.6B, 2.6E) 4 hours following treatment. The enzyme DIO2 is responsible for the intracellular conversion of thyroxine (T4) to the active 3,3,5-triiodothyronine (T3), whose increase in the brown adipocyte ultimately leads to increased *Ucp1* activity, and therefore increased thermogenesis (de Jesus et al., 2001). Accordingly, *Dio2* mRNA levels are upregulated in response to increases in iBAT temperature (Monge-Roffarello et al., 2014). *Ucp1*, a transmembrane protein whose main function is to dissipate the proton gradient generated in the electron transport chain, thus producing heat, represents the main marker of thermogenesis. Sub-chronic administration of nesfatin-1 has been reported to increase *Ucp1* expression (Yuan et al., 2017) and its activity. In this study, intra-PVN nesfatin-1 did not significantly alter the levels of *Ucp1* mRNA expression 4 hours after its injection (Figure 2.6E), suggesting that the increase of thermogenesis mediated by nesfatin-1 happens by enhancing its activity rather than promoting the production of new protein. However, at this timepoint a trend towards increased *Ucp1* mRNA expression could already be seen, possibly indicating that also acute nesfatin-1 might lead to increased *Ucp1* mRNA expression, but at a later time. Notably, a strong correlation between skin temperature increase at sacrifice (Figure A.3.3) and *Ucp1* mRNA levels was present in the nesfatin-1 treated group (Figure 2.6F) but not in the control one (Figure 2.6G).

Finally, levels of Cell Death-Inducing DFFA-Like Effector A (*Cidea*) an inhibitor of iBAT thermogenesis (Sharma et al., 2014) and peroxisomal proliferator-activated receptor gamma (*Pparg*) a gene associated with "browning" of white adipose tissue (Cannon & Nedergaard, 2004) remained unchanged in this study (Figure 2.6C, 2.6D) at 4 hours post-injection. A non-significant decrease of Peroxisome proliferator-activated receptor gamma coactivator 1-alpha (*Pgc1a*) was observed (Figure 2.6A). Notably, while *Pgc1a*

has been associated with brown adipose tissue thermogenesis (Cannon & Nedergaard, 2004) its role in the iBAT thermogenesis is not yet clear.

In summary, we showed that the PVN is of focal importance in mediating the effects of nesfatin-1 with regards to food intake, energy expenditure, and iBAT thermogenesis, as its sole stimulation could fully replicate the effects of i.c.v. administered nesfatin-1. Additionally, we identified the hypothalamic ERK1/2 system as a downstream mediator of these effects.

Experiment IV: effects of viral knockdown of melanocortin type 4 receptors (MC4R) in the brainstem on intra-PVN nesfatin-1 induced effects on energy homeostasis.

The fundamental contribution of the central melanocortin system with regards to homeostasis and its importance in nesfatin-1's effects has been touched on previously. Of the five G protein-coupled receptors, only the melanocortin type 3 (MC3R) and 4 (MC4R) receptors are known to be expressed in the brain, but while the contribution of the MC3R in the context of energy balance is still unclear (Girardet & Butler, 2014) manipulation of the MC4Rs is established to cause severe obesity, hyperphagia, and reduced energy expenditure (Cone, 2005; Huszar et al., 1997). The distribution of the MC4R overlaps with brain areas known to regulate energy balance, being particularly high in the brainstem, IML, and hypothalamic nuclei such as PVN and the arcuate nucleus (Kishi et al., 2003; Mountjoy et al., 1994). Accordingly, the arcuate nucleus is the major site of POMC and AgRP expression in the brain (Cone, 2005) and sends projections to several brain areas of homeostatic importance. For example, the PVN is contacted by both POMC and AgRP neurons (Cowley et al., 1999), and intra-PVN injection of MC4R ligands alters food intake and energy expenditure (Cowley et al., 1999; Giraudo et al., 1998). In the brainstem, the NTS is a central component for the melanocortin system: along with the aforementioned high expression of MC4R, this area is the second largest nucleus to possess POMC-expressing neurons, and site-specific injections of melanocortin receptor ligands affect food intake and energy expenditure (Kishi et al., 2003; H. Liu et al., 2003; Karolina P. Skibicka & Grill, 2009). Lastly, the NTS receives extensive connections from both

POMC and AgRP neurons in the arcuate (Swanson et al., 1980) as well as from the PVN (Geerling et al., 2010; Swanson & Sawchenko, 1983). Furthermore, i.c.v. (Wernecke et al., 2014) or intra-PVN (Maejima et al., 2009) injection of nesfatin-1 leads to increased *Pomc* and *c-fos* mRNA expression, respectively, in the NTS.

As the NTS has been shown to be important for both the melanocortin and nesfatinergic system, and a blockade of MC3/4R could abolish the effects of i.c.v. effects of nesfatin-1 on energy expenditure (Dore, Levata, Gachkar, et al., 2017) we hypothesized that the NTS could be a focal point of the interplay between these two systems. To investigate such interaction, in Experiment IVa MC4R expression was knocked down using an adeno-associated viral (AAV) vectors encoding short hairpin RNAs targeting the MC4R, and the metabolic effects of the knockdown then characterized for six weeks. In this model, we also investigated whether knockdown of the MC4R in the brainstem would affect the effects of intra-PVN injections of nesfatin-1 on iBAT thermogenesis.

AAV-mediated knockdown of the MC4R in the NTS resulted in a mild but significant decrease in body weight along with an increase in food intake through the six weeks of characterization (Figure 4.1A-B). Previous evidences (Balthasar et al., 2005) have shown how re-expression of MC4R exclusively in the PVN and amygdala on MC4R *null* animals (a model characterized by increased food intake and reduced energy expenditure (Huszar et al., 1997)) is sufficient to re-establish a normal feeding phenotype. In accordance with this result, PVN-specific knockdown of MC4R resulted in animals showing highly increased food intake, albeit only when exposed to a high-fat-diet (C Garza et al., 2008). Notably, in Balthasar's study while re-expression of the PVN MC4R in the PVN fully rescued the feeding phenotype it had no effect on the energy expenditure profile, suggesting that different MC4R populations outside the hypothalamus (e.g. the brainstem) would regulate it instead. This hypothesis of a "divergence" of the melanocortin system in the control of feeding and energy expenditure is challenged by the literature, that strongly indicates 1) how MC4R-expressing PVN neurons project to sympathetic premotor neurons involved in iBAT thermogenesis

(Song et al., 2008; Voss-Andreae et al., 2007) 2) by an increase in food intake upon stimulation of MC4R in the NTS (G. Li et al., 2007; Zheng, 2005) and 3) by this study as well, since here the manipulation of the MC4R in the brainstem was sufficient to exert significant effects on both feeding, and energy expenditure (see below). Rather than discrete MC4R-expressing neuronal populations controlling distinct aspects of energy homeostasis, the existence of a "network" of melanocortin-responsive neurons able to provide a certain degree of redundancy seems more likely, as similar cardiovascular and metabolic responses can be obtained by stimulating separate MCR-expressing neurons (Karolina P. Skibicka & Grill, 2008).

As mentioned above, in Experiment IVa the lower body weight despite higher food intake was not reconciled by observable alterations in basal dry heat loss (Figure 4.1D) or basal iBAT activity (Figure 4.1E). Although not measured here, a change in locomotor activity could simply explain this discrepancy. However, while MC4R are implicated in the regulation of locomotion, it's usually their agonism that prompts an increase in locomotion (Karolina P. Skibicka & Grill, 2009) while their antagonism (Tang-Christensen et al., 2004) does the opposite. Importantly, some aspects of the phenotype might be dormant and observable only in the presence of a "challenge", pharmacological or environmental: for example, MC4R *null* mice fed with a low-fat diet tend to have normal food intake and become hyperphagic only after being exposed to high-fat diet (Butler et al., 2001) or in different housing conditions (Butler et al., 2001). But a strong emphasis should be put on the effectiveness of the knockdown itself. The reduction in MC4R in the knockdown group, although present in this study, failed to reach significance compared to the control group. This, along with the aforementioned hypothesis of a redundant central melanocortin network, can lead to speculate that other areas might have compensated for a reduced expression of MC4R in the brainstem, ameliorating or possibly masking some aspects of the phenotype.

Next, using the same setup as in Experiment IIc and IIIb in Experiment IVb we sought to investigate whether brainstem MC4R knockdown animals were still responsive to intra-PVN nesfatin-1-induced increased iBAT thermogenesis. Confirming the observations of the previous experiments, intra-PVN

injection of nesfatin-1 increased iBAT (Figure 4.2A) and core body temperature compared to controls (Figure 4.2C). Strikingly, while no basal differences could be found between MC4R knockdowns and scramble controls, knockdown of the MC4R led to a complete blockade of the effect of nesfatin-1 on iBAT and core body temperature. In conclusion, we show for the first time that intra-PVN nesfatin-1 requires functional MC4R in the brainstem to exert its effects on energy expenditure. Therefore, despite the PVN having direct connections to the iBAT (M Bamshad et al., 1999; Cano et al., 2003; Madden & Morrison, 2009) iBAT activation upon nesfatin-1 administration happens via recruitment of the brainstem. From here, the outflow from the brainstem to the iBAT is likely to proceed through the ILM; accordingly, deletion of the MC4R in this area potently reduces sympathetic outflow towards the periphery (Rossi et al., 2011). However, our setup limits how in-depth we can describe this circuit. As the brain contains two known sources of POMC producing neurons, the arcuate nucleus and the brainstem itself, both areas could plausibly supply the necessary ligands to activate the MC4R in the brainstem. Stimulation of the PVN with nesfatin-1 could activate POMC neurons directly in the brainstem, and the resulting release of melanocortin ligands would then activate the brainstem MC4R, resulting in increased iBAT thermogenesis. Alternatively, stimulation of the PVN with nesfatin-1 could activate POMC neurons in the arcuate nucleus that would then release MC4R ligands in the brainstem resulting in increased iBAT thermogenesis. Further experiments are then necessary to map the areas involved.

Experiment V: role of NTS GLP-1 system on hedonic and homeostatic feeding behavior, and interaction with the NTS nesfatin-1 system

Homeostatic regulation of appetite is the result of a complex interaction between satiety and hunger signals originating from both the periphery and the central nervous system. The production of both satiety and hunger signals reflect perturbations in the nutritional state, coordinating when a meal starts, how much food is ingested, and finally when a meal finishes. Thus, caloric input through feeding is strictly regulated to match the body's caloric expenditure and keep the body weight constant.

But appetite, and ultimately feeding is not controlled solely by the need to eat, meaning the necessity of replenishing a caloric deficit; food is also pleasurable, and its palatability can motivate consumption even when the homeostatic needs of the body are met, opening up to overeating and obesity. Palatable food, especially if rich in fat and sugar, can disrupt hunger and satiety signals shifting the driving force behind eating from the need to replenish a "caloric deficit" towards "gratification". This consumption of food for pleasure rather than for homeostatic needs is defined as "hedonic eating". While the hypothalamus and the brainstem are key areas in the control of homeostatic feeding, palatable food activates the so-called "mesolimbic dopamine system". In simple terms, the mesolimbic dopamine system consists of dopamine-releasing neurons whose cell bodies are located mainly in the VTA – and in the substantia nigra pars compacta (SNpc) – that project mainly to the striatum. While the SNpc sends projections to the dorsal striatum (e.g. caudo-putamen) to control motor-related activities, the projections from the VTA to the ventral striatum (NAc and the olfactory tubercle) are fundamental in controlling hedonic activities (Gardner & Ashby, 2000). Both natural rewards (e.g. sex, food) and the consumption of substances of abuse (e.g. drugs, but also nicotine and alcohol) activate this latter pathway, leading to a release of dopamine from the neurons in the VTA into the NAc.

Glucagon-like peptide-1 (GLP-1) is a peptide mainly secreted from the L cells of the intestine with the main function of regulating insulin secretion in response to a meal. As the half-life of GLP-1 is considered to be extremely short (from ~10 minutes down to 2 minutes) being rapidly degraded by the enzyme dipeptidyl peptidase-4 (DPP-4) (Holst, 2007), GLP-1 is thought to act in a paracrine fashion with its receptor (GLP-1R, a G-protein coupled receptor) expressed on the vagal afferents innervating the intestine (mainly the celiac and gastric branches). While the intestine represents the principal site of GLP-1 production, this system possesses a strong central component: GLP-1 is in fact expressed in a discrete population of neurons in the medial NTS (mNTS), and the GLP-1R is expressed in the majority of the brain (with the exception of cortex and cerebellum) and particularly in the brainstem and hypothalamus (Merchenthaler et al., 1999). Compatible with the distribution of its receptor, central administration of

GLP-1 or its synthetic agonist Exenidin-4 (Ex4, a selective and DDP-4 resistant GLP-1R agonist) suppresses homeostatic food intake following i.c.v. (Tang-Christensen et al., 1996), supramammilary nucleus (López-Ferreras et al., 2019), NAc (Dickson et al., 2012), and NTS administration (Richard et al., 2015). In addition, a role for GLP-1 in the control of hedonic feeding has also been proposed: peripheral, i.c.v., and intra-VTA administration of Ex4 have been shown to decrease the rewarding value of food and motivation to work for sucrose (Dickson et al., 2012). Notably, the NTS neurons that express glucagon-like peptide 1 are known to project to the VTA, where GLP-1 receptors are expressed (Alhadeff et al., 2012), and intra-NTS administration of Ex4 can replicate the anhedonic effects on food-reward related behavior of intra-VTA Ex4 administration.

This involvement of GLP-1 in reward-related behaviors is of particular interest for nesfatin-1, as nesfatin-1 is 1) both expressed (Brailoiu et al., 2007) and active (Mimee et al., 2012) in the NTS, where GLP-1 is strongly represented. 2) nesfatin-1 is expressed in the VTA and has been recently described to act here hyperpolarizing dopamine neurons to reduce motivated behavior and preference for sucrose (Dore et al., 2020; Goebel-Stengel et al., 2011), and its application i.c.v. or intra-VTA reduces food intake and dopamine release in the NAc (X. Chen et al., 2015). And 3) not only peripheral administration of GLP-1 activates nesfatin-1 expressing neurons in the NTS (Saito et al., 2016), but the suppression of homeostatic feeding upon GLP-1 peripheral administration is negated if central nesfatin-1 is blocked (Saito et al., 2016).

Based on these evidences, we hypothesized that nesfatin-1 might interact in the NTS with GLP-1 to control also reward-related feeding behaviors; thus, intra-NTS stimulation with Ex4 would affect motivated behavior through the recruitment of endogenous nesfatin-1 in this same area. To test this hypothesis, in Experiment Va both female and male animals were treated with Nes-1 Ab prior to treatment with Ex4. Animals were then tested during their light phase (when levels of endogenous NUCB2/nesfatin-1 are naturally high (Kohno et al., 2008)) using a progressive ratio operant conditioning task (PR), a high-

effort task where the animals have to perform an increasing number of operant responses (e.g. the press of a lever) to obtain each successive reinforcement (e.g. a sucrose pellet) (Richardson & Roberts, 1996).

In both males and females tested under PR conditions, intra-NTS administration of Ex4 resulted in significantly fewer sucrose pellets obtained (Figure 5.1A and Figure 5.2A) as well as significantly fewer lever presses (Figure 5.1C and Figure 5.2C), indicating a reduction in food-motivated behavior. However, pretreatment with Nes-1 Ab had no effects on both pellets earned and lever pressed after Ex4 treatment, indicating that endogenous NUCB2/nesfatin-1 in the NTS is not required for the effects of intra-NTS Ex4 on food-motivated behavior. Fittingly, in the same animals sacrificed 2 hours after a final Ex4 injection, no alteration in *Nucb2* mRNA could be found (Figure 5.6) suggesting that, at least in the short term, the nesfatinergic system in the NTS is not involved in regulating food reward-related behavior.

While these results seem to rule out the involvement of the NTS, this study can't address the possibility that NUCB2/nesfatin-1 might still be recruited elsewhere. Activation of GLP-1 receptor in the VTA and NAc is sufficient to decrease food-motivated behavior (Dickson et al., 2012) and nesfatin-1 acts has been described to hyperpolarize VTA dopaminergic neurons (Dore et al., 2020), opening to the possibility that endogenous NUCB2/nesfatin-1 might be recruited at the level of the VTA. Additionally, as NUCB2/nesfatin-1 is mainly of peripheral origin, being expressed here roughly 10 times higher than in the brain (Stengel, Goebel, Yakubov, Wang, Witcher, Coskun, Taché, et al., 2009), and its levels are at the highest during the light phase or after a meal (Kohno et al., 2008), has been detected in plasma (Tsuchiya et al., 2010), and can cross the blood-brain barrier by non-saturable mechanism (T. O. Price et al., 2007), the potential involvement of peripheral nesfatin-1 as a confounding factor can't be excluded.

Similarly, the involvement of GLP-1 of non-NTS origin acting as a confounding factor can't be fully excluded. Like nesfatin-1, GLP-1 is mainly produced in the periphery, and can easily cross the blood-brain barrier, potentially supplying the central nervous system in an NTS-independent way (Kastin et al., 2002). However, given the extremely short half-life of GLP-1, it is unlikely that GLP-1 from the periphery can

enter the brain in concentrations sufficient to produce meaningful effects, leaving the NTS as the major source of this peptide in the central nervous system.

In Experiment Vb, food intake and body weight change were monitored 24 hours after the injections of Experiment Va. Consistently with the previous findings, in both male and female animals intra-NTS administration of Ex4 strongly reduced food intake (Figure 5.3A and Figure 5.4A) and body weight (Figure 5.3B and Figure 5.4B). However, while the Ex-4 induced decrease in motivation to obtain food was unaffected by the intra-NTS Nes-1 Ab pretreatment, it was able to prevent both the anorexigenic effect and the reduction in body weight caused by Ex4, but exclusively in male animals. With the exception of smaller (but not statistically significant) loss in body weight, intra-NTS Nes-1 Ab were here completely ineffective against intra-NTS Ex4 stimulation.

In summary, these results suggest that endogenous NUCB2/nesfatin-1 acts in the NTS as a downstream effector of the GLP-1 receptor to control homeostatic feeding but not to control food-motivated behavior. Additionally, we show that this interaction is sex-specific, as endogenous NUCB2/nesfatin-1 seems to be downstream of the GLP-1 receptor only in male animals.

In support of these results, a number of studies have suggested that NUCB2/nesfatin-1 is regulated in a sex-specific regulation fashion in both animals (Bertucci et al., 2016; Senin et al., 2015; L. Xu et al., 2009) and humans (Hofmann et al., 2015). Fittingly, *Nucb2/nesfatin-1* expression in normal cycling female rats seems to be under the control of sex hormone levels: in fact, *Nucb2/nesfatin-1* mRNA expression in the hypothalamus decreases significantly during proestrus, a phase of the estrous cycle when estrogen and progesterone levels are their highest. Conversely, centrally administered nesfatin-1 elevates MAP in normal cycling female animals exclusively during diestrus, a phase of the estrous cycle when both estrogen and progesterone levels are low. The differential response between males and females in this study could then be ascribed to both a different expression of *Nucb2/nesfatin-1* mRNA in male and female animals as well

as an effect of sex hormones on the expression of nesfatin-1's receptor. However, this latter hypothesis can't be tested to date, as the receptor for nesfatin-1 remains undiscovered.

Similarly, activation of GLP-1 receptors with Ex4 has been shown to affect reward-related behavior differentially in males and females (Richard et al., 2016), and the anorectic effects of peripheral GLP-1 seem to vary with estrogen levels (Asarian & Geary, 2013).

Importantly, the estrous cycle and the variation of hormones during its phases affect food-related behavior, from both a homeostatic and hedonic perspective (Asarian & Geary, 2013; Richard et al., 2017). Chow intake is at its lowest during estrous, (Eckel, 2004; Geary & Asarian, 2006) and the motivation to work for a palatable reward follows a similar pattern (Richard et al., 2017), likely by acting on estrogen receptor in the brainstem and hypothalamus (Asarian & Geary, 2013). Given the influence of sex hormones on food intake, a potential limitation of this study lies in the fact that estrous cycle phases were not monitored. Female subjects are commonly considered to have greater variability than males due to hormone fluctuations during the estrous cycle, represent a confounding factor in our findings. However, intra-NTS Ex4 treatments in females in this study were comparable with previous, similar experiments (Anderberg et al., 2017); besides, the real impact of the cycle in studies including female animals has been challenged by recent data showing that the variation in phenotypes in cycling females is not as severe as assumed, being comparable or even less variable than in males (Dayton et al., 2016; Prendergast et al., 2014).

Finally, we sought to confirm that the blockade of the Ex4 anorexigenic effect seen on Experiment Vb was caused by the specific blockade of endogenous NUCB2/nesfatin-1, and not due to unspecific effects of the antibody. Therefore, in Experiment Vc we tested the ability of the Nes-1 Ab to block intra-NTS Ex4-induced anorexia during the first three hours of the dark phase, a time when levels of endogenous NUCB2/nesfatin-1 are at their lowest (Kohno et al., 2008). Accordingly, pretreatment with Nes-1 Ab was ineffective in counteracting the effects of intra-NTS Ex4 on early dark phase food intake and body weight change (Figure 5.5A), thus indicating a specific role for endogenous NUCB2/nesfatin-1 in the anorectic

effect of Ex4 rather than an unspecific effect of the antibody used in this study. Furthermore, direct action on extracellular secreted nesfatin-1 is far more likely, as antibodies are unable to pass the cell membrane due to their large size and hydrophobicity (Trenevska et al., 2017) and can't, therefore, affect intracellular functions of NUCB2/nesfatin-1 but only act after its release.

However, Ex4 still managed to suppress food intake (Figure 5.5A) and reduce body weight (Figure 5.5B) during the first three hours of the dark phase, suggesting that endogenous NUCB2/nesfatin-1 might be recruited as a downstream effector of the GLP-1R in a delayed fashion. Thus, endogenous NUCB2/nesfatin-1 would maintain the anorexigenic effect initiated by Ex4/GLP-1 during the late dark/light phase, as its expression and thus secretion raises within the same timeframe.

Bibliography

Alhadeff, A. L., Rupprecht, L. E., & Hayes, M. R. (2012). GLP-1 neurons in the nucleus of the solitary tract project directly to the ventral tegmental area and nucleus accumbens to control for food intake. *Endocrinology*, *153*(2), 647–658. https://doi.org/10.1210/en.2011-1443

Amir, S. (1990). Stimulation of the paraventricular nucleus with glutamate activates interscapular brown adipose tissue thermogenesis in rats. *Brain Research*, *508*(1), 152–155. https://doi.org/10.1016/0006-8993(90)91129-5

Anderberg, R. H., Eerola, K., Kanoski, S. E., Richard, J. E., Noble, E. E., Taing, L., Hayes, M. R., López-Ferreras, L., Olandersson, K., & Skibicka, K. P. (2017). Lateral hypothalamic GLP-1 receptors are critical for the control of food reinforcement, ingestive behavior and body weight. *Molecular Psychiatry*, *23*(5), 1157–1168. https://doi.org/10.1038/mp.2017.187

Appleyard, S. M., Bailey, T. W., Doyle, M. W., Jin, Y. H., Smart, J. L., Low, M. J., & Andresen, M. C. (2005). Proopiomelanocortin neurons in nucleus tractus solitarius are activated by visceral afferents: Regulation by cholecystokinin and opioids. *Journal of Neuroscience*, *25*(14), 3578–3585. https://doi.org/10.1523/JNEUROSCI.4177-04.2005

Appleyard, S. M., Marks, D., Kobayashi, K., Okano, H., Low, M. J., & Andresen, M. C. (2007). Visceral afferents directly activate catecholamine neurons in the solitary tract nucleus. *Journal of Neuroscience*, *27*(48), 13292–13302. https://doi.org/10.1523/JNEUROSCI.3502-07.2007

Asarian, L., & Geary, N. (2013). Sex differences in the physiology of eating. *American Journal of Physiology-Regulatory, Integrative and Comparative Physiology*, *305*(11), R1215–R1267. https://doi.org/10.1152/ajpregu.00446.2012

Atasoy, D., Betley, J. N., Su, H. H., & Sternson, S. M. (2012). Deconstruction of a neural circuit for hunger. *Nature*, *488*(7410), 172–177. https://doi.org/10.1038/nature11270

Bagnol, D., Lu, X. Y., Kaelin, C. B., Day, H. E., Ollmann, M., Gantz, I., Akil, H., Barsh, G. S., & Watson, S. J. (1999). Anatomy of an endogenous antagonist: relationship between Agouti-related protein and proopiomelanocortin in brain. *The Journal of Neuroscience : The Official Journal of the Society for Neuroscience*, *19*(18), 1–7. https://doi.org/10.1523/jneurosci.19-18-j0004.1999

Balthasar, N., Dalgaard, L. T., Lee, C. E., Yu, J., Funahashi, H., Williams, T., Ferreira, M., Tang, V., McGovern, R. A., Kenny, C. D., Christiansen, L. M., Edelstein, E., Choi, B., Boss, O., Aschkenasi, C., Zhang, C. Y., Mountjoy, K., Kishi, T., Elmquist, J. K., & Lowell, B. B. (2005). Divergence of melanocortin pathways in the control of food intake and energy expenditure. *Cell*, *123*(3), 493–505. https://doi.org/10.1016/j.cell.2005.08.035

Bamshad, M, Song, C. K., & Bartness, T. J. (1999). CNS origins of the sympathetic nervous system outflow to brown adipose tissue. *The American Journal of Physiology*, *276*(6 Pt 2), R1569–R1578. https://doi.org/10.1016/0006-8993(89)91720-4

Bamshad, Maryam, Aoki, V. T., Adkison, M. G., Warren, W. S., & Bartness, T. J. (1998). Central nervous system origins of the sympathetic nervous system outflow to white adipose tissue. *American Journal of Physiology - Regulatory Integrative and Comparative Physiology*, *275*(1 44-1), 291–299. https://doi.org/10.1152/ajpregu.1998.275.1.r291

Barros, V. N., Mundim, M., Galindo, L. T., Bittencourt, S., Porcionatto, M., & Mello, L. E. (2015). The pattern of c-Fos expression and its refractory period in the brain of rats and monkeys. *Frontiers in Cellular Neuroscience*, *9*(March), 1–8. https://doi.org/10.3389/fncel.2015.00072

Berridge, K. C. (1996). Food reward: Brain substrates of wanting and liking. *Neuroscience & Biobehavioral Reviews*, *20*(1), 1–25. https://doi.org/10.1016/0149-7634(95)00033-B

Berridge, K. C., Robinson, T. E., & Aldridge, J. W. (2009). Dissecting components of reward: 'liking', 'wanting', and learning. *Current Opinion in Pharmacology*, *9*(1), 65–73. https://doi.org/10.1016/j.coph.2008.12.014

Bertucci, J. I., Blanco, A. M., Canosa, L. F., & Unniappan, S. (2016). Estradiol and testosterone modulate the tissue-specific expression of ghrelin, ghs-r, goat and nucb2 in goldfish. *General and Comparative Endocrinology*, *228*, 17–23. https://doi.org/10.1016/j.ygcen.2016.01.006

Blevins, J. E., & Baskin, D. G. (2010). Hypothalamic-brainstem circuits controlling eating. *Forum of Nutrition*, *63*, 133–140. https://doi.org/10.1159/000264401

Blouet, C., & Schwartz, G. J. (2012). Brainstem nutrient sensing in the nucleus of the solitary tract inhibits feeding. *Cell Metabolism*, *16*(5), 579–587. https://doi.org/10.1016/j.cmet.2012.10.003

BRADLEY, R. M., & GRABAUSKAS, G. (1998). Neural Circuits for Taste: Excitation, Inhibition, and Synaptic Plasticity in the Rostral Gustatory Zone of the Nucleus of the Solitary Tracta. *Annals of the New York Academy of Sciences*, *855*(1 OLFACTION AND), 467–474. https://doi.org/10.1111/j.1749-6632.1998.tb10607.x

Brailoiu, G. C., Deliu, E., Tica, A. A., Rabinowitz, J. E., Tilley, D. G., Benamar, K., Koch, W. J., & Brailoiu, E. (2013). Nesfatin-1 activates cardiac vagal neurons of nucleus ambiguus and elicits bradycardia in conscious rats. *Journal of Neurochemistry*, *126*(6), 739–748. https://doi.org/10.1111/jnc.12355

Brailoiu, G. C., Dun, S. L., Brailoiu, E., Inan, S., Yang, J., Jaw, K. C., & Dun, N. J. (2007). Nesfatin-1: Distribution and interaction with a G protein-coupled receptor in the rat brain. *Endocrinology*, *148*(10), 5088–5094. https://doi.org/10.1210/en.2007-0701

Butler, A. A., Marks, D. L., Fan, W., Kuhn, C. M., Bartolome, M., & Cone, R. D. (2001). Melanocortin-4 receptor is required for acute homeostatic responses to increased dietary fat. *Nature Neuroscience*, *4*(6), 605–611. https://doi.org/10.1038/88423

C Garza, J., Kim, C. S., Liu, J., Zhang, W., & Lu, X.-Y. (2008). Adeno-associated virus-mediated knockdown of melanocortin-4 receptor in the paraventricular nucleus of the hypothalamus promotes high-fat diet-induced hyperphagia and obesity. *Journal of Endocrinology*, *197*(3), 471–482. https://doi.org/10.1677/JOE-08-0009

CALDEIRA, J. C., FRANCI, C. R., & PELA, I. R. (1998). Bilateral Lesion of Hypothalamic Paraventricular Nucleus Abolishes Fever Induced by Endotoxin and Bradykinin in Ratsa. *Annals of the New York Academy of Sciences*, *856*(1 MOLECULAR MEC), 294–297. https://doi.org/10.1111/j.1749-6632.1998.tb08342.x

Cannon, B., & Nedergaard, J. (2004). *Brown adipose tissue: function and physiological significance*. *84*(1), 277–359.

Cano, G., Passerin, A. M., Schiltz, J. C., Card, J. P., Morrison, S. F., & Sved, A. F. (2003). Anatomical substrates for the central control of sympathetic outflow to interscapular adipose tissue during cold exposure. *Journal of Comparative Neurology*, *460*(3), 303–326. https://doi.org/10.1002/cne.10643

Chen, X., Dong, J., & Jiang, Z. Y. (2012). Nesfatin-1 influences the excitability of glucosensing neurons in the hypothalamic nuclei and inhibits the food intake. *Regulatory Peptides*, *177*(1–3), 21–26. https://doi.org/10.1016/j.regpep.2012.04.003

Chen, X., Shu, X., Cong, Z.-K., Jiang, Z.-Y., & Jiang, H. (2015). Nesfatin-1 acts on the dopaminergic reward pathway to inhibit food intake. *Neuropeptides*, *53*, 45–50. https://doi.org/10.1016/j.npep.2015.07.004

Chen, Z., Xu, Y. Y., Ge, J. F., & Chen, F. H. (2018). CRHR1 Mediates the Up-Regulation of Synapsin I Induced by Nesfatin-1 Through ERK 1/2 Signaling in SH-SY5Y Cells. *Cellular and Molecular Neurobiology*, *38*(3), 627–633. https://doi.org/10.1007/s10571-017-0509-x

Cone, R. D. (2005). Anatomy and regulation of the central melanocortin system. *Nature Neuroscience*, *8*(5), 571–578. https://doi.org/10.1038/nn1455

Cowley, M. A., Pronchuk, N., Fan, W., Dinulescu, D. M., Colmers, W. F., & Cone, R. D. (1999). Integration of npy, agrp, and melanocortin signals in the hypothalamic paraventricular nucleus: Evidence of a cellular basis for the adipostat. *Neuron*, *24*(1), 155–163. https://doi.org/10.1016/S0896-6273(00)80829-6

Dallman, M. F., Pecoraro, N. C., La Fleur, S. E., Warne, J. P., Ginsberg, A. B., Akana, S. F., Laugero, K. C., Houshyar, H., Strack, A. M., Bhatnagar, S., & Bell, M. E. (2006). Chapter 4: Glucocorticoids,

chronic stress, and obesity. *Progress in Brain Research*, *153*, 75–105. https://doi.org/10.1016/S0079-6123(06)53004-3

Darambazar, G., Nakata, M., Okada, T., Wang, L., Li, E. X., Shinozaki, A., Motoshima, M., Mori, M., & Yada, T. (2015). Paraventricular NUCB2/nesfatin-1 is directly targeted by leptin and mediates its anorexigenic effect. *Biochemical and Biophysical Research Communications*, *456*(4), 913–918. https://doi.org/10.1016/j.bbrc.2014.12.065

Dayton, A., Exner, E. C., Bukowy, J. D., Stodola, T. J., Kurth, T., Skelton, M., Greene, A. S., & Cowley, A. W. (2016). Breaking the Cycle. *Hypertension*, *68*(5), 1139–1144. https://doi.org/10.1161/HYPERTENSIONAHA.116.08207

de Jesus, L. A., Carvalho, S. D., Ribeiro, M. O., Schneider, M., Kim, S.-W., Harney, J. W., Larsen, P. R., & Bianco, A. C. (2001). The type 2 iodothyronine deiodinase is essential for adaptive thermogenesis in brown adipose tissue. *Journal of Clinical Investigation*, *108*(9), 1379–1385. https://doi.org/10.1172/JCI13803

Dickson, S. L., Shirazi, R. H., Hansson, C., Bergquist, F., Nissbrandt, H., & Skibicka, K. P. (2012). The Glucagon-Like Peptide 1 (GLP-1) Analogue, Exendin-4, Decreases the Rewarding Value of Food: A New Role for Mesolimbic GLP-1 Receptors. *Journal of Neuroscience*, *32*(14), 4812–4820. https://doi.org/10.1523/JNEUROSCI.6326-11.2012

Dietrich, M. O., & Horvath, T. L. (2009). Feeding signals and brain circuitry. *European Journal of Neuroscience*, *30*(9), 1688–1696. https://doi.org/10.1111/j.1460-9568.2009.06963.x

Dore, R., Iemolo, A., Smith, K. L., Wang, X., Cottone, P., & Sabino, V. (2013). CRF mediates the anxiogenic and anti-rewarding, but not the anorectic effects of PACAP. *Neuropsychopharmacology*, *38*(11), 2160–2169. https://doi.org/10.1038/npp.2013.113

Dore, R., Krotenko, R., Reising, J. P., Murru, L., Sundaram, S. M., Di Spiezio, A., Müller-Fielitz, H., Schwaninger, M., Jöhren, O., Mittag, J., Passafaro, M., Shanabrough, M., Horvath, T. L., Schulz, C., & Lehnert, H. (2020). Nesfatin-1 decreases the motivational and rewarding value of food. *Neuropsychopharmacology*, *April*, 1–11. https://doi.org/10.1038/s41386-020-0682-3

Dore, R., Levata, L., Gachkar, S., Jöhren, O., Mittag, J., Lehnert, H., & Schulz, C. (2017). The thermogenic effect of nesfatin-1 requires recruitment of the melanocortin system. *Journal of Endocrinology*, *235*(2), 111–122. https://doi.org/10.1530/JOE-17-0151

Dore, R., Levata, L., Lehnert, H., & Schulz, C. (2017). Nesfatin-1: Functions and physiology of a novel regulatory peptide. *Journal of Endocrinology*, *232*(1), R45–R65. https://doi.org/10.1530/JOE-16-0361

Eckel, L. A. (2004). Estradiol: A rhythmic, inhibitory, indirect control of meal size. *Physiology and Behavior*, *82*(1), 35–41. https://doi.org/10.1016/j.physbeh.2004.04.023

Ellacott, K. L. J., & Cone, R. D. (2006). The role of the central melanocortin system in the regulation of food intake and energy homeostasis: lessons from mouse models. *Philosophical Transactions of the Royal Society of London. Series B, Biological Sciences*, *361*(1471), 1265–1274. https://doi.org/10.1098/rstb.2006.1861

Fenselau, H., Campbell, J. N., Verstegen, A. M. J., Madara, J. C., Xu, J., Shah, B. P., Resch, J. M., Yang, Z., Mandelblat-Cerf, Y., Livneh, Y., & Lowell, B. B. (2017). A Rapidly Acting Glutamatergic ARC→PVH Satiety Circuit Postsynaptically Regulated by α-MSH. *Nature Neuroscience*, *20*(1), 42–51. https://doi.org/10.1038/nn.4442

Fioramonti, X., Chrétien, C., Leloup, C., & Pénicaud, L. (2017). Recent advances in the cellular and molecular mechanisms of hypothalamic neuronal glucose detection. *Frontiers in Physiology*, *8*(NOV), 1–8. https://doi.org/10.3389/fphys.2017.00875

Foo, K. S., Brismar, H., & Broberger, C. (2008). Distribution and neuropeptide coexistence of nucleobindin-2 mRNA/nesfatin-like immunoreactivity in the rat CNS. *Neuroscience*, *156*(3), 563–579. https://doi.org/10.1016/j.neuroscience.2008.07.054

Foo, Kylie S., Brauner, H., Östenson, C. G., & Broberger, C. (2010). Nucleobindin-2/nesfatin in the endocrine pancreas: Distribution and relationship to glycaemic state. *Journal of Endocrinology*, *204*(3), 255–263. https://doi.org/10.1677/JOE-09-0254

François, M., Torres, H., Huesing, C., Zhang, R., Saurage, C., Lee, N., Qualls-Creekmore, E., Yu, S., Morrison, C. D., Burk, D., Berthoud, H. R., & Münzberg, H. (2019). Sympathetic innervation of the interscapular brown adipose tissue in mouse. *Annals of the New York Academy of Sciences*, *1454*(1), 3–13. https://doi.org/10.1111/nyas.14119

Friedman, J. M. (2004). Modern science versus the stigma of obesity. *Nature Medicine*, *10*(6), 563–569. https://doi.org/10.1038/nm0604-563

García-Galiano, D., Navarro, V. M., Gaytan, F., & Tena-Sempere, M. (2010). Expanding roles of NUCB2/nesfatin-1 in neuroendocrine regulation. *Journal of Molecular Endocrinology*, *45*(5), 281–290. https://doi.org/10.1677/JME-10-0059

Garcia-Galiano, D., Navarro, V. M., Roa, J., Ruiz-Pino, F., Sanchez-Garrido, M. A., Pineda, R., Castellano, J. M., Romero, M., Aguilar, E., Gaytan, F., Dieguez, C., Pinilla, L., Tena-Sempere, M., García-Galiano, D., Navarro, V. M., Roa, J., Ruiz-Pino, F., Sánchez-Garrido, M. A., Pineda, R., … Tena-Sempere, M. (2010). The anorexigenic neuropeptide, nesfatin-1, is indispensable for normal puberty onset in the female rat. *The Journal of Neuroscience : The Official Journal of the Society for Neuroscience*, *30*(23), 7783–7792. https://doi.org/10.1523/JNEUROSCI.5828-09.2010

Gardner, E. L., & Ashby, C. R. (2000). Heterogeneity of the mesotelencephalic dopamine fibers:

Physiology and pharmacology. *Neuroscience and Biobehavioral Reviews*, *24*(1), 115–118. https://doi.org/10.1016/S0149-7634(99)00048-2

Geary, N., & Asarian, L. (2006). Modulation of appetite by gonadal steroid hormones. *Philosophical Transactions of the Royal Society B: Biological Sciences*, *361*(1471), 1251–1263. https://doi.org/10.1098/rstb.2006.1860

Geerling, J. C., Shin, J.-W. W., Chimenti, P. C., & Loewy, A. D. (2010). Paraventricular hypothalamic nucleus: Axonal projections to the brainstem. *The Journal of Comparative Neurology*, *518*(9), 1460–1499. https://doi.org/10.1002/cne.22283

Girardet, C., & Butler, A. A. (2014). Neural melanocortin receptors in obesity and related metabolic disorders. *Biochimica et Biophysica Acta - Molecular Basis of Disease*, *1842*(3), 482–494. https://doi.org/10.1016/j.bbadis.2013.05.004

Giraudo, S. Q., Billington, C. J., & Levine, A. S. (1998). Feeding effects of hypothalamic injection of melanocortin 4 receptor ligands. *Brain Research*, *809*(2), 302–306. https://doi.org/10.1016/S0006-8993(98)00837-3

Goebel-Stengel, M., Wang, L., Stengel, A., & Taché, Y. (2011). Localization of nesfatin-1 neurons in the mouse brain and functional implication. *Brain Research*, *1396*(2), 20–34. https://doi.org/10.1016/j.brainres.2011.04.031

Goebel, M., Stengel, A., Wang, L., Lambrecht, N. W. G., & Taché, Y. (2009). Nesfatin-1 immunoreactivity in rat brain and spinal cord autonomic nuclei. *Neuroscience Letters*, *452*(3), 241–246. https://doi.org/10.1016/j.neulet.2009.01.064

Gonzalez, R., Tiwari, A., & Unniappan, S. (2009). Pancreatic beta cells colocalize insulin and pronesfatin immunoreactivity in rodents. *Biochemical and Biophysical Research Communications*, *381*(4), 643–648. https://doi.org/10.1016/j.bbrc.2009.02.104

Hammond, K. A., Konarzewski, M., Torres, R. M., & Diamond, J. (1994). Metabolic ceilings under a combination of peak energy demands. *Physiological Zoology*, *65*(6), 1479–1506. https://doi.org/10.1086/physzool.67.6.30163908

Harris, R. B. S., Mitchell, T. D., Simpson, J., Redmann, S. M., Youngblood, B. D., & Ryan, D. H. (2002). Weight loss in rats exposed to repeated acute restraint stress is independent of energy or leptin status. *American Journal of Physiology - Regulatory Integrative and Comparative Physiology*, *282*(1 51-1), 77–88. https://doi.org/10.1152/ajpregu.2002.282.1.r77

Haskell-Luevano, C., Chen, P., Li, C., Chang, K., Smith, M. S., Cameron, J. L., & Cone, R. D. (1999). Characterization of the neuroanatomical distribution of agouti-related protein immunoreactivity in the rhesus monkey and the rat. *Endocrinology*, *140*(3), 1408–1415. https://doi.org/10.1210/endo.140.3.6544

Hill, J. (2012). PVN pathways controlling energy homeostasis. *Indian Journal of Endocrinology and Metabolism*, *16*(9), 627. https://doi.org/10.4103/2230-8210.105581

Hisadome, K., Reimann, F., Gribble, F. M., & Trapp, S. (2011). CCK stimulation of GLP-1 neurons involves α 1-adrenoceptor- mediated increase in glutamatergic synaptic inputs. *Diabetes*, *60*(11), 2701–2709. https://doi.org/10.2337/db11-0489

Hofmann, T., Elbelt, U., Ahnis, A., Rose, M., Klapp, B. F., & Stengel, A. (2015). Sex-specific regulation of NUCB2/nesfatin-1: Differential implication in anxiety in obese men and women. *Psychoneuroendocrinology*, *60*, 130–137. https://doi.org/10.1016/j.psyneuen.2015.06.014

Holst, J. J. (2007). The physiology of glucagon-like peptide 1. *Physiological Reviews*, *87*(4), 1409–1439. https://doi.org/10.1152/physrev.00034.2006

Huszar, D., Lynch, C. A., Fairchild-Huntress, V., Dunmore, J. H., Fang, Q., Berkemeier, L. R., Gu, W., Kesterson, R. A., Boston, B. A., Cone, R. D., Smith, F. J., Campfield, L. A., Burn, P., & Lee, F. (1997). Targeted Disruption of the Melanocortin-4 Receptor Results in Obesity in Mice. *Cell*, *88*(1), 131–141. https://doi.org/10.1016/S0092-8674(00)81865-6

Ilango, A., Kesner, A. J., Keller, K. L., Stuber, G. D., Bonci, A., & Ikemoto, S. (2014). Similar Roles of Substantia Nigra and Ventral Tegmental Dopamine Neurons in Reward and Aversion. *The Journal of Neuroscience*, *34*(3), 817–822. https://doi.org/10.1523/JNEUROSCI.1703-13.2014

Ishida, E., Hashimoto, K., Shimizu, H., Okada, S., Satoh, T., Kato, I., Yamada, M., & Mori, M. (2012). Nesfatin-1 Induces the Phosphorylation Levels of cAMP Response Element-Binding Protein for Intracellular Signaling in a Neural Cell Line. *PLoS ONE*, *7*(12), 1–8. https://doi.org/10.1371/journal.pone.0050918

Iwasaki, Y., Nakabayashi, H., Kakei, M., Shimizu, H., Mori, M., & Yada, T. (2009). Nesfatin-1 evokes Ca2+ signaling in isolated vagal afferent neurons via Ca2+ influx through N-type channels. *Biochemical and Biophysical Research Communications*, *390*(3), 958–962. https://doi.org/10.1016/j.bbrc.2009.10.085

Jansen, A. S. P., Hoffman, J. L., & Loewy, A. D. (1997). CNS sites involved in sympathetic and parasympathetic control of the pancreas: A viral tracing study. *Brain Research*, *766*(1–2), 29–38. https://doi.org/10.1016/S0006-8993(97)00532-5

Jeong, J. K., Kim, J. G., & Lee, B. J. (2014). Participation of the central melanocortin system in metabolic regulation and energy homeostasis. *Cellular and Molecular Life Sciences*, *71*(19), 3799–3809. https://doi.org/10.1007/s00018-014-1650-z

Jones, F. N., & Skinner, B. F. (1939). The Behavior of Organisms: An Experimental Analysis. *The American Journal of Psychology*. https://doi.org/10.2307/1416495

Kaiyala, K. J., & Schwartz, M. W. (2011). Toward a more complete (and less controversial) understanding of energy expenditure and its role in obesity pathogenesis. In *Diabetes*. https://doi.org/10.2337/db10-0909

Kastin, A. J., Akerstrom, V., & Pan, W. (2002). *Interactions of Glucagon-Like Peptide-1 (GLP-1) with the Blood-Brain Barrier*. *18*, 7–14.

KENNEDY, G. C. (1953). The role of depot fat in the hypothalamic control of food intake in the rat. *Proceedings of the Royal Society of London. Series B, Biological Sciences*, *140*(901), 578–596. https://doi.org/10.1098/rspb.1953.0009

Kishi, T., Aschkenasi, C. J., Lee, C. E., Mountjoy, K. G., Saper, C. B., & Elmquist, J. K. (2003). Expression of melanocortin 4 receptor mRNA in the central nervous system of the rat. *Journal of Comparative Neurology*, *457*(3), 213–235. https://doi.org/10.1002/cne.10454

KLEIBER, M. (1947). Body size and metabolic rate. *Physiological Reviews*. https://doi.org/10.1152/physrev.1947.27.4.511

Kohno, D., Nakata, M., Maejima, Y., Shimizu, H., Sedbazar, U., Yoshida, N., Dezaki, K., Onaka, T., Mori, M., & Yada, T. (2008). Nesfatin-1 neurons in paraventricular and supraoptic nuclei of the rat hypothalamus coexpress oxytocin and vasopressin and are activated by refeeding. *Endocrinology*, *149*(3), 1295–1301. https://doi.org/10.1210/en.2007-1276

Könczöl, K., Pintér, O., Ferenczi, S., Varga, J., Kovács, K., Palkovits, M., Zelena, D., & Tóth, Z. E. (2012). Nesfatin-1 exerts long-term effect on food intake and body temperature. *International Journal of Obesity (2005)*, *36*(12), 1514–1521. https://doi.org/10.1038/ijo.2012.2

Könczöl, K, Pintér, O., Ferenczi, S., Varga, J., Kovács, K., Palkovits, M., Zelena, D., & Tóth, Z. E. (2012). Nesfatin-1 exerts long-term effect on food intake and body temperature. *International Journal of Obesity (2005)*, *36*(12), 1514–1521. https://doi.org/10.1038/ijo.2012.2

Könczöl, Katalin, Bodnár, I., Zelena, D., Pintér, O., Papp, R. S., Palkovits, M., Nagy, G. M., & Tóth, Z. E. (2010). Nesfatin-1/NUCB2 may participate in the activation of the hypothalamic-pituitary-adrenal axis in rats. *Neurochemistry International*, *57*(3), 189–197. https://doi.org/10.1016/j.neuint.2010.04.012

Kwon Jeong, J., Dae Kim, J., & Diano, S. (2013). Ghrelin regulates hypothalamic prolyl carboxypeptidase expression in mice. *Molecular Metabolism*, *2*(1), 23–30. https://doi.org/10.1016/j.molmet.2013.01.002

Lake, D., Corrêa, S. A. L., & Müller, J. (2016). Negative feedback regulation of the ERK1/2 MAPK pathway. *Cellular and Molecular Life Sciences*, *73*(23), 4397–4413. https://doi.org/10.1007/s00018-016-2297-8

Leibowitz, S. F., Hammer, N. J., & Chang, K. (1981). Hypothalamic paraventricular nucleus lesions produce overeating and obesity in the rat. *Physiology and Behavior*, *27*(6), 1031–1040.

https://doi.org/10.1016/0031-9384(81)90366-8

Levata, L., Dore, R., Jöhren, O., Schwaninger, M., Schulz, C., & Lehnert, H. (2019). Nesfatin-1 Acts Centrally to Induce Sympathetic Activation of Brown Adipose Tissue and Non-Shivering Thermogenesis. *Hormone and Metabolic Research*, *51*(10), 678–685. https://doi.org/10.1055/a-0985-4272

Li, C., Zhang, F., Shi, L., Zhang, H., Tian, Z., Xie, J., & Jiang, H. (2014). Nesfatin-1 decreases excitability of dopaminergic neurons in the substantia nigra. *Journal of Molecular Neuroscience*, *52*(3), 419–424. https://doi.org/10.1007/s12031-013-0169-3

Li, G., Zhang, Y., Rodrigues, E., Zheng, D. H., Matheny, M., Cheng, K. Y., & Scarpace, P. J. (2007). Melanocortin activation of nucleus of the solitary tract avoids anorectic tachyphylaxis and induces prolonged weight loss. *American Journal of Physiology - Endocrinology and Metabolism*, *293*(1), 252–258. https://doi.org/10.1152/ajpendo.00451.2006

Li, Z. L., Xu, L., Sun, X. R., Guo, F. F., Gong, Y. L., & Gao, S. L. (2013). Central nesfatin-1 influences the excitability of ghrelin-responsive gastric distension neurons in the arcuate nucleus and reduces gastric motility in rats. *European Journal of Neuroscience*, *38*(11), 3636–3643. https://doi.org/10.1111/ejn.12366

Liu, H., Kishi, T., Roseberry, A. G., Cai, X., Lee, C. E., Montez, J. M., Friedman, J. M., & Elmquist, J. K. (2003). Transgenic mice expressing green fluorescent protein under the control of the melanocortin-4 receptor promoter. *Journal of Neuroscience*, *23*(18), 7143–7154. https://doi.org/10.1523/jneurosci.23-18-07143.2003

Liu, T., Kong, D., Shah, B. P., Ye, C., Koda, S., Saunders, A., Ding, J. B., Yang, Z., Sabatini, B. L., & Lowell, B. B. (2012). Fasting Activation of AgRP Neurons Requires NMDA Receptors and Involves Spinogenesis and Increased Excitatory Tone. *Neuron*, *73*(3), 511–522. https://doi.org/10.1016/j.neuron.2011.11.027

López-Ferreras, L., Eerola, K., Mishra, D., Shevchouk, O. T., Richard, J. E., Nilsson, F. H., Hayes, M. R., & Skibicka, K. P. (2019). GLP-1 modulates the supramammillary nucleus-lateral hypothalamic neurocircuit to control ingestive and motivated behavior in a sex divergent manner. *Molecular Metabolism*, *20*(November 2018), 178–193. https://doi.org/10.1016/j.molmet.2018.11.005

Luijten, I. H. N., Cannon, B., & Nedergaard, J. (2019). Glucocorticoids and Brown Adipose Tissue: Do glucocorticoids really inhibit thermogenesis? *Molecular Aspects of Medicine*, *68*(July), 42–59. https://doi.org/10.1016/j.mam.2019.07.002

Lutter, M., & Nestler, E. J. (2009). Homeostatic and Hedonic Signals Interact in the Regulation of Food Intake. *The Journal of Nutrition*, *139*(3), 629–632. https://doi.org/10.3945/jn.108.097618

Madden, C. J., & Morrison, S. F. (2009). Neurons in the paraventricular nucleus of the hypothalamus inhibit sympathetic outflow to brown adipose tissue. *American Journal of Physiology - Regulatory Integrative*

and Comparative Physiology, *296*(3). https://doi.org/10.1152/ajpregu.91007.2008

Maejima, Y., Horita, S., Kobayashi, D., Aoki, M., O'hashi, R., Imai, R., Sakamoto, K., Mori, M., Takasu, K., Ogawa, K., Takenoshita, S., Zhao, S., Hazama, A., & Shimomura, K. (2017). Nesfatin-1 inhibits voltage gated K + channels in pancreatic beta cells. *Peptides*, *95*, 10–15. https://doi.org/10.1016/j.peptides.2017.07.001

Maejima, Y., Sedbazar, U., Suyama, S., Kohno, D., Onaka, T., Takano, E., Yoshida, N., Koike, M., Uchiyama, Y., Fujiwara, K., Yashiro, T., Horvath, T. L., Dietrich, M. O., Tanaka, S., Dezaki, K., Hashimoto, K., Shimizu, H., Nakata, M., Mori, M., & Yada, T. (2009). Nesfatin-1-Regulated Oxytocinergic Signaling in the Paraventricular Nucleus Causes Anorexia through a Leptin-Independent Melanocortin Pathway. *Cell Metabolism*, *10*(5), 355–365. https://doi.org/10.1016/j.cmet.2009.09.002

McKay, M. M., & Morrison, D. K. (2007). Integrating signals from RTKs to ERK/MAPK. *Oncogene*, *26*(22), 3113–3121. https://doi.org/10.1038/sj.onc.1210394

Mendel, C. M., & Mendel, D. B. (1985). "Non-specific" binding. The problem, and a solution. *The Biochemical Journal*, *228*(1), 269–272. https://doi.org/10.1042/bj2280269

Merali, Z., Cayer, C., Kent, P., & Anisman, H. (2008). Nesfatin-1 increases anxiety- and fear-related behaviors in the rat. *Psychopharmacology*, *201*(1), 115–123. https://doi.org/10.1007/s00213-008-1252-2

Merchenthaler, I., Lane, M., & Shughrue, P. (1999). *Distribution of Pre-Pro-Glucagon and Glucagon-Like Peptide-1 Receptor Messenger RNAs in the Rat Central*. *280*(February 1998), 261–280.

Mimee, A., Smith, P. M., & Ferguson, A. V. (2012). Nesfatin-1 influences the excitability of neurons in the nucleus of the solitary tract and regulates cardiovascular function. *American Journal of Physiology-Regulatory, Integrative and Comparative Physiology*, *302*(11), R1297–R1304. https://doi.org/10.1152/ajpregu.00266.2011

Miura, K., Titani, K., Kurosawa, Y., & Kanai, Y. (1992). Molecular cloning of nucleobindin, a novel DNA-binding protein that contains both a signal peptide and a leucine zipper structure. *Biochemical and Biophysical Research Communications*, *187*(1), 375–380. https://doi.org/10.1016/S0006-291X(05)81503-7

Mizuno, T. M., Kleopoulos, S. P., Bergen, H. T., Roberts, J. L., Priest, C. A., & Mobbs, C. V. (1998). Hypothalamic Pro-Opiomelanocortin mRNA Is Reduced By Fasting in ob/ob and db/db Mice, but Is Stimulated by Leptin. *Diabetes*, *47*(2), 294–297. https://doi.org/10.2337/diab.47.2.294

Mizuno, T. M., Makimura, H., Silverstein, J., Roberts, J. L., Lopingco, T., & Mobbs, C. V. (1999). Fasting regulates hypothalamic neuropeptide Y, agouti-related peptide, and proopiomelanocortin in diabetic mice independent of changes in leptin or insulin. *Endocrinology*, *140*(10), 4551–4557. https://doi.org/10.1210/en.140.10.4551

Monge-Roffarello, B., Labbe, S. M., Lenglos, C., Caron, A., Lanfray, D., Samson, P., & Richard, D. (2014). The medial preoptic nucleus as a site of the thermogenic and metabolic actions of melanotan II in male rats. *American Journal of Physiology - Regulatory Integrative and Comparative Physiology*, *307*(2), 158–167. https://doi.org/10.1152/ajpregu.00059.2014

Morikawa, Y., Ueyama, E., & Senba, E. (2004). Fasting-induced activation of mitogen-activated protein kinases (ERK/p38) in the mouse hypothalamus. *Journal of Neuroendocrinology*, *16*(2), 105–112. https://doi.org/10.1111/j.0953-8194.2004.01135.x

Morton, G. J., Meek, T. H., & Schwartz, M. W. (2014). Neurobiology of food intake in health and disease. *Nature Reviews Neuroscience*, *15*(6), 367–378. https://doi.org/10.1038/nrn3745

Morton, G., & Schwartz, M. (2006). Central nervous system control of food intake and body weight. *Nature Reviews*, *443*(7109), 289–295. https://doi.org/10.1038/nature05026

Mountjoy, K. G., Mortrud, M. T., Low, M. J., Simerly, R. B., & Cone, R. D. (1994). Localization of the melanocortin-4 receptor (MC4-R) in neuroendocrine and autonomic control circuits in the brain. *Molecular Endocrinology*, *8*(December), 1298–1308. https://doi.org/10.1210/mend.8.10.7854347

Myers, M. G., Olson, D. P., Low, M. J., & Elias, C. F. (2016). Brain Regulation of Feeding and Energy Homeostasis. In *Metabolic Syndrome* (pp. 347–368). Springer International Publishing. https://doi.org/10.1007/978-3-319-11251-0_22

Nakata, M., Manaka, K., Yamamoto, S., Mori, M., & Yada, T. (2011). Nesfatin-1 enhances glucose-induced insulin secretion by promoting Ca(2+) influx through L-type channels in mouse islet β-cells. *Endocrine Journal*, *58*(4), 305–313. https://doi.org/10.1507/endocrj.K11E-056

Nestler, E. J. (2001). Molecular basis of long-term plasticity underlying addiction. *Nature Reviews Neuroscience*, *2*(2), 119–128. https://doi.org/10.1038/35053570

Nestler, E. J. (2005). Is there a common molecular pathway for addiction? *Nature Neuroscience*, *8*(11), 1445–1449. https://doi.org/10.1038/nn1578

Nonogaki, K., Ohba, Y., Sumii, M., & Oka, Y. (2008). Serotonin systems upregulate the expression of hypothalamic NUCB2 via 5-HT2C receptors and induce anorexia via a leptin-independent pathway in mice. *Biochemical and Biophysical Research Communications*, *372*(1), 186–190. https://doi.org/10.1016/j.bbrc.2008.05.010

Oh-I, S., Shimizu, H., Satoh, T., Okada, S., Adachi, S., Inoue, K., Eguchi, H., Yamamoto, M., Imaki, T., Hashimoto, K., Tsuchiya, T., Monden, T., Horiguchi, K., Yamada, M., & Mori, M. (2006). Identification of nesfatin-1 as a satiety molecule in the hypothalamus. *Nature*, *443*(7112), 709–712. https://doi.org/10.1038/nature05162

Ozcan, M., Gok, Z. B., Kacar, E., Serhatlioglu, I., & Kelestimur, H. (2016). Nesfatin-1 increases intracellular calcium concentration by protein kinase C activation in cultured rat dorsal root ganglion neurons. *Neuroscience Letters*, *619*, 177–181. https://doi.org/10.1016/j.neulet.2016.03.018

Pan, W., Hsuchou, H., & Kastin, A. J. (2007). Nesfatin-1 crosses the blood-brain barrier without saturation. *Peptides*, *28*(11), 2223–2228. https://doi.org/10.1016/j.peptides.2007.09.005

Paxinos, G., & Watson, C. (2007). The Rat Brain in Stereotaxic Coordinates Sixth Edition. *Elsevier Academic Press.*

Prendergast, B. J., Onishi, K. G., & Zucker, I. (2014). Female mice liberated for inclusion in neuroscience and biomedical research. *Neuroscience and Biobehavioral Reviews*, *40*, 1–5. https://doi.org/10.1016/j.neubiorev.2014.01.001

Price, C. J., Hoyda, T. D., Samson, W. K., & Ferguson, A. V. (2008). Nesfatin-1 influences the excitability of paraventricular nucleus neurones. *Journal of Neuroendocrinology*, *20*(2), 245–250. https://doi.org/10.1111/j.1365-2826.2007.01641.x

Price, Christopher J, Samson, W. K., & Ferguson, A. V. (2008). Nesfatin-1 inhibits NPY neurons in the arcuate nucleus. *Brain Research*, *1230*(613), 99–106. https://doi.org/10.1016/j.brainres.2008.06.084

Price, T. O., Samson, W. K., Niehoff, M. L., & Banks, W. A. (2007). Permeability of the blood-brain barrier to a novel satiety molecule nesfatin-1. *Peptides*, *28*(12), 2372–2381. https://doi.org/10.1016/j.peptides.2007.10.008

Prinz, P., Teuffel, P., Lembke, V., Kobelt, P., Goebel-Stengel, M., Hofmann, T., Rose, M., Klapp, B. F., & Stengel, A. (2015). Nesfatin-130-59 injected intracerebroventricularly differentially affects food intake microstructure in rats under normal weight and diet-induced obese conditions. *Frontiers in Neuroscience*, *9*(NOV), 1–12. https://doi.org/10.3389/fnins.2015.00422

Rahmouni, K., Sigmund, C. D., Haynes, W. G., & Mark, A. L. (2009). Hypothalamic ERK mediates the anorectic and thermogenic sympathetic effects of leptin. *Diabetes*, *58*(3), 536–542. https://doi.org/10.2337/db08-0822

Ramanjaneya, M., Chen, J., Brown, J. E., Tripathi, G., Hallschmid, M., Patel, S., Kern, W., Hillhouse, E. W., Lehnert, H., Tan, B. K., & Randeva, H. S. (2010). Identification of nesfatin-1 in human and murine adipose tissue: A novel depot-specific adipokine with increased levels in obesity. *Endocrinology*, *151*(7), 3169–3180. https://doi.org/10.1210/en.2009-1358

Richard, J. E., Anderberg, R. H., Göteson, A., Gribble, F. M., Reimann, F., & Skibicka, K. P. (2015). Activation of the GLP-1 receptors in the nucleus of the solitary tract reduces food reward behavior and targets the mesolimbic system. *PLoS ONE*, *10*(3), 1–21. https://doi.org/10.1371/journal.pone.0119034

Richard, J. E., Anderberg, R. H., López-Ferreras, L., Olandersson, K., & Skibicka, K. P. (2016). Sex and estrogens alter the action of glucagon-like peptide-1 on reward. *Biology of Sex Differences*, *7*(1), 1–16. https://doi.org/10.1186/s13293-016-0059-9

Richard, J. E., López-Ferreras, L., Anderberg, R. H., Olandersson, K., & Skibicka, K. P. (2017). Estradiol is a critical regulator of food-reward behavior. *Psychoneuroendocrinology*, *78*, 193–202. https://doi.org/10.1016/j.psyneuen.2017.01.014

Richardson, N. R., & Roberts, D. C. S. (1996). Progressive ratio schedules in drug self-administration studies in rats: a method to evaluate reinforcing efficacy. *Journal of Neuroscience Methods*, *66*(1), 1–11. https://doi.org/10.1016/0165-0270(95)00153-0

Roh, E., Song, D. K., & Kim, M. S. (2016). Emerging role of the brain in the homeostatic regulation of energy and glucose metabolism. *Experimental and Molecular Medicine*, *48*(3), e216-12. https://doi.org/10.1038/emm.2016.4

Rossi, J., Balthasar, N., Olson, D., Scott, M., Berglund, E., Lee, C. E., Choi, M. J., Lauzon, D., Lowell, B. B., & Elmquist, J. K. (2011). Melanocortin-4 receptors expressed by cholinergic neurons regulate energy balance and glucose homeostasis. *Cell Metabolism*, *13*(2), 195–204. https://doi.org/10.1016/j.cmet.2011.01.010

Rui, L. (2013). Brain Regulation of energy balanmce and body weigts. *Rev Endocr Metab Disord.*, *14*(4), 1–35. https://doi.org/10.1007/s11154-013-9261-9.Brain

Saito, R., So, M., Motojima, Y., Matsuura, T., Yoshimura, M., Hashimoto, H., Yamamoto, Y., Kusuhara, K., & Ueta, Y. (2016). Activation of Nesfatin-1-Containing Neurones in the Hypothalamus and Brainstem by Peripheral Administration of Anorectic Hormones and Suppression of Feeding via Central Nesfatin-1 in Rats. *Journal of Neuroendocrinology*, *28*(9). https://doi.org/10.1111/jne.12400

Saper, C.B., Loewy, A. D., Swanson, L. W., & Cowan, W. M. (1976). Direct hypothalamo-autonomic connections. *Brain Research*, *117*(2), 305–312. https://doi.org/10.1016/0006-8993(76)90738-1

Saper, Clifford B., Chou, T. C., & Elmquist, J. K. (2002). The need to feed: Homeostatic and hedonic control of eating. *Neuron*, *36*(2), 199–211. https://doi.org/10.1016/S0896-6273(02)00969-8

Schwartz, M. W., Seeley, R. J., Woods, S. C., Weigle, D. S., Campfield, L. A., Burn, P., & Baskin, D. G. (1997). Leptin increases hypothalamic pro-opiomelanocortin mRNA expression in the rostral arcuate nucleus. *Diabetes*, *46*(12), 2119–2123. https://doi.org/10.2337/diab.46.12.2119

Seidah, N. G., & Prat, A. (2002). Precursor convertases in the secretory pathway, cytosol and extracellular milieu. *Essays in Biochemistry*, *38*, 79–94. https://doi.org/10.1042/bse0380079

Senin, L. L., Al-Massadi, O., Barja-Fernandez, S., Folgueira, C., Castelao, C., Tovar, S. A., Leis, R.,

Lago, F., Baltar, J., Baamonde, I., Dieguez, C., Casanueva, F. F., & Seoane, L. M. (2015). Regulation of NUCB2/nesfatin-1 production in rat's stomach and adipose tissue is dependent on age, testosterone levels and lactating status. *Molecular and Cellular Endocrinology*, *411*(March), 105–112. https://doi.org/10.1016/j.mce.2015.04.016

Sharma, B. K., Patil, M., & Satyanarayana, A. (2014). Negative Regulators of Brown Adipose Tissue (BAT)-Mediated Thermogenesis. *Journal of Cellular Physiology*, *229*(12), 1901–1907. https://doi.org/10.1002/jcp.24664

Shimizu, H., Oh-I, S., Hashimoto, K., Nakata, M., Yamamoto, S., Yoshida, N., Eguchi, H., Kato, I., Inoue, K., Satoh, T., Okada, S., Yamada, M., Yada, T., & Mori, M. (2009). Peripheral administration of nesfatin-1 reduces food intake in mice: The leptin-independent mechanism. *Endocrinology*, *150*(2), 662–671. https://doi.org/10.1210/en.2008-0598

Sims, J. S., & Lorden, J. F. (1986). Effect of paraventricular nucleus lesions on body weight, food intake and insulin levels. *Behavioural Brain Research*, *22*(3), 265–281. https://doi.org/10.1016/0166-4328(86)90071-9

Singru, P. S., Wittmann, G., Farkas, E., Zséli, G., Fekete, C., & Lechan, R. M. (2012). Refeeding-activated glutamatergic neurons in the hypothalamic paraventricular nucleus (PVN) mediate effects of melanocortin signaling in the nucleus tractus solitarius (NTS). *Endocrinology*, *153*(8), 3804–3814. https://doi.org/10.1210/en.2012-1235

Skibicka, K. P., Hansson, C., Alvarez-Crespo, M., Friberg, P. A., & Dickson, S. L. (2011). Ghrelin directly targets the ventral tegmental area to increase food motivation. *Neuroscience*, *180*, 129–137. https://doi.org/10.1016/j.neuroscience.2011.02.016

Skibicka, Karolina P. (2013). The central GLP-1: Implications for food and drug reward. *Frontiers in Neuroscience*, *7*(7 OCT), 1–10. https://doi.org/10.3389/fnins.2013.00181

Skibicka, Karolina P., & Grill, H. J. (2008). Energetic responses are triggered by caudal brainstem melanocortin receptor stimulation and mediated by local sympathetic effector circuits. *Endocrinology*, *149*(7), 3605–3616. https://doi.org/10.1210/en.2007-1754

Skibicka, Karolina P., & Grill, H. J. (2009). Hypothalamic and hindbrain melanocortin receptors contribute to the feeding, thermogenic, and cardiovascular action of melanocortins. *Endocrinology*, *150*(12), 5351–5361. https://doi.org/10.1210/en.2009-0804

Sohn, J.-W., Harris, L. E., Berglund, E. D., Liu, T., Vong, L., Lowell, B. B., Balthasar, N., Williams, K. W., & Elmquist, J. K. (2013). Melanocortin 4 Receptors Reciprocally Regulate Sympathetic and Parasympathetic Preganglionic Neurons. *Cell*, *152*(3), 612–619. https://doi.org/10.1016/j.cell.2012.12.022

Song, C. K., Vaughan, C. H., Keen-Rhinehart, E., Harris, R. B. S., Richard, D., & Bartness, T. J. (2008).

Melanocortin-4 receptor mRNA expressed in sympathetic outflow neurons to brown adipose tissue: neuroanatomical and functional evidence. *AJP: Regulatory, Integrative and Comparative Physiology*, *295*(2), R417–R428. https://doi.org/10.1152/ajpregu.00174.2008

Stanley, S., Pinto, S., Segal, J., Pérez, C. A., Viale, A., DeFalco, J., Cai, X., Heisler, L. K., & Friedman, J. M. (2010). Identification of neuronal subpopulations that project from hypothalamus to both liver and adipose tissue polysynaptically. *Proceedings of the National Academy of Sciences of the United States of America*, *107*(15), 7024–7029. https://doi.org/10.1073/pnas.1002790107

Stengel, A., Goebel, M., Wang, L., Rivier, J., Kobelt, P., Mönnikes, H., Lambrecht, N. W. G., & Taché, Y. (2009). Central nesfatin-1 reduces dark-phase food intake and gastric emptying in rats: Differential role of corticotropin-releasing factor2 receptor. *Endocrinology*, *150*(11), 4911–4919. https://doi.org/10.1210/en.2009-0578

Stengel, A., Goebel, M., Yakubov, I., Wang, L., Witcher, D., Coskun, T., Taché, Y., Sachs, G., & Lambrecht, N. W. G. (2009). Identification and characterization of nesfatin-1 immunoreactivity in endocrine cell types of the rat gastric oxyntic mucosa. *Endocrinology*, *150*(1), 232–238. https://doi.org/10.1210/en.2008-0747

Stengel, A., Goebel, M., Yakubov, I., Wang, L., Witcher, D., Coskun, T., Taché, Y., Sachs, G., & Lambrecht, N. W. G. (2009). Identification and Characterization of Nesfatin-1 Immunoreactivity in Endocrine Cell Types of the Rat Gastric Oxyntic Mucosa. *Endocrinology*, *150*(1), 232–238. https://doi.org/10.1210/en.2008-0747

Sutton, G. M., Duos, B., Patterson, L. M., & Berthoud, H. R. (2005). Melanocortinergic modulation of cholecystokinin-induced suppression of feeding through ERK signaling in rat solitary nucleus. *Endocrinology*, *146*(9), 3739–3747. https://doi.org/10.1210/en.2005-0562

Sutton, G. M., Patterson, L. M., & Berthoud, H. R. (2004). Extracellular signal-regulated kinase 1/2 signaling pathway in solitary nucleus mediates cholecystokinin-induced suppression of food intake in rats. *Journal of Neuroscience*, *24*(45), 10240–10247. https://doi.org/10.1523/JNEUROSCI.2764-04.2004

Suzuki, S., Takagi, K., Miki, Y., Onodera, Y., Akahira, J. I., Ebata, A., Ishida, T., Watanabe, M., Sasano, H., & Suzuki, T. (2012). Nucleobindin 2 in human breast carcinoma as a potent prognostic factor. *Cancer Science*, *103*(1), 136–143. https://doi.org/10.1111/j.1349-7006.2011.02119.x

Swanson, L. W. (1977). Immunohistochemical evidence for a neurophysin-containing autonomic pathway arising in the paraventricular nucleus of the hypothalamus. *Brain Research*, *128*(2), 346–353. https://doi.org/10.1016/0006-8993(77)91000-9

Swanson, L. W., & Sawchenko, P. E. (1983). Hypothalamic integration: Organization of the paraventricular and supraoptic nuclei. *Annual Review of Neuroscience*, *Vol. 6*, 269–324.

https://doi.org/10.1146/annurev.ne.06.030183.001413

Swanson, L. W., Sawchenko, P. E., Wiegand, S. J., & Price, J. L. (1980). Separate neurons in the paraventricular nucleus project to the median eminence and to the medulla or spinal cord. *Brain Research*, *198*(1), 190–195. https://doi.org/10.1016/0006-8993(80)90354-6

Swart, I., Jahng, J. W., Overton, J. M., & Houpt, T. a. (2002). Hypothalamic NPY, AGRP, and POMC mRNA responses to leptin and refeeding in mice. *American Journal of Physiology. Regulatory, Integrative and Comparative Physiology*, *283*(5), R1020–R1026. https://doi.org/10.1152/ajpregu.00501.2001

Tagaya, Y., Miura, A., Okada, S., Ohshima, K., & Mori, M. (2012). Nucleobindin-2 is a positive modulator of EGF-dependent signals leading to enhancement of cell growth and suppression of adipocyte differentiation. *Endocrinology*, *153*(7), 3308–3319. https://doi.org/10.1210/en.2011-2154

Tang-Christensen, M., Larsen, P. J., Göke, R., Fink-Jensen, A., Jessop, D. S., Møller, M., & Sheikh, S. P. (1996). Central administration of GLP-1-(7-36) amide inhibits food and water intake in rats. *American Journal of Physiology - Regulatory Integrative and Comparative Physiology*, *271*(4 40-4). https://doi.org/10.1152/ajpregu.1996.271.4.r848

Tang-Christensen, M., Vrang, N., Ortmann, S., Bidlingmaier, M., Horvath, T. L., & Tschöp, M. (2004). Central administration of ghrelin and agouti-related protein (83-132) increases food intake and decreases spontaneous locomotor activity in rats. *Endocrinology*, *145*(10), 4645–4652. https://doi.org/10.1210/en.2004-0529

Tanida, M., Gotoh, H., Yamamoto, N., Wang, M., Kuda, Y., Kurata, Y., Mori, M., & Shibamoto, T. (2015). Hypothalamic nesfatin-1 stimulates sympathetic nerve activity via hypothalamic ERK signaling. *Diabetes*, *64*(11), 3725–3736. https://doi.org/10.2337/db15-0282

Tanida, M., & Mori, M. (2011). Nesfatin-1 stimulates renal sympathetic nerve activity in rats. *Neuroreport*, *22*(6), 309–312. https://doi.org/10.1097/WNR.0b013e328346107f

Trenevska, I., Li, D., & Banham, A. H. (2017). Therapeutic antibodies against intracellular tumor antigens. *Frontiers in Immunology*, *8*(AUG). https://doi.org/10.3389/fimmu.2017.01001

Tsuchiya, T., Shimizu, H., Yamada, M., Osaki, A., Oh-I, S., Ariyama, Y., Takahashi, H., Okada, S., Hashimoto, K., Satoh, T., Kojima, M., & Mori, M. (2010). Fasting concentrations of nesfatin-1 are negatively correlated with body mass index in non-obese males. *Clinical Endocrinology*, *73*(4), 484–490. https://doi.org/10.1111/j.1365-2265.2010.03835.x

Ueta, Y., Ozaki, Y., Saito, J., & Onaka, T. (2003). Involvement of Novel Feeding-Related Peptides in Neuroendocrine Response to Stress. *Experimental Biology and Medicine*, *228*(10), 1168–1174. https://doi.org/10.1177/153537020322801011

Ueyama, E., Morikawa, Y., Yasuda, T., & Senba, E. (2004). Attenuation of fasting-induced phosphorylation of mitogen-activated protein kinases (ERK/p38) in the mouse hypothalamus in response to refeeding. *Neuroscience Letters*, *371*(1), 40–44. https://doi.org/10.1016/j.neulet.2004.08.035

Van Den Beukel, J. C., Grefhorst, A., Quarta, C., Steenbergen, J., Mastroberardino, P. G., Lombés, M., Delhanty, P. J., Mazza, R., Pagotto, U., Van Der Lely, A. J., & Themmen, A. P. N. (2014). Direct activating effects of adrenocorticotropic hormone (ACTH) on brown adipose tissue are attenuated by corticosterone. *FASEB Journal*, *28*(11), 4857–4867. https://doi.org/10.1096/fj.14-254839

Villanueva, E. C., & Myers, M. G. (2008). Leptin receptor signaling and the regulation of mammalian physiology. *International Journal of Obesity*, *32*, S8–S12. https://doi.org/10.1038/ijo.2008.232

Voss-Andreae, A., Murphy, J. G., Ellacott, K. L. J., Stuart, R. C., Nillni, E. A., Cone, R. D., & Fan, W. (2007). Role of the central melanocortin circuitry in adaptive thermogenesis of brown adipose tissue. *Endocrinology*, *148*(4), 1550–1560. https://doi.org/10.1210/en.2006-1389

Wallingford, N., Perroud, B., Gao, Q., Coppola, A., Gyengesi, E., Liu, Z. W., Gao, X. B., Diament, A., Haus, K. A., Shariat-Madar, Z., Mahdi, F., Wardlaw, S. L., Schmaier, A. H., Warden, C. H., & Diano, S. (2009). Prolylcarboxypeptidase regulates food intake by inactivating α-MSH in rodents. *Journal of Clinical Investigation*, *119*(8), 2291–2303. https://doi.org/10.1172/JCI37209

Wang, Q., Guo, F., Sun, X., Gao, S., Li, Z., Gong, Y., & Xu, L. (2014). Effects of exogenous nesfatin-1 on gastric distention-sensitive neurons in the central nucleus of the amygdala and gastric motility in rats. *Neuroscience Letters*, *582*, 65–70. https://doi.org/10.1016/j.neulet.2014.09.003

Wernecke, K., Lamprecht, I., Jöhren, O., Lehnert, H., & Schulz, C. (2014). Nesfatin-1 increases energy expenditure and reduces food intake in rats. *Obesity*, *22*(7), 1662–1668. https://doi.org/10.1002/oby.20736

Wesolowski, T., Schaarschmidt, B., & Lamprecht, I. (1985). A poor man's calorimeter (PMC) for small animals. *Journal of Thermal Analysis*, *30*(6), 1403–1413. https://doi.org/10.1007/BF01914314

Xu, L., Bloem, B., Gaszner, B., Roubos, E. W., & Kozicz, T. (2009). Sex-specific effects of fasting on urocortin 1, cocaine- and amphetamine-regulated transcript peptide and nesfatin-1 expression in the rat Edinger-Westphal nucleus. *Neuroscience*, *162*(4), 1141–1149. https://doi.org/10.1016/j.neuroscience.2009.05.003

Xu, Luo, Wang, Q., Guo, F., Pang, M., Sun, X., Gao, S., & Gong, Y. (2015). Nesfatin-1 signaling in the basom edial amygdala modulates the gastric distension-sensitive neurons discharge and decreases gastric motility via melanocortin 3/4 receptors and modified by the arcuate nucleus. *European Journal of Pharmacology*, *764*, 164–172. https://doi.org/10.1016/j.ejphar.2015.07.002

Xu, Y. Y., Ge, J. F., Qin, G., Peng, Y. N., Zhang, C. F., Liu, X. R., Liang, L. C., Wang, Z. Z., Chen, F. H., & Li, J. (2015). Acute, but not chronic, stress increased the plasma concentration and hypothalamic

mRNA expression of NUCB2/nesfatin-1 in rats. *Neuropeptides*, *54*, 47–53. https://doi.org/10.1016/j.npep.2015.08.003

Yamada, M., Horiguchi, K., Umezawa, R., Hashimoto, K., Satoh, T., Ozawa, A., Shibusawa, N., Monden, T., Okada, S., Shimizu, H., & Mori, M. (2010). Troglitazone, a ligand of peroxisome proliferator-activated receptor-γ, stabilizes NUCB2 (nesfatin) mRNA by activating the ERK1/2 pathway: Isolation and characterization of the human NUCB2 gene. *Endocrinology*, *151*(6), 2494–2503. https://doi.org/10.1210/en.2009-1169

Yang, Y., Atasoy, D., Su, H. H., & Sternson, S. M. (2011). Hunger states switch a flip-flop memory circuit via a synaptic AMPK-dependent positive feedback loop. *Cell*, *146*(6), 992–1003. https://doi.org/10.1016/j.cell.2011.07.039

Yilmaz, M. S., Altinbas, B., Guvenc, G., Erkan, L. G., Avsar, O., Savci, V., Kucuksen, D. U., Arican, I., & Yalcin, M. (2015). The role of centrally injected nesfatin-1 on cardiovascular regulation in normotensive and hypotensive rats. *Autonomic Neuroscience: Basic and Clinical*, *193*, 63–68. https://doi.org/10.1016/j.autneu.2015.07.009

Yosten, G. L. C., & Samson, W. K. (2009). Nesfatin-1 exerts cardiovascular actions in brain: possible interaction with the central melanocortin system. *AJP: Regulatory, Integrative and Comparative Physiology*, *297*(2), R330–R336. https://doi.org/10.1152/ajpregu.90867.2008

Yosten, Gina L. C., & Samson, W. K. (2009). Nesfatin-1 exerts cardiovascular actions in brain: possible interaction with the central melanocortin system. *AJP: Regulatory, Integrative and Comparative Physiology*, *297*(2), R330–R336. https://doi.org/10.1152/ajpregu.90867.2008

Yosten, Gina L C, & Samson, W. K. (2010). The anorexigenic and hypertensive effects of nesfatin-1 are reversed by pretreatment with an oxytocin receptor antagonist. *American Journal of Physiology-Regulatory, Integrative and Comparative Physiology*, *298*(6), R1642–R1647. https://doi.org/10.1152/ajpregu.00804.2009

YOUNG, J. B., & LANDSBERG, L. (1977). Stimulation of the sympathetic nervous system during sucrose feeding. *Nature*, *269*(5629), 615–617. https://doi.org/10.1038/269615a0

Young, J. B., Rosa, R. M., & Landsberg, L. (1984). Dissociation of sympathetic nervous system and adrenal medullary responses. *The American Journal of Physiology*, *247*(1 Pt 1).

Young, J B, Saville, E., Rothwell, N. J., Stock, M. J., & Landsberg, L. (1982). Effect of diet and cold exposure on norepinephrine turnover in brown adipose tissue of the rat. *The Journal of Clinical Investigation*, *69*(5), 1061–1071. https://doi.org/10.1172/jci110541

Young, James B. (2003). Developmental plasticity in sympathetic nervous system response to fasting in adipose tissues of male rats. *Metabolism: Clinical and Experimental*, *52*(12), 1621–1626.

https://doi.org/10.1016/S0026-0495(03)00331-7

Young, James B., & Landsberg, L. (1977). Suppression of sympathetic nervous system during fasting. *Science*, *196*(4297), 1473–1475. https://doi.org/10.1126/science.867049

Young, James B, & Landsberg, L. (1979). Effect of diet and cold exposure on norepinephrine turnover in pancreas and liver. *American Journal of Physiology-Endocrinology and Metabolism*, *236*(5), E524. https://doi.org/10.1152/ajpendo.1979.236.5.E524

Yu, C. H., Hsieh, Y. S., Chen, P. N., Chen, J. R., & Kuo, D. Y. (2018). Knockdown of the transcript of ERK in the brain modulates hypothalamic neuropeptide-mediated appetite control in amphetamine-treated rats. *British Journal of Pharmacology*, *175*(4), 726–739. https://doi.org/10.1111/bph.14120

Yuan, J. H., Chen, X., Dong, J., Zhang, D., Song, K., Zhang, Y., Wu, G. B., Hu, X. H., Jiang, Z. Y., & Chen, P. (2017). Nesfatin-1 in the lateral parabrachial nucleus inhibits food intake, modulates excitability of glucosensing neurons, and enhances UCP1 expression in brown adipose tissue. *Frontiers in Physiology*, *8*(APR), 1–11. https://doi.org/10.3389/fphys.2017.00235

Zhang, J., Zhou, Y., Chen, C., Yu, F., Wang, Y., Gu, J., Ma, L., & Ho, G. (2015). ERK1/2 mediates glucose-regulated pomc gene expression in hypothalamic neurons. *Journal of Molecular Endocrinology*, *54*(2), 125–135. https://doi.org/10.1530/JME-14-0330

Zhao, Z. J., Chi, Q. S., Cao, J., & Han, Y. D. (2010). The energy budget, thermogenic capacity and behavior in Swiss mice exposed to a consecutive decrease in temperatures. *Journal of Experimental Biology*, *213*(23), 3988–3997. https://doi.org/10.1242/jeb.046821

Zheng, H. (2005). Brain stem melanocortinergic modulation of meal size and identification of hypothalamic POMC projections. *AJP: Regulatory, Integrative and Comparative Physiology*, *289*(1), R247–R258. https://doi.org/10.1152/ajpregu.00869.2004

Appendix

List of tables

Table M.1 – Stereotactic coordinates

Area of interest	Direction	Coordinates (mm)
Lateral ventricle	antero-posterior	-1.00
	medio-lateral	+1.50
	dorso-ventral	-2.30 (+1.50 protrusion)
PVN	antero-posterior	-1.80
	medio-lateral	+0.30
	dorso-ventral	-5. 90 (+2.00 protrusion)
NTS	antero-posterior	on occipital suture

Coordinates used for site-specific cannula implantation and virus injection, according to Paxinos and Watson's rat brain atlas (2007). Dorso-ventral coordinates are indicated as depth of the implanted cannula plus additional depth reached by the injector.

Table M.2 - Chemicals & reagents

Bromphenol-blue	Sigma Aldrich, Saint Louis, MO, US
Carprofen, Rimadyl®	Pfizer Inc., New York, NY, USA
Injectable water, Ampuwa®	Fresenius Kabi Deutschland GmbH, Bad Homburg vor der Höhe, Germany
Ketamin 10%	Medistar, Serumwerk Bernburg AG, Bernburg, Germany
Xylazin 20mg/mL	Medistar, Serumwerk Bernburg AG, Bernburg, Germany
Paladur®	Heraeus, Hanau, Germany
Nesfatin-1	Phoenix Europe GmbH, Karlsruhe, Germany
U0126	Sigma Aldrich, Saint Louis, MO,US
Exendin-4	Tocris Bioscience, Bristol (UK)
Angiotensin II	Sigma Aldrich, Saint Louis, MO,US

Table M.3 - Mastermix composition for qPCR

Volume [µL]	Reagent
1.6	cDNA
0.75	Forward primer 5 pmol/µL
0.75	Revers primer 5 pmol/µL
12.5	Platinum® SYBR® Green
9	Water

Table M.4 - Composition of the mastermix per reaction for cDNA synthesis

Volume [µL]	Reagent
4	$MgCl_2$
2	Reverse transcription 10x buffer
2	dNTP mix
0.5	Recombinant RNasin® Ribonuclease inhibitor
0.5	AMV Reverse transcriptase
1	Oligo(dT)15 primer

Table M.5 - Parameters for cDNA synthesis and qPCR

Reaction	Tcycle	Usage	Time	Rep
Reverse Transcription	70	RNA incubator	10 min	1
	42	Annealing, reverse transcription	15 min	1
	95	Denaturation of the RT	5 min	1
	4	Inactivation and storage	∞	∞
qPCR	50	Activation of UDG	2 min	
	95	Initial denaturation and inactivation of UDG	2 min	
	95	Denaturation of the RT	15 s	40
	60	Anealing & elongation	1 min	40
	95	Dissociation	15 s	
	60	Dissociation	20 s	
	95	Dissociation	15 s	

Cycle temperature in °C is given in Tcycle; number of cycle repetitions is given in Rep

Table M.6 - Kits

Absolutely RNA Nanoprep Kit	Agilent Technologies, Texas, USA
cDNA synthesis Kit, Reverse Transcription System	Promega Corporation, Madison, USA
NucleoSpin® RNA	Macherey-Nagel GmbH & Co. KG, Düren, Germany
qPCR Kit, Platinum® SYBR® Green	invitrogen, Thermo Fisher Scientific, Carlsbad, USA
Sepharose Column, AVB Sepharose High Performance	VWR International GmbH, Hannover Germany

Table M.7 - Consumables

96-Well plate half skirt	Sarstedt AG & Co. KG, Nümbrecht, Germany
Acrodisc® Syringe Filter, 0,2 µm	Pall Corporation, Port Washington, NY, USA
Amicon Ultra 4 Centrifugal Filter	Merck Millipore, Darmstadt, Germany
Cannula, dummy, C315DCS-5-SPC	PlasticsOne®, Roanoke, VA, USA
Cannula, guide, C315GS-5-SP, 3.3 mm protrusion/below pedestal	PlasticsOne®, Roanoke, VA, USA
Cannula, dummy, C315DCS-5-SPC	PlasticsOne®, Roanoke, VA, USA
Cannula, guide, C315GS-5-SP, 3.9 mm protrusion/below pedestal	PlasticsOne®, Roanoke, VA, USA
Cannula, dummy C23DC-1.5-SPC	PlasticsOne®, Roanoke, VA, USA
Dust cap 41023 Flat Top, 8K000303DCFT	PlasticsOne®, Roanoke, VA, USA
Cannula, guide, C235G-1.5-SPC 8.0 mm protrusion/below pedestal	PlasticsOne®, Roanoke, VA, USA
Tubing, C232CT-PKG	PlasticsOne®, Roanoke, VA, USA
Teklad Global 16% Protein Rodent Diet, (2016)	Envigo, Huntingdon, UK
Chow food for rats and mice, #1320	Altromin Spezialfutter GmbH & Co. KG, Germany
Disposable Scalpel	Feather safety razor Co., Japan
Injector, C315IS-5-SPC with 2.0 mm protrusion	PlasticsOne®, Roanoke, VA, USA
Injector, C315IS-5-SPC with 1.5 mm protrusion	PlasticsOne®, Roanoke, VA, USA
Disposable cannulas, BD Microlance™3, 27G x 3/4	Becton, Dickinson and Company Limited, Ireland
MembraneSlide, 1.0 mm, PEN-membrane covered	Carl Zeiss Microscopy GmbH, Göttingen, Germany
Micro tube 1.5 mL	Sarstedt AG & Co. KG, Nümbrecht, Germany
Slides, MENZEL-Gläser Superfrost™Plus	Thermo scientific, Gerhard Menzel B.V. & Co. KG, Braunschweig, Germany
Syringe, 1 mL, Injekt®-F B.	Braun Melsungen AG, Melsungen, Germany
Tissue-Tek O.C.T™Compound	Sakura Fintek Europe, Alphen aan den Rijn, Netherlands
Tube 0.2 mL, Multiply® - µStrip Pro 8-strip	Sarstedt AG & Co. KG, Nümbrecht, Germany
Tube 15 mL	Sarstedt AG & Co. KG, Nümbrecht, Germany
Tube 50 mL	Sarstedt AG & Co. KG, Nümbrecht, Germany

Table M.8 - Primers

Gene	Forward	Reverse	Base pairs
Agrp	GCAGACCGAGCAGAAGATGT	CTTGAAGAAGCGGCAGTAGC	177
Cart	ACTGTCCCCGAGGAACTTCT	ATTTTGAAGCAGCAGGGAAA	191
cFOS	TCAATGACCCTGAGCCCAA	TGATGCCGGAAACAAGAAGTC	101
Cidea	TATCCGCTGCACAAGCTTCA	CACATAAGCGCCCGCATAA	88
Crf	AAAGGGGAAAGGCAAAGAAA	GTTTAGGGGCGCTCTCTTCT	137
Dio2	CTTCAGACCATGCCATGTGGT	CCAACATTCCCTACCCCAAGA	112
Mc4r	TGTCCACATGTTCCTGATGGC	GGTAATTGCGCCCTTCATGTT	83
Npy	TAACAAACGAATGGGGCTGT	TGTCTCAGGGCTGGATCTCT	208
Nucb2	TTTCTCTTGGTTCCGTGCGT	TGGCGGTTCTATCCTTGCA	142
Oxytocin	ATCTCGGACTGAACACCAACG	TTGCGCATATCCAGGTCTAGC	111
Pomc	GAAGGTGTACCCCAATGTCG	CTTCTCGGAGGTCATGAAGC	192
PparΥ	TGCTGAACGTGAAGCCCAT	TCATCTTCTGGAGCACCTTGG	99
Ppgcα	CAATGAGCACGAAAGGCTGA	CACACGGCGCTCTTCAATT	100
Th	CCAGGACATTGGACTTGCATC	TGCACCATAAGCCTTCAGCTC	127
Ucp1	AACTTCCGAAGTGCAACCCAC	GGCCTTCACCTTGGATCTGAA	108
β-actin	TGTTGCCCTAGACTTCGAGCA	ATGCCACAGGATTCCATACCC	168

Table M.8 - Softwares

7000 System SDS Software RQ Study Application, Version 1.2.3	Applied Biosystems, USA
Leica LAS AF	Leica Microsystems CMS GmbH., Wetzlar, Germany
Measure minispec PLUS NF .Ink	Bruker Biospin GmbH, Rheinstetten, Germany
NanoDrop 2000, Version 1.4.0.1	Thermo Fisher Scientific Inc., Carlsbad, USA
OPUS 7.0 Ink.	Bruker Biospin GmbH, Rheinstetten, Germany
PALM Robo 4.8 Pro	Carl Zeiss AG, Oberkochen, Germany
Graphpad Prism 8.0	GraphPad Inc., USA
Quick Report	FLIR® Systems, Inc., Wilsonville, USA
ResearchIR FLIR®	FLIR® Systems, Inc., Wilsonville, USA
MED-PC V Software Suit	Med Associates, Georgia, VT, USA
Statistica 7.0	StatSoft (Europe) GmbH, Hamburg

Table M.9 - Settings used for ResearchIR FLIR®

Parameter	Setting used
Emissivity	0.95
Distance	30 cm
Reflected temperature	As measured
Relative humidity	50%
Palette	User defined

User-defined settings only. All remaining settings to default. Infrared resolution 640 × 512 pixels, thermal sensitivity 0.05˚C at 30 C

Table M.10 - In-hose built direct calorimeter parameters

Aluminum box	Lenght	180 mm
	Width	125 mm
	Height	160 mm
Distances from the main cooling box	From side walls	2 mm
	From bottom/front walls	6 mm
Air exchange slit	Height	5 mm
	Width	125 mm
Air pump	Flow rate	200 mL/min

Table S.1a - Experiment I - 3-way ANOVA main effects

Parameter	**F value**	**p value**
Nesfatin-1	19.3920	0.000162
Feeding state	15.5049	0.000550
Time	121.0227	0.000000
Time * Nesfatin-1	6.6735	0.000000
Time * Feeding	1.0631	0.389155
Nesfatin-1 * Feeding	0.0026	0.959862
Nesfatin-1 * Feeding * Time	1.0243	0.415670

Relative to figure 1.1A

Table S.1b - Experiment I - 2-way ANOVA for each timepoint

Parameter	Nesfatin-1		Feeding state		Nesfatin-1 * Feeding	
	F value	p value	F value	p value	F value	p value
Hour 1	4.1670	0.051488	21.655	0.000084	1.467	0.236667
Hour 2	12.3885	0.0016132	15.213793	0.0006057	0.5262175	0.4746806
Hour 3	34.2745	3.586E-06	17.62112	0.0002787	0.0298561	0.8641551
Hour 4	33.8593	3.933E-06	17.736069	0.0002689	0.2513759	0.6203268
Hour 5	24.4103	3.93E-05	6.4328576	0.0175498	0.3736825	0.5463119
Hour 6	15.6321	0.0005274	5.2319386	0.0305586	0.1497778	0.7018975
Hour 7	6.3812	0.0179622	8.4046861	0.0075086	0.0025917	0.9597872
Hour 8	2.6560	0.1152158	6.8531449	0.0145581	0.0316841	0.8601023

Table S.1c - Experiment I - 2-way ANOVA

Parameter	F value	p value
Nesfatin-1	19.390	0.959900
Feeding state	15.510	0.000200
Nesfatin-1 * Feeding	0.003	0.000500

Relative to figure 1.1B

Table S.1d - Experiment I - BW loss/DHL correlation

Parameter	R^2	p value	n
Nesfatin-1. both groups	0.4634	0.0037	16
PBS. both groups	0.1374	0.1919	14
Nesfatin-1. *ad libitum*	0.2581	0.2433	9
Nesfatin-1. food deprived	0.4203	0.0590	7

Table S.1e - Experiment I - 2-way ANOVA

Parameter	F value	p value
Nesfatin-1	0.081	0.778200
Feeding state	13.740	0.001000
Nesfatin-1 * Feeding	0.507	0.482600

Relative to figure 1.3A

Table S.2a - Experiment IIa - 2-way ANOVA Food Intake

Parameter	Cumulative		Incremental	
	F value	p value	F value	p value
Nesfatin-1	9.488	0.000400	2.211	0.1216
Time	222.600	<0.0001	22.24	<0.0001
Nesfatin-1 * Time	17.580	0.000400	18.29	0.0003

Table S.2b - Experiment IIb - 2-way ANOVA Direct Calorimetry

Parameter	Cumulative	
	F value	p value
Nesfatin-1	0.524	0.814800
Time	18.150	<0.0001
Nesfatin-1 * Time	7.723	0.013400

Table S.2c - Experiment IIc - 2-way ANOVA Infrared Thermography

Parameter	iBAT		Ear		Tail	
	F value	p value	F value	p value	F value	p value
Nesfatin-1	3.105	0.008200	3.964	0.0015	0.6789	0.667
Time	15.770	<0.0001	12.14	<0.0001	7.806	0.0004
Nesfatin-1 * Time	12.190	0.003300	12.55	0.003	0.07581	0.7868

Table S.2d - Experiment IId - UCP1/iBATΔ correlation

Parameter	R^2	p value	n
Nesfatin-1	0.9777	0.0002	6
PBS	0.0016	0.9329	7

Table S.2e - Experiment IIe - cFOS/iBATΔ correlation

Parameter	R^2	p value	n
NTS	0.3767	0.0196	14
PVN	0.0749	0.3894	12

Table S.3a - Experiment IIIa - 3-way ANOVA main effects

Parameter	F value	p value
Nesfatin-1	17.104	0.002026
U0126	14.127	0.003731
Time	351.346	0.000000
Time * Nesfatin-1	22.565	0.000007
Time * U0126	3.0072	0.072137
Nesfatin-1 * U0126	11.977	0.006115
Nesfatin-1 * U0126 * Time	6.752	0.005746

Table S.3b - Experiment IIIa - 2-way ANOVA for each timepoint

Parameter	Nesfatin-1		U0126		Nesfatin-1 * U0126	
	F value	p value	F value	p value	F value	p value
Hour 1	2.0437	0.183328	1.8833	0.199957	1.1092	0.317041
Hour 3	10.5611	0.008724	8.342	0.016156	1.5186	0.246018
Hour 6	31.045	0.000237	8.0939	0.017399	12.9053	0.00491

Relative to figure 3.1A

Table S.3c - Experiment IIb - 3-way ANOVA main effects

Parameter	iBAT		Ear		Tail	
	F value	p value	F value	p value	F value	p value
Nesfatin-1	17.483	0.000924	4.933871	0.043338	2.29305	0.152201
U0126	3.177	0.096361	2.144931	0.165134	0.08558	0.77417
Time	10.343	0.000000	1.078778	0.379697	17.85187	0.000000
Time * Nesfatin-1	0.634	0.674426	0.574564	0.719239	1.37625	0.243756
Time * U0126	1.21021	0.31347	3.486737	0.082941	0.35863	0.875004
Nesfatin-1 * U0126	4.447	0.053447	1.174011	0.330703	3.10012	0.100104
Nesfatin-1 * U0126 * Time	1.137	0.349173	0.557855	0.73185	0.06651	0.996849

Table S.3d - Experiment IIb - 2-way ANOVA for each timepoint

	Parameter	Nesfatin-1		U0126		Nesfatin-1 * U0126	
		F value	p value	F value	p value	F value	p value
iBAT	15 min	2.291	0.152371	0.00088	0.976807	8.10607	0.012923
	30 min	16.18772	0.001257	5.24376	0.03807	2.88653	0.111426
	45 min	2.88653	0.111426	4.86392	0.044643	5.78225	0.030596
	60 min	14.88764	0.001738	3.60743	0.078323	1.13714	0.304303
	75 min	6.010711	0.027954	1.384727	0.258918	4.430522	0.053845
	90 min	4.656322	0.048798	0.946568	0.347105	0.201636	0.660276

Table S.4a - Experiment IVa - 2-way ANOVA main effects

Parameter	MC4R KD		Time		Time * MC4R KD	
	F value	p value	F value	p value	F value	p value
Body Weight	7.031	0.029200	48.790	<0.0001	0.101	>0.9999
Food intake	5.903	0.0412	6.625	<0.0001	0.9512	0.5075
Direct calorimetry	0.5186	0.4816	42.18	<0.0001	0.0019	4.181
Body composition	0.01566	0.9035	3.621	0.032400	1.159	0.3473
Thermography	0.2139	0.656	1.943	0.170700	0.3467	0.7918

Table S.4b - Experiment IVb - 3-way ANOVA main effects

Parameter	iBAT		Ear		Tail	
	F value	p value	F value	p value	F value	p value
MC4R KD	2.549	0.149003	1.52838	0.251419	0.466259	0.513997
Nesfatin-1	17.964	0.002844	9.12052	0.016559	0.306715	0.594839
Time	3.408	0.011710	4.86779	0.001431	2.314481	0.061490
Time * MC4R KD	1.250	0.304280	0.77849	0.571095	0.830898	0.535462
Time * Nesfatin-1	1.2061	0.323884	1.66679	0.164952	1.125956	0.362372
MC4R KD * Nesfatin-1	4.440	0.068168	12.71645	0.007336	0.396907	0.54626
MC4R KD * Nesfatin-1 * Time	0.389	0.853485	0.32458	0.895204	0.482451	0.787224

Table S.4c - Experiment IVb - 2-way ANOVA for each timepoint

	Parameter	M4C4 KD		Nesfatin-1		MC4R KD * Nesfatin-1	
		F value	p value	F value	p value	F value	p value
iBAT	15 min	0.59524	0.462578	9.87313	0.01376	3.04726	0.119019
	30 min	0.08319	0.780346	8.79296	0.018	1.69147	0.229619
	45 min	7.139	0.028279	26.53158	0.000873	1.52105	0.252467
	60 min	6.27709	0.036632	15.29101	0.004479	4.28571	0.072207
	75 min	0.15022	0.708431	3.362	0.104065	2.178	0.178236
	90 min	0.66117	0.439673	2.30084	0.167778	0.74118	0.414341
Ear	15 min	2.82888	0.131087	13.61111	0.006136	22.5	0.001458
	30 min	0.26178	0.62272	3.15847	0.113432	3.54098	0.096645
	45 min	3.01176	0.120878	3.84053	0.085694	2.24585	0.172355
	60 min	4.559267	0.065258	6.278261	0.036618	3.248309	0.109167
	75 min	0.14177	0.716316	0.15629	0.70293	3.9072	0.083478
	90 min	0.25903	0.624524	2.59875	0.145613	1.83368	0.2127

Table S.5a - Experiment Va - 2-way ANOVA main effects - Males

Parameter	Exendin 4		Nesfatin-1 Ab		Nesfatin-1 Ab * Exendin 4	
	F value	p value	F value	p value	F value	p value
Pellets earned	5.283	0.033700	0.009	0.926800	0.217	0.646900
Breakpoint	3.802	0.0669	0.06981	0.7946	3.562	0.0754
Active lever presses	1.544	0.23	3.115	0.094500	0.09863	0.7571
Inactive lever presses	3.187	0.0911	0.08446	0.774700	3.856	0.0652
Horizontal activity	0.4783	0.498	4.668	0.044500	1.986	0.1758
Head entries	0.625	0.4395	0.1462	0.706700	0.3034	0.5886

Table S.5b - Experiment Va - 2-way ANOVA main effects - Females

Parameter	Exendin 4		Nesfatin-1 Ab		Nesfatin-1 Ab * Exendin 4	
	F value	p value	F value	p value	F value	p value
Pellets earned	0.307	0.587100	12.280	0.002700	0.007	0.935300
Breakpoint	0.00372	0.9521	14	0.0016	0.08162	0.7786
Active lever presses	0.3389	0.5681	9.495	0.006800	0.000271	0.9871
Inactive lever presses	2.027	0.1726	8.474	0.009700	1.56	0.2286
Horizontal activity	3.76	0.0693	9.806	0.006100	6.034	0.0251
Head entries	0.07279	0.7906	7.562	0.013700	1.178	0.2929

Table S.5c - Experiment Vb - 2-way ANOVA 24 h Food Intake - Males

Parameter	Food intake		Body weight change	
	F value	p value	F value	p value
Exendin 4	22.230	0.000200	32.98	<0.0001
Nesfatin-1 Ab	17.690	0.000500	26.42	<0.0001
Nesfatin-1 Ab * Exendin 4	13.050	0.002000	22.36	0.0002

Table S.5d - Experiment Vb - 2-way ANOVA 24 h Food Intake - Females

Parameter	Food intake		Body weight change	
	F value	p value	F value	p value
Exendin 4	30.620	<0.0001	27.83	0.0001
Nesfatin-1 Ab	0.690	0.417600	3.089	0.0968
Nesfatin-1 Ab * Exendin 4	0.188	0.669800	0.1567	0.6972

Table S.5e - Experiment Vc - 2-way ANOVA 3 h Food Intake - Males

Parameter	Food intake		Body weight change	
	F value	p value	F value	p value
Exendin 4	3.446	0.079900	2.179	<0.0001
Nesfatin-1 Ab	0.454	0.509200	43.42	0.2556
Nesfatin-1 Ab * Exendin 4	4.997	0.038300	1.379	0.1572

Table A.A1a - Efficiency time. Best fit values

Parameter	Ad libitum	Food deprived
Bmax	5.5390	6.152000
h	1.9600	2.404000
Kd	22.2500	15.810000

Table A.A1b - Body weight loss after direct calorimetry

Parameter	F value	p value
Nesfatin-1	0.081	0.778200
Feeding state	13.740	0.001000
Nesfatin-1 * Feeding	0.507	0.482600

Table A.A3a - 24 hours Cumulative Food Intake and body weight change

	Body weight change		Food intake	
Parameter	**F value**	**p value**	**F value**	**p value**
Nesfatin-1	26.140	0.000500	20.730	0.001100
U0126	3.673	0.084300	0.693	0.424600
Nesfatin-1 * U0126	3.137	0.106900	0.246	0.630700

Table A.A3a - Effect of the injection

Parameter	**F value**	**p value**
Nesfatin-1	2.322	0.149800
U0126	0.019	0.893200
Nesfatin-1 * U0126	0.971	0.341100

Additional figures

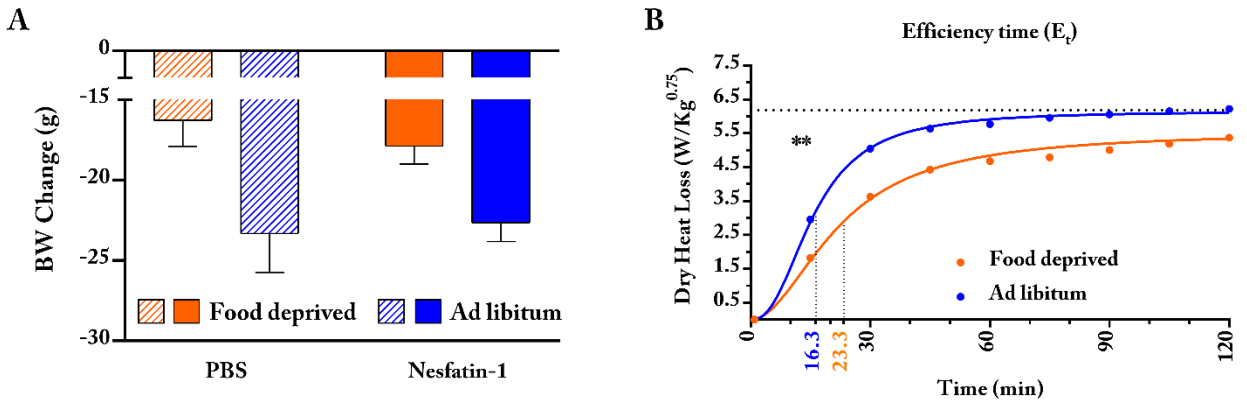

Figure A.1.: Bodyweight change and efficiency time curve.

Effect of i.c.v. administration of nesfatin-1 (100 pmol/rat) or PBS as a control solution on A) body weight change after 8 hours of direct calorimetry; B) efficiency time, or time to reach 50% of the peak dry heat loss on Experiment I. **P < 0.01 (Student's *t*-test). All data are represented as mean ± SEM.

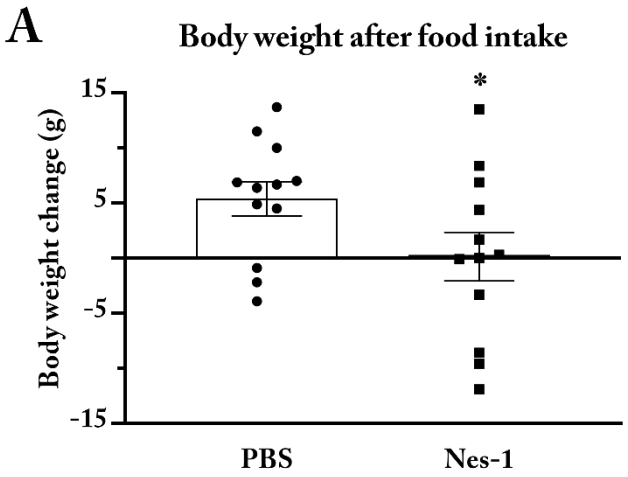

Figure A.2.1.: Bodyweight change after intra-PVN nesfatin-1 injection.

Effect of intra-PVN administration of nesfatin-1 (50 pmol/rat) or PBS as a control solution on body weight change 6 hours after injection (12/group) on Experiment IIa. *P < 0.05 (Student's *t*-test).

All data are represented as mean ± SEM.

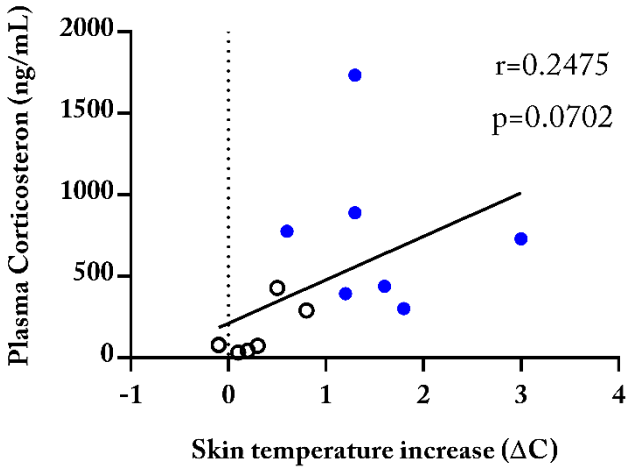

Figure A.2.2.: Correlation between plasma CTS levels and iBAT thermogenesis.

Correlation analysis (Spearman´s coefficient) between skin temperature increase from baseline at sacrifice and plasma corticosterone levels in both intra-PVN nesfatin-1 (50 pmol/rat) and PBS injected animals (6-7/group) from Experiment IIe.

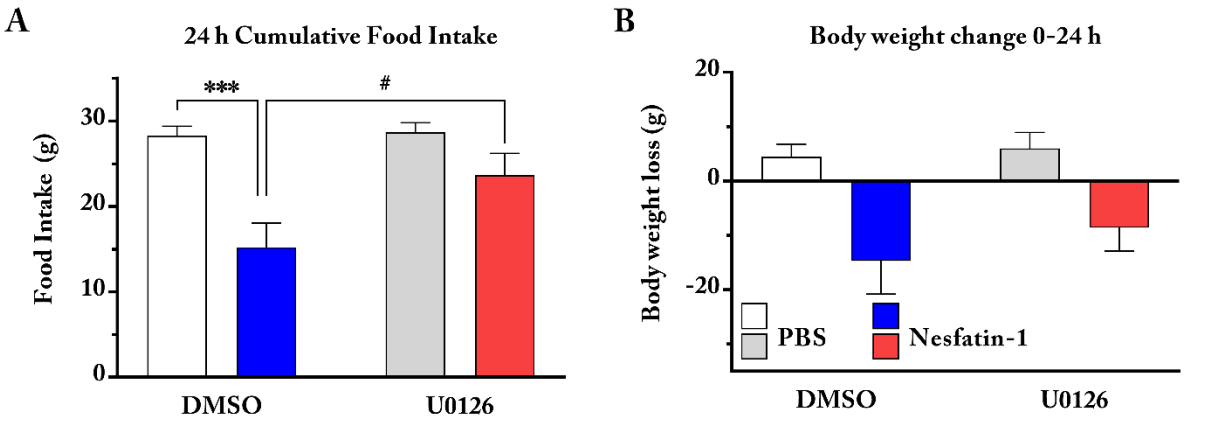

Figure A.3.1.: Erk1/2 antagonism of intra-PVN nesfatin-1 effects on food intake and body weight at 24 hours.

Effect of pretreatment with U0126 (25ng/rat) on intra-PVN administration of nesfatin-1 (50 pmol/rat) or PBS as a control solution (12/group) on *ad libitum* fed rats on Experiment IIIa.

A) 24 hours food intake. B) Body weight change. 2-way ANOVA, #P < 0.1, *P < 0.05, ***P < 0.001 (Sidak's multiple comparison test). All data are represented as mean ± SEM.

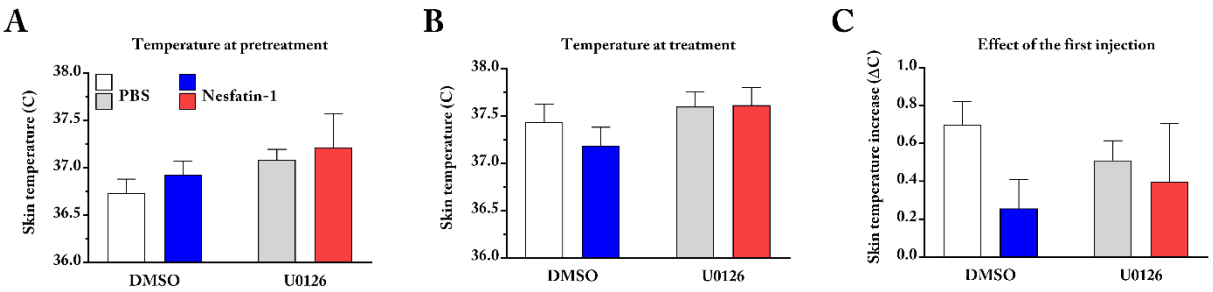

Figure A.3.2.: Aspecific effect of the pretreatment injection on the intra-PVN nesfatin-1 effects on iBAT thermogenesis.

Change in temperature generated by the pretreatment solution injection on *ad libitum* fed rats on Experiment IIIb. A) Skin temperature over the iBAT before pretreatment injection; B) Skin temperature after 30 minutes from A), before treatment injection; C) Skin temperature increase for each group. 2-way ANOVA, all data are represented as mean ± SEM.

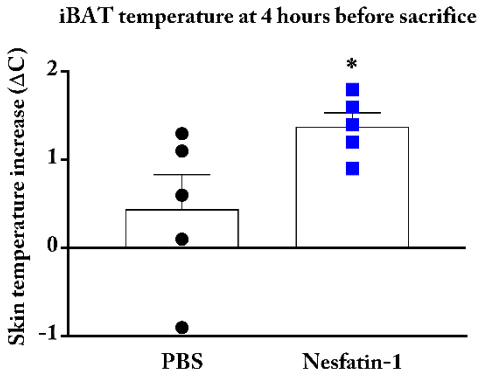

Figure A.3.3.: Skin over the iBAT temperature at the sacrifice.

Effect of intra-PVN administration of nesfatin-1 (50 pmol/rat) or PBS as a control solution on skin temperature over the iBAT (12/group) 4 hours after injection, before sacrifice, on Experiment IIc. *P < 0.05 (Student's *t*-test). All data are represented as mean ± SEM.

Figure A.4: Intra-PVN cannula placement.

Representative image of the cannula placement for intra-PVN surgeries. Immediately before killing, 1 µL of 1% bromphenol-blue was injected into the brain. The darker region above the left PVN represents the implanted cannula track.